

From the Center of Experimental Orthopaedics

Saarland University

Director: Prof. Dr. med. Henning Madry

**Novel therapeutic strategies  
for osteochondral repair *ex vivo* and *in vivo***

*Dissertation for the degree of Doctor of Medicine and Natural Sciences (MD-PhD)*

**Faculty of Medicine**

**SAARLAND UNIVERSITY**

2021

submitted by:

Xiaoyu Cai

born on: 18.04.1992 in Shandong, P. R. China

## Declaration

I hereby declare that this thesis is my own original work and effort. All experiments, except for those specified, were exclusively performed by me. Except for the publications written by myself listed in the publication list, the data presented here have not been submitted elsewhere for any award. Where other sources of information and help have been used, they have been indicated and acknowledged.

Homburg, 07.06.2021

*Xiaoyu Cai*

---

Xiaoyu Cai

Tag der Promotion: 11.03.2022

Dekan: Prof. Dr. M. D. Menger

Berichterstatter:

Prof. H. Madry

Prof. T. Pohlemann

Prof. H. Schmal

# CONTENT

List of Abbreviations .....	1
List of Figures .....	4
List of Tables .....	6
<b>1. ABSTRACT .....</b>	<b>7</b>
<b>2. ZUSAMMENFASSUNG .....</b>	<b>8</b>
<b>3. INTRODUCTION .....</b>	<b>9</b>
<b>3.1. Scaffold-guided delivery of rAAV via polymeric micelles/hydrogels.....</b>	<b>13</b>
<b>3.2. Scaffold-guided delivery of rAAV via solid scaffolds.....</b>	<b>15</b>
<b>4. HYPOTHESES .....</b>	<b>16</b>
<b>5. MATERIALS .....</b>	<b>17</b>
<b>5.1. Chemicals .....</b>	<b>17</b>
<b>5.2. Solutions and buffers .....</b>	<b>18</b>
<b>5.3. Antibodies.....</b>	<b>19</b>
<b>5.4. Software .....</b>	<b>20</b>
<b>5.5. Instrumentation .....</b>	<b>20</b>
<b>5.6. Equipment.....</b>	<b>21</b>
<b>6. METHODS .....</b>	<b>22</b>
<b>6.1. Study design.....</b>	<b>22</b>
<b>6.2. SOX9 and IGF-I <i>in vivo</i> studies .....</b>	<b>24</b>
6.2.1. <i>Plasmids and rAAV vectors.....</i>	24
6.2.2. <i>Preparation of the rAAV/scaffold systems.....</i>	25
6.2.3. <i>Evaluation of rAAV controlled release efficacy from the                 rAAV/scaffold systems.....</i>	25
6.2.4. <i>Surgeries .....</i>	25
6.2.5. <i>Macroscopic evaluation of cartilage repair.....</i>	27
6.2.6. <i>Histological scoring of cartilage repair.....</i>	27

6.2.7. Immunohistochemical evaluations .....	28
6.2.8. Histomorphometric analyses of cartilage repair .....	29
6.2.9. Qualitative evaluation of subchondral bone alterations and status .....	32
<b>6.3. TGF-<math>\beta</math> ex vivo study .....</b>	<b>33</b>
6.3.1. Samples .....	33
6.3.2. Preparation of the poly( $\epsilon$ -caprolactone) (PCL) films.....	33
6.3.3. Generation of the rAAV vectors.....	33
6.3.4. rAAV immobilization on PCL films.....	34
6.3.5. rAAV gene transfer.....	34
6.3.6. Transgene expression.....	35
6.3.7. Biological analyses.....	35
6.3.8. Histology and immunohistochemistry.....	35
6.3.9. Histomorphometric analyses .....	36
6.3.10. Real-time RT-PCR analysis .....	36
<b>6.4. Statistical analysis .....</b>	<b>37</b>
<b>7. RESULTS.....</b>	<b>38</b>
<b>7.1. SOX9 in vivo study.....</b>	<b>38</b>
7.1.1. Effects of SOX9 overexpression via rAAV-FLAG-hsox9/PEO-PPO-PEO hydrogel mediated gene transfer on the repair processes in minipig chondral defects.....	38
7.1.2. Effects of SOX9 overexpression via rAAV-FLAG-hsox9/PEO-PPO-PEO hydrogel mediated gene transfer on the immune response in minipig chondral defects.....	42
7.1.3. Effects of SOX9 overexpression via rAAV-FLAG-hsox9/PEO-PPO-PEO hydrogel mediated gene transfer on collagen orientation and distribution in minipig chondral defects.....	44
7.1.4. Effects of SOX9 overexpression via rAAV-FLAG-hsox9/PEO-PPO-PEO hydrogel mediated gene transfer on the chondrogenesis and osteogenesis in minipig chondral defects.....	47
7.1.5. Effects of SOX9 overexpression via rAAV-FLAG-hsox9/PEO-PPO-PEO hydrogel mediated gene transfer on the entire region below the cartilage defect in minipig chondral defects.....	50

<b>7.2. IGF-I <i>in vivo</i> study</b> .....	<b>57</b>
7.2.1. <i>Effective overexpression of IGF-I via rAAV/alginate-mediated gene transfer in chondral defects in minipigs in vivo</i> .....	57
7.2.2. <i>Effects of IGF-I overexpression via rAAV/alginate-mediated gene transfer on the repair processes in minipig chondral defects over time</i> .....	58
7.2.3. <i>Effects of IGF-I overexpression via rAAV/alginate-mediated gene transfer on the inflammatory responses and perifocal OA in minipig chondral defects over time</i> .....	62
<b>7.3. TGF-<math>\beta</math> <i>ex vivo</i> study</b> .....	<b>65</b>
7.3.1. <i>Effective TGF-<math>\beta</math> overexpression via rAAV/pNaSS-grafted PCL films in human bone marrow aspirates</i> .....	65
7.3.2. <i>Effects of TGF-<math>\beta</math> overexpression via rAAV/pNaSS-grafted PCL films on the deposition of proteoglycans and type-II collagen and on cell viability in human bone marrow aspirates</i> .....	68
7.3.3. <i>Effects of TGF-<math>\beta</math> overexpression via rAAV/pNaSS-grafted PCL films on mineralization and type-X collagen deposition in human bone marrow aspirates</i> .....	69
7.3.4. <i>Effects of TGF-<math>\beta</math> overexpression via rAAV/pNaSS-grafted PCL films on the chondrogenic expression profiles in human bone marrow aspirates</i> .....	72
<b>8. DISCUSSION</b> .....	<b>74</b>
<b>8.1. SOX9 <i>in vivo</i> study</b> .....	<b>74</b>
<b>8.2. IGF-I <i>in vivo</i> study</b> .....	<b>76</b>
<b>8.3. TGF-<math>\beta</math> <i>ex vivo</i> study</b> .....	<b>78</b>
<b>8.4. Conclusions</b> .....	<b>80</b>
<b>9. REFERENCES</b> .....	<b>82</b>
<b>10. PUBLICATIONS AND PRESENTATIONS</b> .....	<b>94</b>
<b>10.1. Publications</b> .....	<b>94</b>
<b>10.2. Oral presentations</b> .....	<b>95</b>
<b>10.3. Poster presentations</b> .....	<b>95</b>
<b>11. ACKNOWLEDGEMENTS</b> .....	<b>96</b>
<b>12. CURRICULUM VITAE</b> .....	<b>97</b>

## List of Abbreviations

2D	two-dimensional
3D	three-dimensional
AAV	adeno-associated virus
ABC	avidin-biotin complex
ACAN	aggrecan
AlgPH155	alginate
$\beta$ -gal	$\beta$ -galactosidase
BMD	bone mineral density
BSA	bovine serum albumin
BS/BV	specific bone surface
BS/TV	bone surface density
BV/TV	bone volume fraction
BW	body weight
CD	cluster of differentiation
cDNA	complementary deoxyribonucleic acid
CMC	critical micellar concentration
CMV-IE	cytomegalovirus immediate-early (promoter)
COL1A1	type-I collagen (gene)
COL2A1	type-II collagen (gene)
COL10A1	type-X collagen (gene)
Ct	threshold cycle
Ct.Th	cortical thickness
CT	computed tomography
DA	degree of anisotropy
DAB	diaminobenzidine
DMEM	Dulbecco's modified Eagle's medium
DNA	deoxyribonucleic acid
DNase	deoxyribonuclease
ECM	extracellular matrix

ELISA	enzyme-linked immunosorbent assay
FD	fractal dimension
GAPDH	glyceraldehyde-3-phosphate dehydrogenase
HE	hematoxylin and eosin
HLA-DR $\alpha$	class II major histocompatibility complex antigen
HMG	high mobility group box
hMSCs	human mesenchymal stromal cells
ICRS	International Cartilage Regeneration & Joint Preservation Society
IGF-I	insulin-like growth factor I
IL-1 $\beta$	interleukin 1 beta
MBBH	maximal bone bridge height
micro-CT	micro-computed tomography
microRNA	micro-ribonucleic acid
MH	maximal height
MHD	maximal horizontal distance
MOI	multiplicity of infection
mRNA	messenger ribonucleic acid
MSCs	mesenchymal stromal cells
MTDA	maximal two-dimensional area
MVD	maximal vertical distance
MW	maximal width
n.a.	not applicable
n.s.	not significant
NIH	National Institutes of Health
OA	osteoarthritis
PBS	phosphate-buffered saline
PEO	poly(ethylene oxide)
PCL	poly( $\epsilon$ -caprolactone)
PCR	polymerase chain reaction
PGA	poly(glycolic acid)
pNaSS	poly(sodium styrene sulfonate)

PPO	poly(propylene oxide)
rAAV	recombinant adeno-associated viral vector
RNA	ribonucleic acid
RNase	ribonuclease
ROI	region of interest
RT-PCR	reverse transcriptase polymerase chain reaction
Safranin O	safranin orange/fast green
SAS	subarticular spongiosa
SBP	subchondral bone plate
SD	standard deviation
SMI	structure model index
SOX9	sex-determining region Y-type high-mobility group box 9
Tb.N	trabecular number
Tb.Pf	trabecular pattern factor
Tb.Sp	trabecular separation
Tb.Th	trabecular thickness
TNF- $\alpha$	tumor necrosis factor alpha
TGF- $\beta$	transforming growth factor beta
VOI	volume of interest

## List of Figures

<b>Figure 1.</b>	Schematic view of the osteochondral unit	9
<b>Figure 2.</b>	Structure of a normal and osteoarthritic knee joint	10
<b>Figure 3.</b>	Generation and features of rAAV gene therapy vectors	11
<b>Figure 4.</b>	Limitations to effective rAAV-mediated gene transfer <i>in vivo</i> and current strategies to circumvent such barriers	12
<b>Figure 5.</b>	Principle of scaffold-guided delivery of rAAV vectors via polymeric micelles/hydrogels	13
<b>Figure 6.</b>	Principle of scaffold-guided delivery of rAAV (TGF- $\beta$ ) vectors via pNaSS-grafted PCL films	15
<b>Figure 7.</b>	Intraoperative view of the full-thickness chondral defect creation and treatment with microfracture augmented with <i>in situ</i> gelation of the rAAV/hydrogels	22
<b>Figure 8.</b>	Treatments performed in the <i>in vivo</i> studies	23
<b>Figure 9.</b>	Design of the <i>ex vivo</i> study	24
<b>Figure 10.</b>	Measurement of defect filling and repair tissue thickness	30
<b>Figure 11.</b>	Cartilage repair in minipig chondral defects upon microfracture and application of <i>sox9</i> /hydrogel <i>versus lacZ</i> /hydrogel and free vector treatment	39
<b>Figure 12.</b>	CD3, CD11b, and HLA-DR $\alpha$ expression in minipig chondral defects upon microfracture and application of <i>sox9</i> /hydrogel <i>versus lacZ</i> /hydrogel and free vector treatment	43
<b>Figure 13.</b>	Collagen orientation in minipig chondral defects upon microfracture and application of <i>sox9</i> /hydrogel <i>versus lacZ</i> /hydrogel	45
<b>Figure 14.</b>	Quantitative analyses of collagen fiber orientation in minipig chondral defects upon microfracture and application of <i>sox9</i> /hydrogel <i>versus lacZ</i> /hydrogel	46

<b>Figure 15.</b>	Histomorphometric analyses of chondrogenesis and osteogenesis in the osteochondral unit of minipig chondral defects upon microfracture and application of <i>sox9</i> /hydrogel versus <i>lacZ</i> /hydrogel	48
<b>Figure 16.</b>	Qualitative analyses of subchondral bone changes in minipig chondral defects upon microfracture and application of <i>sox9</i> /hydrogel versus <i>lacZ</i> /hydrogel	51
<b>Figure 17.</b>	Quantitative analysis of subchondral bone changes in minipig chondral defects upon microfracture and application of <i>sox9</i> /hydrogel versus <i>lacZ</i> /hydrogel	54
<b>Figure 18.</b>	Transgene (IGF-I) expression in rAAV/AlgPH155-treated minipig chondral defects	57
<b>Figure 19.</b>	Macroscopic repair of rAAV/AlgPH155-treated minipig chondral defects	58
<b>Figure 20.</b>	Histological repair of rAAV/AlgPH155-treated minipig chondral defects	60
<b>Figure 21.</b>	Expression of ECM components in rAAV/AlgPH155-treated minipig chondral defects	62
<b>Figure 22.</b>	Histological analyses of the cartilage adjacent to rAAV/AlgPH155-treated minipig chondral defects	63
<b>Figure 23.</b>	Inflammatory responses in the repair tissue and surrounding cartilage of rAAV/AlgPH155-treated minipig chondral defects	65
<b>Figure 24.</b>	Detection of transgene (TGF- $\beta$ ) overexpression in human bone marrow aspirates treated with rAAV TGF- $\beta$ -coated PCL films	66
<b>Figure 25.</b>	Chondroreparative activities in human bone marrow aspirates treated with rAAV-TGF- $\beta$ -coated PCL films	70
<b>Figure 26.</b>	Mineralization and type-I and -X collagen deposition in human bone marrow aspirates treated with rAAV-hTGF- $\beta$ -coated PCL films	71
<b>Figure 27.</b>	Gene expression profiles in human bone marrow aspirates treated with rAAV-hTGF- $\beta$ -coated PCL films	73

## List of Tables

<b>Table 1.</b>	Chemicals used in the studies	17
<b>Table 2.</b>	Solutions and buffers used in the studies	18
<b>Table 3.</b>	Antibodies used in the studies	19
<b>Table 4.</b>	Software used in the studies	20
<b>Table 5.</b>	Instruments used for the surgeries	20
<b>Table 6.</b>	Equipment used in the studies	21
<b>Table 7.</b>	Macroscopic scoring of cartilage repair in the defects (SOX9 study)	40
<b>Table 8.</b>	Filling and thickness of the defects	41
<b>Table 9.</b>	Histological scoring of cartilage repair in the defects (SOX9 study)	41
<b>Table 10.</b>	Type-II collagen deposition and SOX9 expression in the defects	42
<b>Table 11.</b>	Analyses of CD3, CD11b, and HLA-DR $\alpha$ expression in the defects	44
<b>Table 12.</b>	Estimation of chondrogenic foci and stereological cells in the defects	49
<b>Table 13.</b>	Areas occupied by marrow cavity, mature bone, new bone, and repair tissue in ROIs of subchondral bone	52
<b>Table 14.</b>	Intralesional osteophytes in the defects	52
<b>Table 15.</b>	Subchondral bone changes in the defects	53
<b>Table 16.</b>	Micro-CT parameters of the subchondral bone plate and subarticular spongiosa in the defects	56
<b>Table 17.</b>	Macroscopic scoring of cartilage repair in the defects (IGF-I study)	58
<b>Table 18.</b>	Histological scoring of cartilage repair in the defects (IGF-I study)	61
<b>Table 19.</b>	Cell densities and type-II/-I collagen deposition in the defects	61
<b>Table 20.</b>	OA signs in the cartilage adjacent to the defects	64
<b>Table 21.</b>	Histomorphometric and biological analyses in human bone marrow aspirates treated with rAAV-coated PCL films	67
<b>Table 22.</b>	Transgene (TGF- $\beta$ ) expression in human bone marrow aspirates treated with rAAV-coated PCL films	68

# 1. ABSTRACT

Adult articular cartilage, a highly specialized connective tissue, does not regenerate upon injury. Articular cartilage defects may further initiate the development of osteoarthritis (OA), a clinically and socioeconomically debilitating joint disorder. Gene transfer of growth and transcription factors is a therapeutic strategy to improve the repair of articular cartilage defects. Advanced biomaterial-guided delivery of gene carriers such as those based on the clinically adapted recombinant adeno-associated virus (rAAV) vector is an exceptionally attractive treatment protocol to improve cartilage repair via minimally invasive, controlled delivery of therapeutic genes in a spatiotemporally precise manner, reducing intra-articular vector spread and a possible loss of the therapeutic gene product.

Here, a thermosensitive hydrogel based on poly(ethylene oxide) and poly(propylene oxide) was first used to release an rAAV vector coding for the chondrogenic sex-determining region Y-type high-mobility group box 9 (SOX9) transcription factor in clinically relevant, full-thickness chondral defects in minipigs to evaluate its potential beneficial effects on cartilage repair *in vivo*. Delivery of a therapeutic rAAV construct coding for the reparative insulin-like growth factor I (IGF-I) via an alginate (AlgPH155) hydrogel was also tested in similar minipig chondral defects to further evidence workable approaches to enhance cartilage repair *in vivo*. As an alternative to hydrogel systems, a focus was also given to rAAV-mediated delivery of the chondrogenic transforming growth factor beta (TGF- $\beta$ ) using solid poly( $\epsilon$ -caprolactone) (PCL) films to test the ability of this system to trigger chondroreparative processes in human bone marrow aspirates *ex vivo* as future implantable platforms in cartilage defects.

Effective release of the rAAV SOX9 and IGF-I vectors using thermosensitive or alginate hydrogels, respectively, improved cartilage repair for at least 4 weeks (SOX9) and one year (IGF-I), with a reduction of perifocal OA when using IGF-I over a longer period of time. Effective release of the rAAV TGF- $\beta$  vector using PCL films (especially those grafted with poly(sodium styrene sulfonate) - pNaSS) activated the chondrogenic differentiation of human bone marrow aspirates for at least 3 weeks.

These data support the concept of applying biomaterial-guided rAAV gene delivery as an off-the-shelf, minimally invasive option for cartilage repair in translational applications.

## 2. ZUSAMMENFASSUNG

Der adulte hyaline Gelenkknorpel, ein hochspezialisiertes Bindegewebe, regeneriert nicht nach einer Verletzung. Knorpeldefekte können zudem die Entstehung der klinisch und sozioökonomisch folgenschweren Arthrose einleiten. Die biomaterialgesteuerte Abgabe von Genvektoren, die auf klinisch adaptierten rekombinanten adeno-assoziierten viralen (rAAV) Vektoren basieren, ist eine attraktive Strategie zur Verbesserung der Knorpelreparatur durch eine minimalinvasive und kontrollierte Abgabe therapeutischer Gene in zeitlich und räumlich präziser Weise, welche eine intraartikuläre Vektorausbreitung und möglichen Verlust des therapeutischen Genprodukts reduziert.

Die vorliegende Arbeit verwendete ein thermosensitives Hydrogel auf Basis von Polyethylenoxid und Polypropylenoxid, um einen rAAV-Vektor, der für das Gen des chondrogenen Transkriptionsfaktors SOX9 (geschlechtsbestimmende Region Y-Typ-Hochmobilitätsgruppenbox 9) kodiert, in vollschichtige chondrale Defekte in Mischschweinen freizusetzen, um seinen Effekt auf die Knorpelreparatur *in vivo* zu analysieren. Zudem wurde die Abgabe eines therapeutischen rAAV-Konstrukts, das für den insulinartigen Wachstumsfaktor I (IGF-I) kodiert, über ein Alginate (AlgPH155)-Hydrogel im gleichen Tiermodell als weiterer Ansatz zur Verbesserung der Knorpelreparatur *in vivo* getestet. Als Alternative zu Hydrogelsystemen wurde ein zusätzlicher Schwerpunkt auf die rAAV-vermittelte Abgabe des transformierenden Wachstumsfaktors  $\beta$  (TGF- $\beta$ ) unter Verwendung fester Poly( $\epsilon$ -Caprolacton) (PCL)-Filme gelegt, um die Fähigkeit dieses Systems zu überprüfen, chondroreparative Prozesse in humanen Knochenmarkaspiraten *ex vivo* als zukünftige implantierbare Plattformen in Knorpeldefekte zu initiieren.

Die Ergebnisse zeigen, daß die effektive Freisetzung der rAAV-SOX9- und IGF-I-Vektoren durch thermosensitive bzw. Alginate-Hydrogele die Knorpelreparatur für mindestens 4 Wochen (SOX9) bzw. ein Jahr (IGF-I) signifikant verbesserte. Zudem führt IGF-I zu gleichzeitiger signifikanter Verringerung der perifokalen Arthrose über einen längeren Zeitraum. Die wirksame Freisetzung des rAAV-TGF- $\beta$ -Vektors unter Verwendung von PCL-Filmen (insbesondere wenn mit Polynatriumstyrolsulfonat - pNaSS liiert) aktivierte die chondrogene Differenzierung humaner Knochenmarkaspirate für mindestens 3 Wochen.

Diese Daten unterstützen das Konzept einer Anwendung von biomaterialgesteuerter rAAV-Genabgabe als vielversprechende minimalinvasive Option für die klinische Knorpelreparatur.

### 3. INTRODUCTION

Articular cartilage, the highly specialized connective tissue of diarthrodial joints, providing a smooth lubricated surface for articulation and facilitating the transmission of loads in a low frictional manner (**Figure 1**) (Sophia Fox et al., 2009).

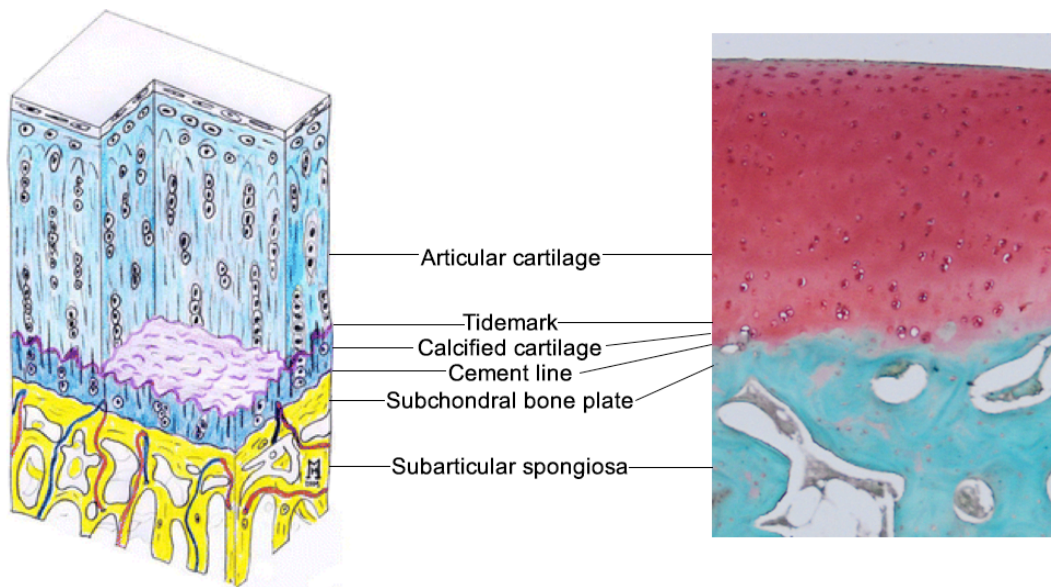


**Figure 1.** Schematic view of the osteochondral unit (source: Madry et al., 2010).

Knee osteochondral defects are focal areas with injuries involving both the superficial cartilage and underlying subchondral bone, which are difficult to treat and cause considerable musculoskeletal morbidity with significant economic and social implications (Gomoll et al., 2010). Articular cartilage lesions (focal defects), especially those affecting the knee joint, as in acute trauma or osteoarthritis (OA) (Guermazi et al., 2017) (**Figure 2**), remain a major unsolved clinical problem due to the extremely limited self-renewal capacity of this highly specialized tissue with neither innervated nor vascularized (Kwon et al., 2019; Medvedeva et al., 2018; O'Driscoll, 1998; Orth et al., 2014).

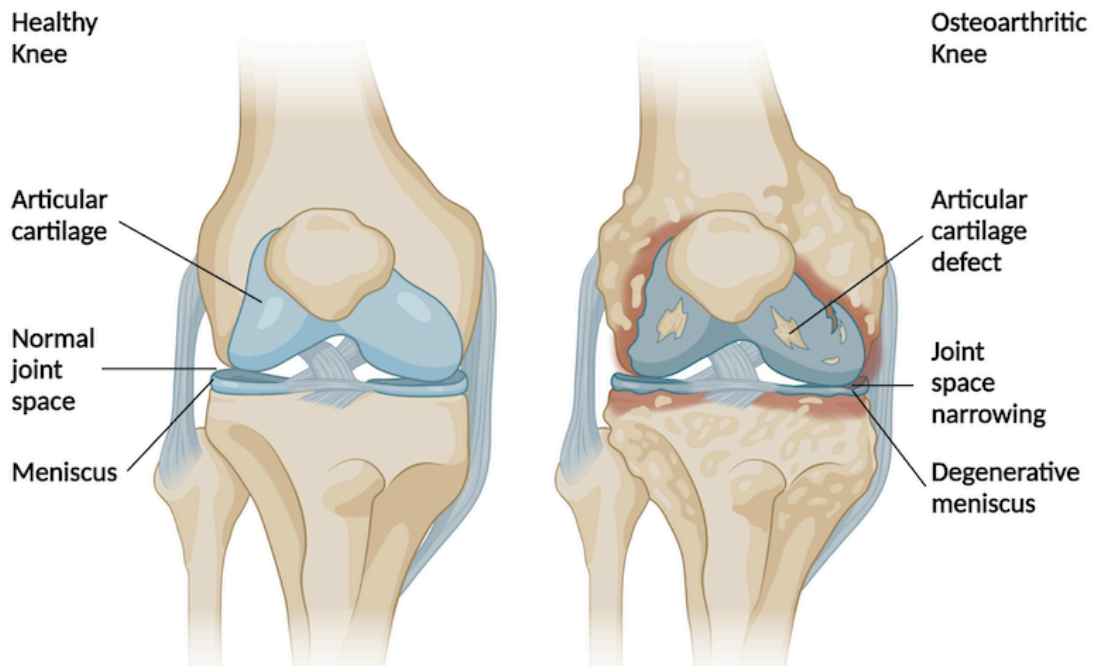


**Figure 2.** Structure of a normal and osteoarthritic knee joint (created with BioRender.com).

Most research efforts currently focus on the restoration of cartilage lesions in connection with trauma or OA. The current area of cartilage repair is multidimensional, and some of the out-of-date views have been reevaluated with state-of-the-art technology now accessible (Grande et al., 2013). The use of essential science tools including cells, genes, and biomaterials combining different approaches as 3D printing of engineered constructs efficiently differentiated chondrocytes, proper lubrication, and approaches affecting the pro-inflammatory milieu might open new avenues of clinically adapted research in articular cartilage repair (Cucchiari et al., 2015; Fahy et al., 2015; Visser et al., 2013).

The concept of gene therapy for cartilage repair originates from the idea of transferring genes encoding therapeutic factors in cartilage defects, resulting in a temporarily and spatially defined delivery of therapeutic molecules within sites of injury (Madry et al., 2011). Current vectors include nonviral systems (naked deoxyribonucleic acid - DNA, physical/chemical methods) and viral (adenoviral, herpes simplex viral, retroviral, lentiviral, recombinant adeno-associated viral - rAAV) vehicles, with rAAV (**Figure 3**) being well-suited carriers for durable treatments for cartilage lesions

(Cucchiarini et al., 2015; Rey-Rico et al., 2018). SOX9, a member of the sex-determining region Y-type (SRY) high mobility group box (HMG) family of DNA binding proteins, plays a crucial role in cartilage formation, offering a strong candidate for gene therapy for cartilage repair (Tao et al., 2016b, 2017), similarly to the chondroreparative insulin-like growth factor I (IGF-I) and transforming growth factor beta (TGF- $\beta$ ) (**Figure 3**) (Cucchiarini et al., 2015, 2018; Cucchiarini, Madry, 2014; Nixon et al., 1999).

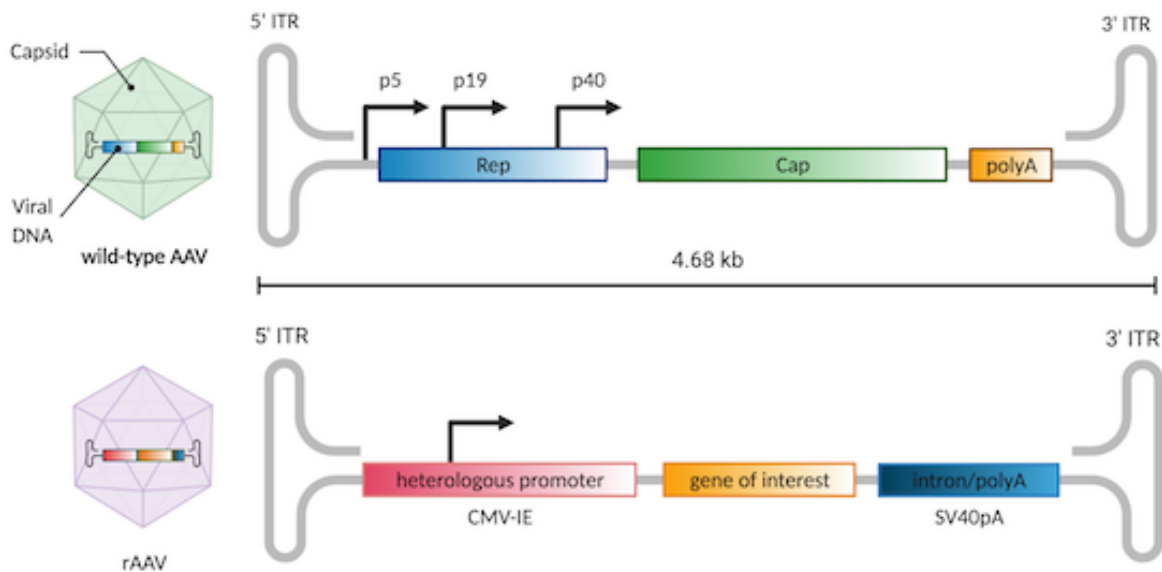


**Figure 3.** Generation and features of rAAV gene therapy vectors. The figure shows classical rAAV vectors with the genes of interest employed in the studies (e.g., SOX9, IGF-I, and TGF- $\beta$ ) (created with BioRender.com).

Still, a direct application of vectors *in vivo* may be limited by a possible degradation of the vectors, their dissemination to nontarget sites like upon systemic injection, and most importantly by their neutralization by immune (humoral) responses and by cellular barriers, all potentially impairing their processing and therapeutic actions (**Figure 4**) (Cucchiarini, Madry, 2019; Madry et al., 2020b; Venkatesan et al., 2018). A number of actions have been taken to address these issues (use of alternative routes of administration, transient host immunosuppression, injection of higher vector doses, manipulation of alternative AAV serotypes different from the classically employed AAV-2, use of capsid decoys, capsid modification, use of self-complementary AAV that bypass

intracellular rate-limiting steps of AAV processing retarding transgene expression like the transition from single-stranded to double-stranded viral DNA, etc) (**Figure 4**) (Cucchiarini, Madry, 2019; Madry et al., 2020b; Venkatesan et al., 2018), but their application in human gene therapy protocols *in vivo* is complex and relatively invasive. In this regard, the administration of vectors via biocompatible materials allowing for a vector controlled release is a novel, promising approach to circumvent such hurdles and afford effective gene transfer in the musculoskeletal system (Cucchiarini, Madry, 2019; Madry et al., 2020b; Venkatesan et al., 2018).

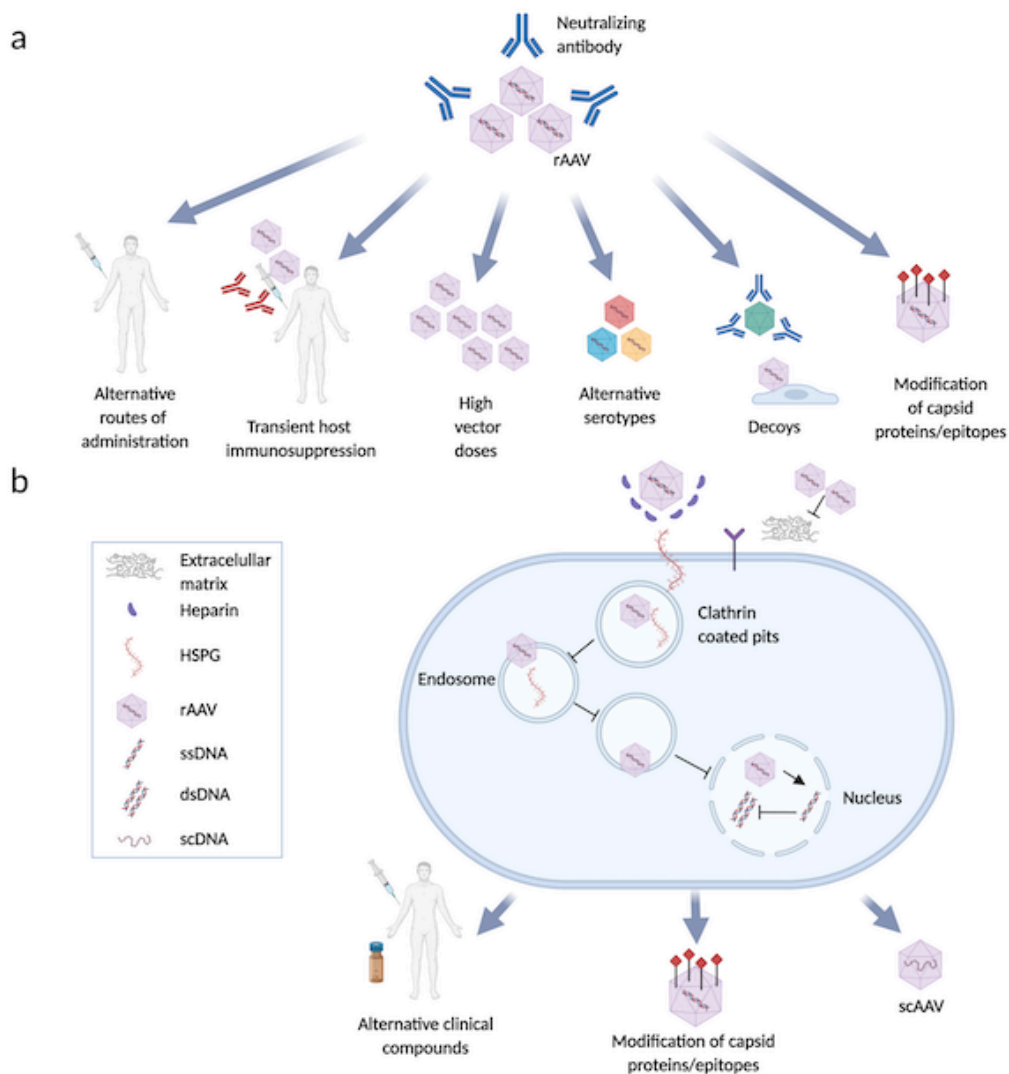


**Figure 4.** Limitations to effective rAAV-mediated gene transfer *in vivo* and current strategies to circumvent such barriers. (a) Pre-existing humoral immunity and (b) cellular barriers (created with BioRender.com).

### 3.1. Scaffold-guided delivery of rAAV via polymeric micelles/hydrogels

Delivery of rAAV via polymeric micelles/hydrogels can increase both their stability and bioactivity while overcoming the barriers that preclude effective gene transfer (Rey-Rico et al., 2017; Tao et al., 2016b, 2017). PEO-PPO-PEO copolymers are nonionic triblock copolymers based on hydrophilic poly(ethylene oxide) (PEO) and hydrophobic poly(propylene oxide) (PPO) (**Figure 5a**). They are self-assembling and temperature-sensitive, i.e., at concentrations higher than the critical micellar concentration (CMC), the individual block copolymers can self-assemble in micelles. By increasing their temperature and concentration, the micelles can form 3D networks (gels) with high viscosity (Oh et al., 2004), displaying a sol-gel transition around 37°C that enables a minimally invasive *in vivo* injection as an attractive approach to treat cartilage defects *in vivo* (**Figure 5b**).

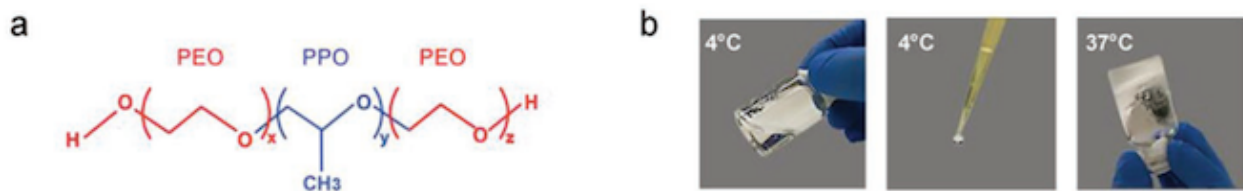


**Figure 5.** Principle of scaffold-guided delivery of rAAV via polymeric micelles/hydrogels. (a) Structure of the PEO-PPO-PEO (PF127) block copolymer. (b) Thermosensitive characteristics of the copolymer (liquid form at 4°C, solid form at 37°C) (source: Madry\*, Gao\* et al., 2020a).

Controlled release of rAAV from PEO-PPO-PEO micelles/hydrogels can enhance both rAAV vector stability and bioactivity and offer protection against viral vector immune neutralization (Alvarez-Lorenzo et al., 2011; Rey-Rico et al., 2018). We showed that delivery of rAAV vectors carrying a reporter (*lacZ*) gene or a sequence coding for the potent transcription factor SOX9 in PEO-PPO-PEO micelles led to higher levels of transgene (*lacZ*, SOX9) expression relative to free vector treatments in human OA chondrocytes, in human bone marrow-derived mesenchymal stromal cells (hMSCs), and in a human model of osteochondral defect, allowing for an improved chondrocyte

phenotype, enhanced MSC chondrogenesis, and improved cartilage repair, respectively (Díaz-Rodríguez et al., 2015; Rey-Rico, Cucchiarini, 2018; Rey-Rico et al., 2016a, 2017, 2018). However thus far, there is no report on the therapeutic potential of rAAV-mediated overexpression of chondroreparative SOX9 via thermosensitive PEO-PPO-PEO hydrogel-guided gene therapy to repair cartilage defects *in vivo*. Therefore, we study the effects of injecting a thermosensitive hydrogel based on PEO-PPO-PEO poloxamers for the *in situ* release of an rAAV encoding for chondrogenic SOX9 transcription factor on the repair of full-thickness chondral defects in a clinically relevant animal model *in vivo*.

While nanoparticles have been successfully employed to nonvirally deliver plasmidic IGF-I and micro-ribonucleic acids (microRNAs) in models of cartilage lesions *in vivo* (Zhao et al., 2019), hydrogels are also well adapted for translational applications in cartilage repair (Rey-Rico et al., 2016b; Vega et al., 2017) as they may be derived from or composed of structural compounds similar to those present in the extracellular matrix (ECM) of the cartilage (Vega et al., 2017) and can be conveniently delivered using direct injections or minimally invasive arthroscopic interventions (Cucchiarini, Madry, 2019; McCarty et al., 2011; Moreira Teixeira et al., 2012). Application of rAAV via hydrogels (e.g., fibrin, alginate, self-assembling peptides, polypseudorotaxanes, and poloxamers/poloxamines) has been a potent approach to deliver rAAV in a controlled manner in musculoskeletal targets for cartilage repair (Lee et al., 2011; Madry et al., 2020a; Rey-Rico et al., 2015b, 2017). We previously developed hydrogels based on the highly biocompatible alginate (AlgPH155) compound that is widely used in the pharmaceutical technology field as a tool to release rAAV vectors for the genetic modification of hMSCs (Díaz-Rodríguez et al., 2015). However thus far, there is no report on the therapeutic potential of rAAV-mediated overexpression of chondroreparative IGF-I via AlgPH155-guided gene therapy to repair cartilage defects *in vivo*. The goal of the present study is to examine whether a therapeutic rAAV/AlgPH155 hydrogel system may improve cartilage repair and reduce OA development in the long-term in a clinically relevant setting in a large animal.

### 3.2. Scaffold-guided delivery of rAAV via solid scaffolds

Scaffold-guided gene therapy emerged as a promising tool to enhance translational cartilage repair by supporting the controlled delivery of therapeutic gene vectors for prolonged, safe expression of gene-based products in cartilage defects (Cucchiarini, Madry, 2019; Kelly et al., 2019). Moreover, scaffold-guided rAAV gene therapy has the potential to protect the rAAV capsid proteins from neutralization by host immune responses (Cottard et al., 2004) that may prevent direct rAAV therapy in patients (Cucchiarini, Madry, 2019). rAAV vectors have been utilized for experimental cartilage research upon release from solid scaffolds (poly( $\epsilon$ -caprolactone) - PCL) (Venkatesan et al., 2020a, 2020b). Solid materials such as PCL display a number of features that are critical for cartilage repair strategies as they offer biocompatible, solid, and mechanically stable scaffolding systems to support cell viability, activation, and targeting with rAAV (Leroux et al., 2019; Moutos, Guilak, 2010; Rohman et al., 2015; Venkatesan et al., 2018) especially when further grafted with poly(sodium styrene sulfonate) (pNaSS), a compound that upholds reparative biological responses in musculoskeletal cells (Leroux et al., 2019; Rohman et al., 2015; Venkatesan et al., 2020a, 2020b). We previously provided evidence of the potential of pNaSS-grafted PCL films as an efficient rAAV gene controlled release system to safely modify chondroreparative human bone marrow aspirates (Venkatesan et al., 2020a). In the current study, we focus on the therapeutic potential of rAAV-mediated overexpression of chondroreparative TGF- $\beta$  via PCL-guided gene therapy to enhance the chondrogenic processes in such aspirates as future implantable reparative platforms in cartilage defects (**Figure 6**).

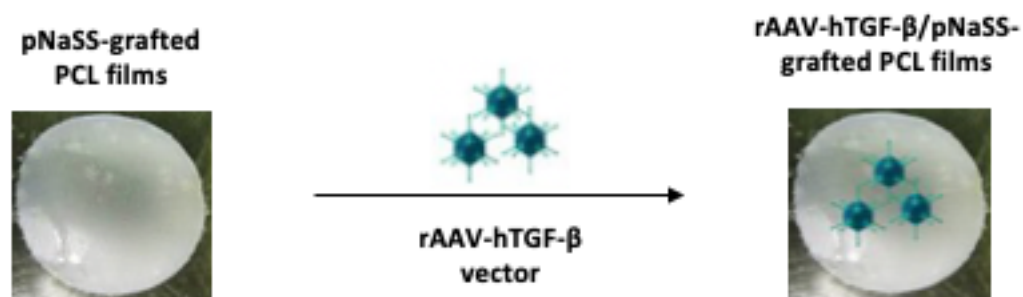


**Figure 6.** Principle of scaffold-guided delivery of rAAV (TGF- $\beta$ ) vectors via pNaSS-grafted PCL films.

## 4. HYPOTHESES

In the present study, we tested the following three hypotheses:

- (1) a thermosensitive PEO-PPO-PEO hydrogel (PF127) can efficiently transfer and overexpress the rAAV SOX9 vector as a means to heal chondral defects *in vivo*,
- (2) an alginate hydrogel can efficiently transfer and overexpress the rAAV IGF-I vector as a means to heal chondral defects *in vivo*, and
- (3) PCL films can efficiently transfer and overexpress the rAAV TGF- $\beta$  vector as a means to enhance the chondrogenic potential of human bone marrow aspirates *ex vivo* as possible material for future transplantation in cartilage defects.

## 5. MATERIALS

### 5.1. Chemicals

**Table 1.** Chemicals used in the studies

<b>Product</b>	<b>Manufacturer</b>
1 <sup>st</sup> Strand cDNA Synthesis kit	Roche Applied Science
4-styrenesulfonic acid sodium salt hydrate (NaSS)	Sigma-Aldrich, Munich, Germany
AAVanced Concentration Reagent	System Bioscience, Heidelberg, Germany
AAV Titration ELISA	Progen, Heidelberg, Germany
ABC-Reagent (Avidin-Biotin-Peroxidase-Reagent)	Vector, Burlingame, California, USA
Alginate (AlgPH155)	Copenhagen, Denmark
Atropine	B. Braun, Melsungen, Germany
BSA (bovine serum albumin)	Sigma, Taufkirchen, Germany
Cell Proliferation Reagent WST-1	Roche Applied Science, Mannheim, Germany
DAB reagent	Vector, Burlingame, California, USA
Eosin G	Roth, Karlsruhe, Germany
Fast Green	ICN Biomedicals, Eschwege, Germany
Fibrinogen/thrombin	Baxter, Volketswil, Switzerland
Formalin stock solution (37%)	Sigma, Taufkirchen, Germany
Hematoxylin	Roth, Karlsruhe, Germany
Hydrogen peroxide	Sigma, Taufkirchen, Germany
Isoflurane	Baxter, Unterschleißheim, Germany
IGF-I Quantikine ELISA	R&D Systems, Wiesbaden, Germany
Ketamine	Ketanest S, Pfizer, Berlin, Germany
Pluronic® F127	BASF, Ludwigshafen, Germany
Pierce Thermo Scientific Protein Assay	Thermo Fisher Scientific, Schwerte, Germany
Propofol	AstraZeneca, Wedel, Germany
RNeasy Protect Mini Kit	Qiagen, Hilden, Germany
RNase-Free DNase Set	Qiagen, Hilden, Germany
Sterile saline	Ecotainer, B. Braun, Melsungen, Germany
Safranin Orange	Roth, Karlsruhe, Germany
TGF- $\beta$ Quantikine ELISA	R&D Systems, Mannheim, Germany

Xylazine	Rompun, Bayer, Leverkusen, Germany
Xylene	Fischer, Saarbrücken, Germany

## 5.2. Solutions and buffers

**Table 2.** Solutions and buffers used in the studies

Solution, Buffer	Ingredient	Weight or volume
Blocking buffer	BSA	6 ml
	PBS	200 ml
DAB solution	H <sub>2</sub> O	5 ml
	Buffer (pH 7.5)	2 drops
	DAB substrate reagent	4 drops
	H <sub>2</sub> O <sub>2</sub>	2 drops
Decalcifying solution	Natrium citrate	100 g
	Formic acid (90%)	250 ml
	H <sub>2</sub> O	ad 750 ml
Eosin solution	Eosin G	10 g
	H <sub>2</sub> O	ad 2,000 ml
	KH <sub>2</sub> PO <sub>4</sub>	9.07 g
	Na <sub>2</sub> HPO <sub>4</sub>	11.86 g
Fast green solution	Fast green	200 mg
	H <sub>2</sub> O	ad 1,000 ml
Formalin solution (pH 7.4)	Formalin stock solution	140 ml
	H <sub>2</sub> O	ad 1,000 ml
Hematoxylin solution (according to Harris)	Hematoxylin	10 g
	Ethanol (100%)	120 ml
	Sodium iodate	10 g
	ALKSO <sub>4</sub>	200 g
	H <sub>2</sub> O	ad 2,000 ml
Hydrogen peroxide solution (0.3%)	H <sub>2</sub> O <sub>2</sub>	0.6 ml
	H <sub>2</sub> O	200 ml
PBS	KCl (pH 7.2)	2.7 mM
	K <sub>2</sub> HPO <sub>4</sub>	1.7 mM

	NaCl	136 mM
	Na <sub>2</sub> HPO <sub>4</sub> ·7H <sub>2</sub> O	10 mM
Safranin orange solution	Safranin orange	1 g
	H <sub>2</sub> O	ad 1,000 ml
Trypsin solution (0.1%)	Trypsin stock solution (25%)	800 µl
	PBS	ad 200 ml
Trypsin stock solution	Trypsin	25% (v/v)
	PBS	75% (v/v)

### 5.3. Antibodies

**Table 3.** Antibodies used in the studies

Antibody	Manufacturer
Anti-CD3 (PC3/188A)	Santa Cruz Biotechnology, Heidelberg, Germany
Anti-CD11b (Ly-40)	Acris, Hiddenhausen, Germany
Anti-HLA-DR $\alpha$ (TAL-1B5)	Dako, Agilent, Waldbronn, Germany
Anti-IGF-I (NBP2-16929)	Novus Biologicals, Centennial, CO, USA
Anti-IL-1 $\beta$ (3553)	Novus Biologicals, Centennial, CO, USA
Anti-SOX9 (C-20)	Santa Cruz Biotechnology, Heidelberg, Germany
Anti-TGF- $\beta$ (V)	Santa Cruz Biotechnology, Heidelberg, Germany
Anti-TNF- $\alpha$ (abx069528)	Abxexa, Cambridge, UK
Anti-type-I collagen	Acris, Hiddenhausen, Germany
Anti-type-II collagen	Acris, Hiddenhausen, Germany
Anti-type-X collagen	Sigma-Aldrich, Munich, Germany
Biotinylated secondary antibodies	Vector Laboratories, Alexis Deutschland GmbH, Grünberg, Germany

## 5.4. Software

**Table 4.** Software used in the studies

Software	Company
Adobe Photoshop	Adobe Systems, Unterschleissheim, Germany
CTAnalyzer	Bruker Skyscan, Kontich, Belgium
ImageJ	National Institutes Health, Maryland, USA
Microsoft Excel	Microsoft, Redmond, Washington, USA
SIS analySIS	Olympus Soft Imaging System GmbH, Münster, Germany
SPSS	IBM SPSS 20; SPSS Inc., Chicago, Illinois, USA
BioRender	BioRender, Toronto, Ontario, Canada

## 5.5. Instrumentation

**Table 5.** Instruments used for the surgeries

Instrument	Manufacturer
Antiseptic spray	Aluminium-Spray, Albrecht, Aulendorf, Germany
Biopsy punch	Kai Europe, Solingen, Germany
Collier-Anderson forceps	Aesculap, Tuttlingen, Germany
De Bakey-Collier forceps	Aesculap, Tuttlingen, Germany
De Bakey needle forceps	Aesculap, Tuttlingen, Germany
Disposable electrode handle	Erbe, Tübingen, Germany
Electric hair shaver	Electra II, Aesculap, Tuttlingen, Germany
High-frequency generator	Erbotom ICC 350, Erbe, Tübingen, Germany
Microfracture awl	Aesculap, Tuttlingen, Germany
Micropipette (20 µl)	Eppendorf, Hamburg, Germany
Mixer forceps	Aesculap, Tuttlingen, Germany
Nelson Metzenbaum scissors	Aesculap, Tuttlingen, Germany
Pipette tips (100 µl)	Eppendorf, Hamburg, Germany
Polypropylene sutures	Prolene, Ethicon, Somerville, New Jersey, USA
Retractor	Aesculap, Tuttlingen, Germany
Ring curette	Aesculap, Tuttlingen, Germany

Scalpel blade (#15)	KLS Martin, Tuttlingen, Germany
Skin disinfectant (polyvidon-iodine, propan-1-ol solution)	Braunoderm, B. Braun, Melsungen, Germany
Skin punch	Kai Europe, Solingen, Germany
Sterile drape (75 x 90 cm)	Foliodrape, Paul Hartmann AG, Heidenheim, Germany
Sterile drape (50 x 60 cm)	Secu-Drape, Sengewald, Germany
Sterile drape (75 x 75 cm)	Raucodrape, Lohmann & Rauscher, Rengsdorf, Germany
Syringe (20 ml)	Braun-Inject, B. Braun, Melsungen, Germany
TC Mayo scissors	Aesculap, Tuttlingen, Germany
TC Mayo Masson needle holder	Aesculap, Tuttlingen, Germany

## 5.6. Equipment

**Table 6.** Equipment used in the studies

Equipment	Manufacturer
Autoclave AMA-240	Astell, Sidcup, England
Digital Camera CC-12 (on Microscope BX-45)	Soft Imaging System, Münster, Germany
Embedding Machine EG 1140-C	Leica, Nussloch, Germany
GENios microplate reader	TECAN, Crailsheim, Germany
Heat plate HI 1220	Leica, Nussloch, Germany
Incubator CB 150 (37°C)	Binder, Tuttlingen, Germany
Magnetic stirrer RH basic 2	IKA, Staufen, Germany
Microfocus X-ray scanner Skyscan 1172	Skyscan, Kontich, Belgium
Microscope BX-45	Olympus, Hamburg, Germany
Microscope CK-2	Olympus, Hamburg, Germany
Mx3000P QPCR system	Stratagene, Agilent Technologies, Waldbronn, Germany
Refrigerator -20°C	Bosch, Gerlingen-Schillerhöhe, Germany
Refrigerator -74°C Platinum 550	Angelantoni Industrie, Massa Martana PG, Italy
Rotational microtome RM 2135	Leica, Nussloch, Germany
SPIN150-v3 SPS	Stratagene, Agilent Technologies, Waldbronn, Germany
Water-bath HI 1210	Leica, Nussloch, Germany

## 6. METHODS

### 6.1. Study design

For the SOX9 *in vivo* study, adult minipigs received full-thickness circular chondral defects in a standardized fashion (4-mm diameter) in the trochlear groove of both stifle joints. The defects were treated with three microfracture holes at identical distances from each other (awl diameter, 1.0 mm) (**Figures 7 and 8**). PF127 hydrogels carrying the candidate rAAV-FLAG-hsox9 vector (a construct carrying a FLAG-tagged human *sox9* complementary DNA (cDNA) that allows to discriminate the *sox9* transgene from the endogenous *sox9* gene) *versus* control rAAV-*lacZ* vectors and promoting rAAV controlled release were injected in the defects (**Figures 7 and 8**). For the IGF-I *in vivo* study, adult minipigs received full-thickness circular chondral defects in a standardized fashion (4-mm diameter) in the weight-bearing area of the distal lateral femoral trochlea groove of each joint. The defects were treated with three uniform microfracture holes (1.2-mm diameter, 5 mm-depth) (**Figures 7 and 8**). AlgPH155 hydrogels carrying the candidate rAAV-hIGF-I vector (a construct carrying a human IGF-I cDNA) *versus* control rAAV-*lacZ* vectors and promoting rAAV controlled release were implanted in the defects (**Figures 7 and 8**).

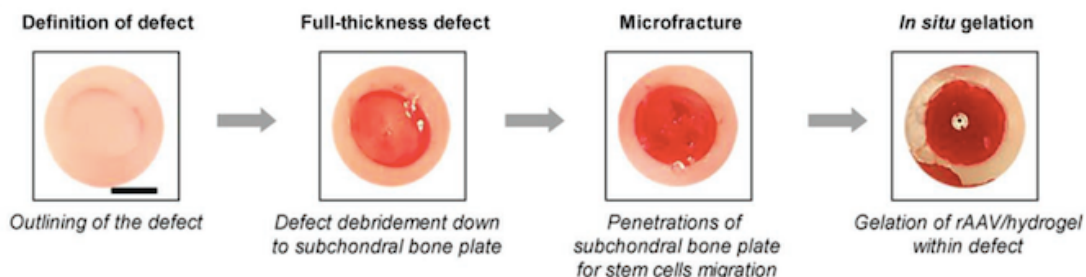


**Figure 7.** Intraoperative view of the full-thickness chondral defect creation and treatment with microfracture augmented with *in situ* gelation of the rAAV/hydrogels. The defects were outlined in the superior region of the lateral trochlear facets of both knees with a biopsy punch and debrided down to the subchondral bone plate after removal of the calcified cartilage layer. Three microfracture holes were always introduced per defect in a standardized manner and the PEO-PPO-PEO systems with rAAV-FLAG-hsox9 *versus* rAAV-*lacZ* or the AlgPH155 hydrogels with rAAV-hIGF-I *versus* rAAV-*lacZ* were applied to the defects, allowing for *in situ* gelation (source: Madry\*, Gao\* et al., 2020a).

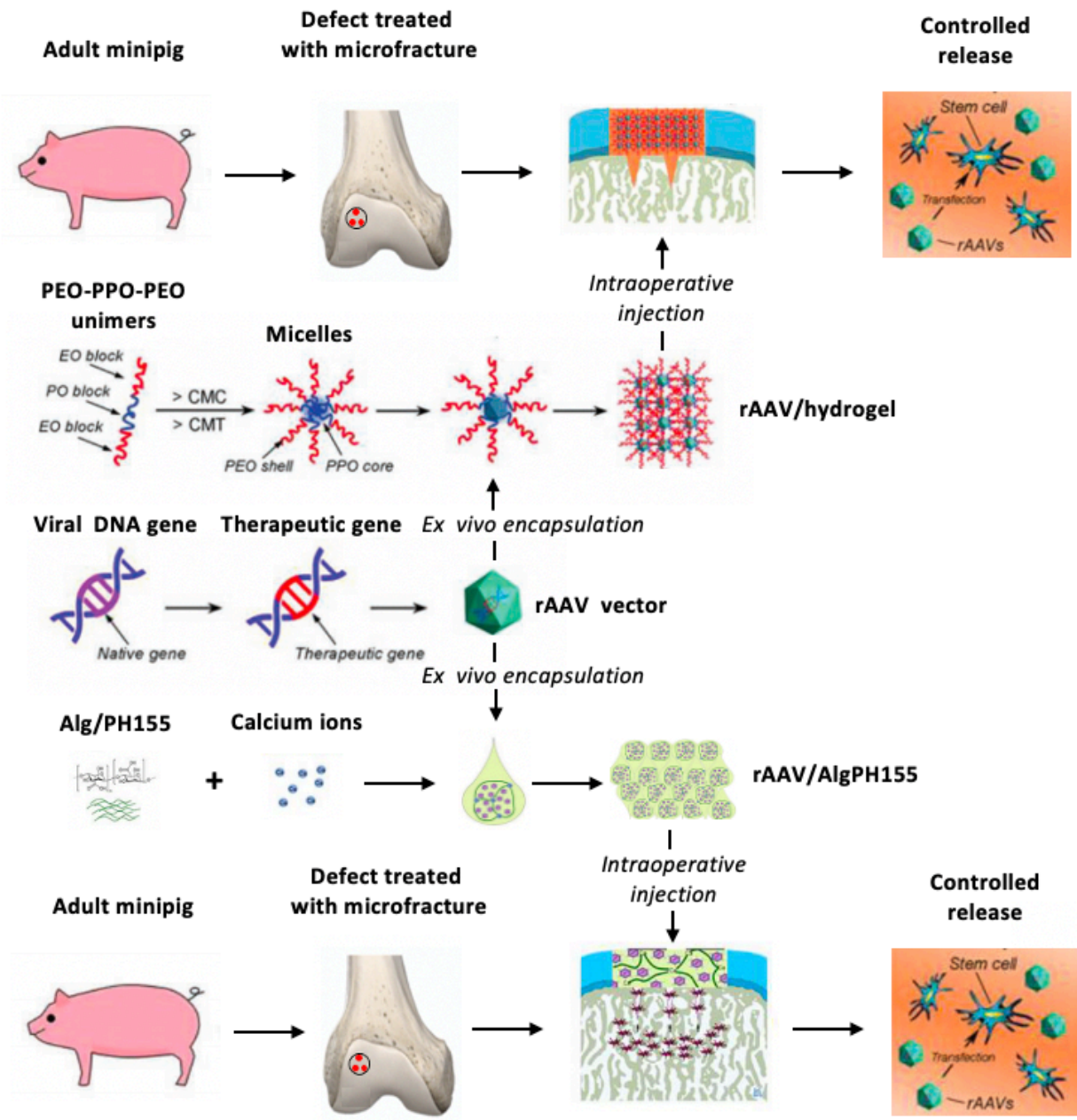


**Figure 8.** Treatments performed in the *in vivo* studies (source: Madry\*, Gao\* et al., 2020a).

For the TGF- $\beta$  *ex vivo* study, human bone marrow aspirates were incubated with pNaSS-grafted (*versus* ungrafted) PCL films carrying the candidate rAAV-hTGF- $\beta$  vector (a construct carrying a human TGF- $\beta$  cDNA) *versus* lack of vector treatment and promoting rAAV controlled release (**Figure 9**).

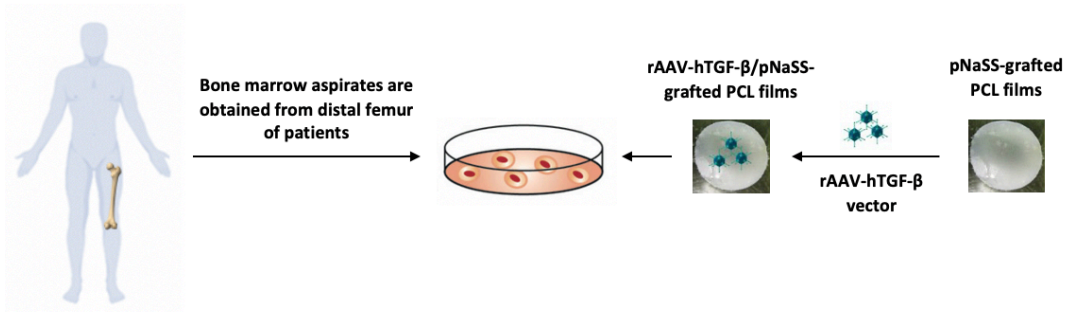


**Figure 9.** Design of the *ex vivo* study.

## 6.2. SOX9 and IGF-I *in vivo* studies

### 6.2.1. Plasmids and rAAV vectors

The vectors were all derived from pSSV9, an AAV-2 genomic clone (Samulski et al., 1987, 1989). rAAV-FLAG-hsox9 carries a FLAG-tagged human sox9 cDNA (Cucchiariini et al., 2007; Tao et al., 2017; Venkatesan et al., 2012, 2020a), rAAV-hIGF-I a human IGF-I cDNA (Cucchiariini et al., 2007), and rAAV-*lacZ* the *lacZ* gene encoding *E. coli*  $\beta$ -galactosidase ( $\beta$ -gal) (Frisch et al., 2014a; Rey-Rico et al., 2015a, 2017). All vectors contained the cytomegalovirus immediate-early (CMV-IE) promoter.

The vectors were produced as conventional (not self-complementary) vectors by using a helper-free, two-plasmid transfection system in 293 cells with the packaging plasmid pXX2 and the adenovirus helper plasmid pXX6 (Rey-Rico et al., 2017).

The vector preparations were purified by dialysis and titrated by real-time polymerase chain reaction (PCR) (Frisch et al., 2014a; Rey-Rico et al., 2015a, 2017), showing an average of  $10^{10}$  transgene copies/ml (1/500 functional recombinant viral particles).

### *6.2.2. Preparation of the rAAV/scaffold systems*

PF127 (BASF, Ludwigshafen, Germany) was used to prepare a thermosensitive hydrogel (24% w/v, > CMC) by dissolution in 10% sucrose at 4°C and incubation with rAAV on ice for 30 minutes prior to use, with sol-gel transition at 37°C (Rey-Rico et al., 2015a, 2016a).

Alginate (AlgPH155) (Copenhagen, Denmark) was employed to prepare hydrogels. The rAAV-loaded capsules were prepared by directly mixing the alginate solution with the rAAV vector dispersions with subsequent crosslinking in calcium chloride at room temperature in a 2-ml tube using a syringe with a stainless steel 21-gauge needle to generate the rAAV/alginate hydrogel systems (Díaz-Rodríguez et al., 2015).

### *6.2.3. Evaluation of rAAV controlled release efficacy from the rAAV/scaffold systems*

Copolymer solutions containing rAAV-*lacZ* (30 µl with polymer concentration 16% w/v and  $0.25 \times 10^9$  transgene copies) were added to the upper chamber of a permeable support device (Transwell Permeable Supports, Life Technologies, Darmstadt, Germany; pore size: 0.4 µm) in 96-well plates containing DMEM (600 µl in the lower chamber). DMEM (70 µl) was then added to the upper chamber to achieve the final polymer concentration 2% w/v with  $0.25 \times 10^9$  transgene copies. Plates were incubated at 37°C for 10 days with an oscillating agitation (50 osc/min). Aliquots of the conditioned medium were collected and immediately frozen at -20°C at the denoted time points in the lower chamber to assess the copolymer-delivered rAAV-*lacZ* diffusion. Diffusion of free rAAV-*lacZ* without polymer was quantified under similar conditions and used as the control. Viral particle concentrations within the culture medium were evaluated with the AAV Titration enzyme-linked immunosorbent assay (ELISA) (Rey-Rico et al., 2015b).

### *6.2.4. Surgeries*

All animal experiments were conducted in agreement with the national legislation on protection of animals and the National Institutes of Health (NIH) Guidelines for the Care and Use of Laboratory Animals (NIH Publication 85-23, Rev 1985) and were approved by the Saarland University Animal Committee according to German guidelines. The minimal sample size was calculated as previously described (Orth et al., 2013b).

In the defect preparation and treatment surgery, six skeletally mature, healthy female Göttingen minipigs (age between 18-22 months; average body weight - BW: 38.9 ± 5.3 kg) were fed *ad libitum* with a standard diet and continuously monitored by a veterinarian for the SOX9 *in vivo* study. Eight healthy, skeletally mature female Aachener minipigs (age 18-22 months, average BW: 42.75 ± 6.54 kg) were fed by standard diet and received water *ad libitum* for the IGF-I *in vivo* study.

The animals were sedated following a 12-hour fast with intramuscular injection of 30 mg ketamine/animal (Ketanest S, Pfizer, Berlin, Germany), 2 mg xylazine/animal (Rompun, Bayer, Leverkusen, Germany), and 1 mg atropine/animal (B. Braun, Melsungen, Germany). General anaesthesia was initially achieved following endotracheal intubation with intravenous administration of 20 ml of 2% propofol (AstraZeneca, Wedel, Germany) and further maintained with inhalation of 1.5% isoflurane (Baxter, Unterschleissheim, Germany) and intravenous administration of propofol (6-20 mg/kg BW/h). A standardized bilateral approach was performed with scheduled treatments in the hind legs with right and left knees alternating within groups (Christensen et al., 2015).

Standardized circular full-thickness chondral defects (diameter 4 mm) were defined on the superior region of lateral trochlea facets using a machine-made skin punch (Kai Europe, Solingen, Germany). The full-thickness chondral defect with a vertical defect edge was achieved with meticulous debridement of the entire cartilage layers, including calcified cartilage, downwards to the subchondral bone plate. Three uniform microfracture holes were introduced using a microfracture awl with a straight trihedral cutting tip and a penetration stop as previously described (Gao et al., 2017). Particular attention was paid to ensure the introduced holes perpendicular to the local subchondral bone plate.

For the SOX9 *in vivo* study, sterile liquid PF127 hydrogel containing rAAV-*lacZ* or rAAV-FLAG-*hsox9* were loaded into all defects (25 µl per defect) via a 100 µl micropipette (Eppendorf, Hamburg, Germany). For the IGF-I *in vivo* study, the hydrogel systems (IGF-I/AlgPH155 or *lacZ*/AlgPH155) (25 µl per defect; 3.6 × 10<sup>5</sup> transgene copies) were implanted in the defects that were prior blotted dry using a spatula where they adhered to the subchondral bone plate treated with microfracture (Díaz-Rodríguez et al., 2015).

Following implantation, the joint was taken through several ranges of motion to test the stability of the hydrogel. *In situ* gelation and arresting of bleeding occurred after a 2-3

minutes delay and the joints were closed in layers. Immediate full weight-bearing was allowed after surgery. Fentanyl pain patch (release rate 100 µg/h) was used only for the first 72 hours postoperatively, and oral carprofen (4 mg/kg BW) was applied orally if needed throughout the entire postoperative phase. For the SOX9 *in vivo* study, the animals were sacrificed at 4 weeks postoperatively. For the IGF-I *in vivo* study, the animals were sacrificed at one year postoperatively.

The entire defect area was photographed intraoperatively for the macroscopic evaluation (Sellers et al., 1997). Osteochondral specimens containing the cartilage defects were standardizedly prepared, retained in 4% formalin for 24 hours, and then stored in 70% ethanol. After the micro-CT analysis, specimens were decalcified with 5% formic acid, trimmed, and prepared for further histological, immunohistological, and histomorphometric analyses.

#### *6.2.5. Macroscopic evaluation of cartilage repair*

Defect photographs for each group were independently evaluated by two blinded experienced investigators using a validated semiquantitative macroscopic scoring system (20 = no repair; 0 = normal articular cartilage) (Goebel et al., 2012).

#### *6.2.6. Histological scoring of cartilage repair*

Paraffin-embedded microtome-cut sections (4 µm for the SOX9 *in vivo* study and 3 µm for the IGF-I *in vivo* study) were stained with safranin orange/fast green (safranin O) and hematoxylin and eosin (HE) as previously described.

A total of 192 stained sections (8 sections per defect) for the SOX9 *in vivo* study were evaluated by two blinded independent investigators using the histological scoring system described by Fortier *et al.* (Fortier et al., 2002). Values ranged from 20 (empty defect without repair tissue) to 0 points (complete regeneration).

The 96 stained sections (12 sections per defect) for the IGF-I *in vivo* study were analyzed using an inverse complex cartilage repair score (0 = normal articular cartilage; 31 = no repair tissue) (Sellers et al., 1997).

The cell densities (cells/mm<sup>2</sup>) in the defects were assessed on safranin O and HE-stained sections by two blinded observers using four defined image excerpts at

magnification x20 (Cucchiarini, Madry, 2014; Frisch et al., 2014b). Samples were examined under light microscopy (BX-45, Olympus, Hamburg, Germany).

#### *6.2.7. Immunohistochemical evaluations*

For the evaluation of the immunoreactivity to SOX9, IGF-I, type-II/-I collagen, CD3 (T lymphocytes), CD11b (activated macrophages), HLA-DR $\alpha$  (class II major histocompatibility complex antigen), IL-1 $\beta$ , and TNF- $\alpha$ , histological sections were deparaffinized and placed in 0.3% hydrogen peroxide for 30 minutes (Cucchiarini, Madry, 2014; Frisch et al., 2014b). The sections were then washed with phosphate-buffered saline (PBS) and incubated in 0.1% trypsin for 10 minutes at 37°C, washed with PBS, and placed in blocking buffer (3% bovine serum albumin in PBS) for 30 minutes at room temperature (Cucchiarini, Madry, 2014). The antibodies were then diluted in blocking buffer and applied to the sections for 12 hours at 4°C (Cucchiarini, Madry, 2014). Control conditions lacking primary antibodies were also evaluated to check for secondary immunoglobulins. The sections were next washed with PBS and incubated with biotinylated secondary antibodies (1/200) for 1 hour at room temperature (Cucchiarini, Madry, 2014). The sections were washed with PBS and incubated with avidin-biotin-peroxidase reagent for 30 minutes at room temperature, washed with PBS, and revealed with diaminobenzidine (DAB) (Cucchiarini, Madry, 2014). Samples were examined under light microscopy.

Expression of SOX9, IGF-I, CD3, CD11b, HLA-DR $\alpha$ , IL-1 $\beta$ , and TNF- $\alpha$  was assessed by two blinded observers by measuring the percentage of immunostained cells for each marker per total cell numbers using three standardized random sites in the defects with the SIS analySIS program (Olympus Soft Imaging System GmbH, Münster, Germany) and Adobe Photoshop (Adobe Systems, Unterschleissheim, Germany) (Cucchiarini, Madry, 2014), with analyses also performed for some markers (SOX9, IGF-I, IL-1 $\beta$ , TNF- $\alpha$ ) in the surrounding cartilage and at broader sites (synovium, quadriceps muscle adjacent to the patella, infrapatellar pad, subchondral bone marrow).

Expression of type-II and -I collagen was graded by two blinded observers using a semiquantitative score (0 = no immunoreactivity; 1 = significantly reduced immunoreactivity; 2 = moderately reduced immunoreactivity; 3 = similar immunoreactivity;

4 = stronger immunoreactivity compared with the controls) at three standardized random sites with the SIS analySIS program (Olympus) and Adobe Photoshop (Adobe Systems) (Xiao et al., 1996). For type-II collagen, the adjacent cartilage was defined as the normal control, and for type-I collagen, the subchondral bone plate was used as the control.

#### *6.2.8. Histomorphometric analyses of cartilage repair*

Safranin O-stained sections (n = 10) were randomly selected from each group to measure the defect filling and repair tissue thickness with the SIS analySIS program (Olympus).

The projected cartilage zone was defined according to the guidelines of the International Cartilage Regeneration & Joint Preservation Society (ICRS) (Hoemann et al., 2011). Defect filling was calculated as the area ratio of the measured cartilaginous repair tissue to the projected cartilage zone (**Figure 10**).

The repair tissue thickness was determined as the mean values of 3 measurements at the middle of one-thirds of the repair tissue, which was defined horizontally within the projected cartilage zone. The normal cartilage was measured from the minipig trochleae without any treatments. To assess perifocal OA in the articular cartilage adjacent to the chondral defects, safranin O-stained sections (n = 6 per animal) were scored by two blinded observers using an inverse OA score (0 = no OA; 25 = severe OA) (Little et al., 2010). Samples were examined under light microscopy (BX-45, Olympus, Hamburg, Germany).

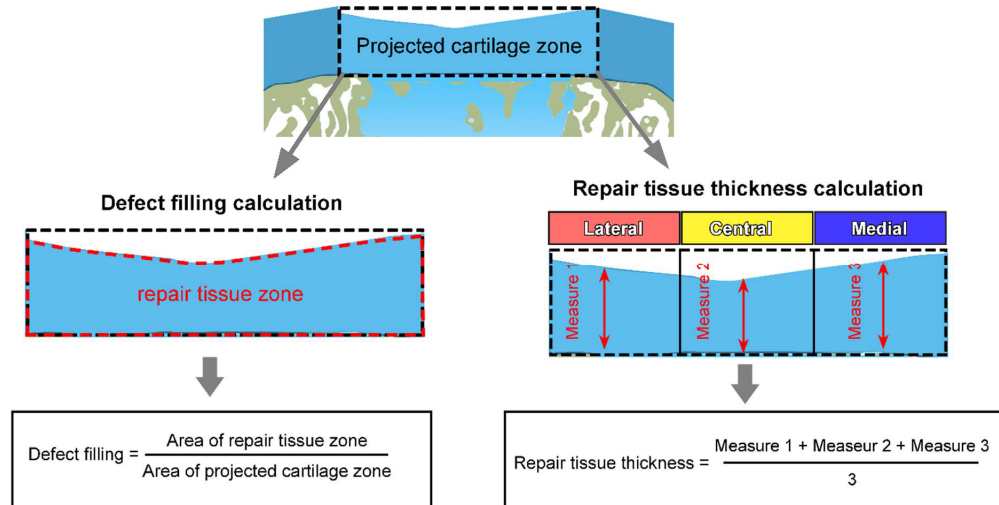


**Figure 10.** Measurement of defect filling and repair tissue thickness. The projected cartilage zone (black dashed region) on microscopic images was defined according to the recommended guidelines by the International Cartilage Regeneration & Joint Preservation Society (ICRS). The defect filling was calculated as the area ratio of the cartilaginous repair tissue (red dashed region) to the projected cartilage zone. The repair tissue thickness was determined as the mean values of 3 measurements at the middle of one-thirds of the repair tissue, which was defined horizontally within the projected cartilage zone (source: Madry\*, Gao\* et al., 2020a).

Visualization of the collagen network was performed on safranin O-stained histological sections using polarized light microscopy (BX-45, Olympus, Hamburg, Germany). A region of interest (ROI) (height 0.5 mm, width 2.0 mm) within the repair tissue showing visually best cartilage repair was selected for further analysis of collagen orientation. Three sub-ROIs were defined including a superficial, an intermediate, and a deep zone (each height 200  $\mu\text{m}$ , width 1,000  $\mu\text{m}$ ). The polarized light microscopy images were analyzed using the ImageJ software package (Version 1.51) with DiameterJ and OrientationJ plugins (Hotaling et al., 2015; Rezakhaniha et al., 2012; Schneider et al., 2012). A HSB color coded mapping file of entire ROI and a weighted histogram of the orientation of all collagen fibers within each sub-ROIs were outputted, as described elsewhere (Mandal et al., 2014).

ROI of the osteochondral unit was defined to include both articular cartilage (ROI-cartilage, 1.0 mm x 4.0 mm; black dashed rectangle) and subchondral bone (ROI-bone, 3.0 mm x 4.0 mm; yellow dashed rectangle). In blinded safranin O-stained sections, chondrogenic foci were identified by the presence of positive safranin O stain and of chondrocyte morphology which was further confirmed by positive immunostaining for type-II collagen in the same area of the defect in the adjacent section (Chevrier et al., 2011). The incidence of chondrogenic foci per defect, total area of chondrogenic foci and soft repair tissue in each defect, and their relative ratio (foci area/soft tissue area; %) within both ROI-cartilage and ROI-bone were calculated.

Quantification of chondrocytes and bone marrow-derived MSCs was achieved microscopically at a magnification x100 in safranin O-stained sections within the center of the osteochondral unit within up to three additional defined ROIs (ROI1-3, 400  $\mu$ m x 400  $\mu$ m; black rectangles), which was modulated to satisfy stereological requirements of a minimal 300 cell counts per ROI, depending on the depth of the soft osteochondral repair tissue. Chondrocytes were defined as cells with typical chondrocyte morphology and a positive safranin O-stained matrix. MSCs were identified as a fibroblast cell shape where incompletely differentiated cells in spindle-like or rounder shapes were also included in the stromal cell count in our study (Chevrier et al., 2007). The densities of chondrocytes and MSCs and the cellularity ratios of chondrocytes to MSCs were reported. Measures from different ROIs in the same defects were averaged and the mean data were used for statistical analysis.

Quantification of osteogenesis was performed within the ROI-bone of Masson-Goldner trichrome-stained sections through the central region of defects (3 sections per defect) using Map\_Bonemicrostructure, a plugin for ImageJ, and Adobe Photoshop (Adobe Systems) as previously described (Gao et al., 2017). Two-dimensional (2D) bone histomorphometric parameters were reported including bone volume fraction (BV/TV; %), mean trabecular thickness (Tb.Th; mm), mean trabecular separation (Tb.Sp;  $\mu$ m), and mean trabecular number per length unit (Tb.N; 1/mm) (Parfitt et al., 1983). Osteoclast and osteoblast density was quantified by manual point counting within 3 zones (each zone 1.0 mm x 4.0 mm) of the entire ROI-bone using previously standardized criterion (Haffner-

Luntzer et al., 2016). The percentage of marrow cavity, mature bone, new bone (osteoid), and repair tissue was also quantified.

#### *6.2.9. Qualitative evaluation of subchondral bone alterations and status*

The subchondral bone plate and subarticular spongiosa beneath cartilage defects and laterally adjacent to the defects (internal controls) were individually evaluated as previously described using a micro-CT scanner (Skyscan 1172; Bruker, Belgium) (Orth et al., 2012). For each osteochondral specimen, four distinct volumes of interest (VOIs) were established without overlapping within the subchondral bone compartment, including "subchondral bone plate-defect (SBP-defect)", "subarticular spongiosa-defect (SAS-defect)", "subchondral bone plate-lateral adjacent (SBP-adjacent)", and "subarticular spongiosa-lateral adjacent (SAS-adjacent; placed peripherally on the femoral trochlea)" (Gao et al., 2017). The vertical and horizontal length of each VOI was restricted to 3.0 mm and 4.0 mm, respectively. Subchondral bone alterations were qualitatively evaluated using a previously established micro-CT-based algorithm and alteration patterns were reported (if any) including intralesional osteophytes, residual microfracture holes, peri-hole bone resorption, and subchondral bone cysts (Gao et al., 2016). The maximal height, maximal width, maximal 2D area, and relative location of each osteophyte were recorded. The maximal height of bone bridges (if existing), maximal horizontal diameter, maximal vertical diameter, and maximal 2D area of residual microfracture holes, peri-hole bone resorption, and subchondral bone cysts were reported as previously described (Gao et al., 2016).

The subchondral bone plate quantitative analysis of the subchondral bone compartment was separately undertaken within the four VOIs. Three-dimensional (3D) bone microstructural parameters were reported including bone mineral density (BMD), bone volume fraction (BV/TV), specific bone surface (BS/BV), bone surface density (BS/TV) (Gao et al., 2017). Cortical thickness (Ct.Th) of the subchondral bone plate and trabecular thickness (Tb.Th), trabecular separation (Tb.Sp), trabecular pattern factor (Tb.Pf), trabecular number (Tb.N), structure model index (SMI), degree of anisotropy (DA), and fractal dimension (FD) of the subarticular spongiosa were additionally recorded.

### 6.3. TGF- $\beta$ *ex vivo* study

#### 6.3.1. Samples

Bone marrow aspirates (~ 15 ml) were obtained from the distal femurs of patients undergoing total knee arthroplasty (n = 12, age 74  $\pm$  3 years as ultimate targets for therapy) with approval from the Ethics Committee of the Saarland Physicians Council (*Ärztchamber des Saarlandes*, reference number Ha06/08). All patients gave their informed consent prior to inclusion in the evaluation performed according to the Helsinki Declaration. Aspirates containing hMSCs (0.5-1.2  $\times$  10<sup>9</sup> cells/ml) were placed in 96-well plates (150  $\mu$ l aspirate/well, 6.1  $\times$  10<sup>7</sup> cells) at 37°C (Frisch et al., 2016; Venkatesan et al., 2020a, 2020b) until immediate application of the various films as described below.

#### 6.3.2. Preparation of the poly( $\epsilon$ -caprolactone) (PCL) films

The PCL films were generated by spin-coating as described (Rohman et al., 2015). Briefly, PCL (60% (w/v) in dichloromethane) was dropped for spinning on a glass slide (30 seconds at 1,500 rpm) using a SPIN150-v3 SPS. The films were air-dried for 2 hours, vacuum-dried for 24 hours, and cut in 4-mm disks for grafting with pNaSS (1.3  $\times$  10<sup>-5</sup> mol/g) via ozonation (10 minutes at 30°C), followed by incubation in degassed NaSS (15% (w/v) in distilled water) for graft polymerization (3 hours, 45°C). The films were washed in distilled water, 0.15 M NaCl, and PBS and rinsed for vacuum-drying. Some films were left ungrafted as controls.

#### 6.3.3. Generation of the rAAV vectors

The vectors were created using a parental AAV-2 genomic clone (pSSV9) (Samulski et al., 1987, 1989). rAAV-hTGF- $\beta$  carries a 1.2-kb human transforming growth factor beta 1 (hTGF- $\beta$ ) cDNA sequence controlled by the CMV-IE promoter (Frisch et al., 2016).

Packaging of conventional vectors (not self-complementary) was performed via helper-free (two-plasmid) transfection in 293 cells using the packaging plasmid pXX2 and the adenovirus helper plasmid pXX6 (Venkatesan et al., 2020a, 2020b).

Vector purification was then performed using the AAVanced Concentration Reagent (Venkatesan et al., 2020a, 2020b) and vector titration was managed via real-time PCR (Frisch et al., 2016; Venkatesan et al., 2020a, 2020b). The method allowed to generate vector solutions at about  $10^{10}$  transgene copies/ml (i.e., about 1/500 functional recombinant viral particles).

#### 6.3.4. rAAV immobilization on PCL films

The rAAV vectors (40  $\mu$ l,  $8 \times 10^5$  transgene copies) were incubated with 0.002% poly-L-lysine (overnight at 37°C) and then immobilized on the PCL films for 2 hours by dropping at 37°C (Brunger et al., 2014; Venkatesan et al., 2020a, 2020b). rAAV-coated PCL films, while some PCL films were left without vector coating as controls. Vector coating on the films using a reporter (rAAV-*lacZ*) vector (Venkatesan et al., 2020a) was not performed as we already showed that rAAV-*lacZ* gene transfer via such films has no effect on the chondrogenesis of bone marrow aspirates (Venkatesan et al., 2020a). Controlled release studies were not performed as we already showed that the various PCL films can properly release rAAV over an extended period of time (at least 21 days) (Venkatesan et al., 2020a).

#### 6.3.5. rAAV gene transfer

Aliquots of human bone marrow aspirates (150  $\mu$ l/well in 96-well plates) containing hMSCs ( $6.1 \times 10^7$  cells) (Frisch et al., 2016; Venkatesan et al., 2020a, 2020b) were incubated with rAAV-coated PCL films (multiplicity of infection - MOI = 75) in the presence of fibrinogen/thrombin (17 mg/ml/5 U/ml) (Venkatesan et al., 2020a, 2020b). The systems were placed either in defined chondrogenic differentiation medium (DMEM high glucose 4.5 g/l, 100 U/ml penicillin, 100  $\mu$ g/ml streptomycin, 0.1  $\mu$ M dexamethasone, 50  $\mu$ g/ml ascorbic acid, 40  $\mu$ g/ml proline, 110  $\mu$ g/ml pyruvate, 6.25  $\mu$ g/ml of insulin, 6.25  $\mu$ g/ml transferrin, 6.25  $\mu$ g/ml selenious acid, 1.25  $\mu$ g/ml bovine serum albumin, 5.55  $\mu$ g/ml linoleic acid, and 10 ng/ml TGF- $\beta$ 3) (Frisch et al., 2016; Venkatesan et al., 2020a, 2020b) or in osteogenic differentiation medium (StemPro Osteogenesis Differentiation kit with 100 U/ml penicillin, 100  $\mu$ g/ml streptomycin) where indicated (Frisch et al., 2016;

Venkatesan et al., 2020a, 2020b) (Life Technologies GmbH, Darmstadt, Germany) at 37°C under 5% CO<sub>2</sub> for up to 21 days prior to the analyses.

#### *6.3.6. Transgene expression*

TGF-β expression was monitored by immunohistochemistry using a specific primary antibody, a biotinylated secondary antibody, and the avidin-biotin complex (ABC) method with DAB as a chromogen for evaluation under light microscopy (Frisch et al., 2016). TGF-β expression was also detected with a specific ELISA (Frisch et al., 2016). Measurements were performed on a GENios spectrophotometer/fluorometer (Tecan, Crailsheim, Germany).

#### *6.3.7. Biological analyses*

The systems were digested with papain and the proteoglycan contents were measured by binding to dimethylmethylene blue dye via normalization to the total cellular proteins (Pierce Thermo Scientific Protein Assay; Thermo Fisher Scientific, Schwerte, Germany) (Frisch et al., 2016; Venkatesan et al., 2020a, 2020b). Measurements were performed on a GENios spectrophotometer/fluorometer (Tecan). Cell viability was monitored with the Cell Proliferation Reagent WST-1 with OD<sup>450</sup> nm being proportional to the cell numbers (Frisch et al., 2016; Venkatesan et al., 2020a, 2020b) on a GENios spectrophotometer/fluorometer (Tecan).

#### *6.3.8. Histology and immunohistochemistry*

The systems were fixed in 4% formalin, dehydrated in graded alcohols, embedded in paraffin, and sectioned (3 μm). Sections were stained with HE for cellularity, with toluidine blue for matrix proteoglycans, and with alizarin red for mineralization (Frisch et al., 2016; Venkatesan et al., 2020a, 2020b). Immunohistochemistry was performed to monitor the type-II, -I, and -X collagen expression with specific primary antibodies, biotinylated secondary antibodies, and the ABC method with DAB (Frisch et al., 2016; Venkatesan et al., 2020a, 2020b). Controls with lack of primary antibodies were tested to check for secondary immunoglobulins. Sections were examined under light microscopy.

### 6.3.9. *Histomorphometric analyses*

The % of TGF- $\beta$ <sup>+</sup> cells (TGF- $\beta$ <sup>+</sup> cells/total cell numbers on immunohistochemical sections), the intensities of toluidine blue and alizarin red staining (histological sections) and of type-II, -I, and -X collagen deposition (immunohistochemical sections), and the cell densities (cells/mm<sup>2</sup>) on HE histological sections were assessed using four sections per condition with the SIS AnalySIS program (Olympus) and Adobe Photoshop (Adobe Systems) (Frisch et al., 2016; Venkatesan et al., 2020a, 2020b). Sections (toluidine blue, alizarin red, type-II/-I/-X collagen) were scored blind by two individuals for uniformity and density with a modified Bern grading score (Venkatesan et al., 2020a, 2020b) as follows: 0 = no staining, 1 = heterogeneous and/or weak staining, 2 = homogeneous and/or moderate staining, 3 = homogeneous and/or intense staining, and 4 = very intense staining.

### 6.3.10. *Real-time reverse transcriptase PCR (RT-PCR) analysis*

Total cellular RNA was extracted using the RNeasy Protect Mini Kit and an on-column RNase-free DNase treatment (Qiagen, Hilden, Germany). The RNA was eluted in 30  $\mu$ l RNase-free water. Reverse transcription was next performed with 8  $\mu$ l eluate using the 1<sup>st</sup> Strand cDNA Synthesis kit for RT-PCR (AMV) (Roche Applied Science). Real-time RT-PCR amplification was performed on an Mx3000P QPCR system (Stratagene, Agilent Technologies, Waldbronn, Germany) with 3  $\mu$ l cDNA product using the Brilliant SYBR Green QPCR Master Mix (Stratagene) (Frisch et al., 2016; Venkatesan et al., 2020a, 2020b) and with the following conditions: 10 minutes at 95°C, 55 amplification cycles (30 seconds denaturation, 95°C; 1 minute annealing, 55°C; 30 seconds extension, 72°C), denaturation 1 minute at 95°C, and final incubation 30 seconds at 55°C.

The primers (Invitrogen GmbH) were SOX9 (chondrogenic marker; forward 5'-ACACACAGCTCACTCGACCTTG-3'; reverse 5'-GGAATTCTGGTTGGTCCTCT-3'), type-II collagen (COL2A1; chondrogenic marker; forward 5'-GGACTTTTCTCCCCTCTCT-3'; reverse 5'-GACCCGAAGGTCTTACAGGA-3'), aggrecan (ACAN; chondrogenic marker; forward 5'-GAGATGGAGGGTGAGGTC-3'; reverse 5'-ACGCTGCCTCGGGCTTC-3'), type-I collagen (COL1A1; osteogenic marker; forward 5'-ACGTCCTGGTGAAGTTGGTC-3'; reverse 5'-ACCAGGGAAGCCTCTCTCTC-3'), type-X collagen (COL10A1; marker of hypertrophy; forward 5'-CCCTCTTGTTAGTGCCAACC-3'; reverse 5'-

AGATTCCAGTCCTTGGGTCA-3'), and glyceraldehyde-3-phosphate dehydrogenase (GAPDH; housekeeping gene and internal control; forward, 5'-GAAGGTGAAGGTCGGAGTC-3'; reverse, 5'-GAAGATGGTGATGGGATTTC-3') (all at a final concentration of 150 nM) (Frisch et al., 2016; Venkatesan et al., 2020a, 2020b). Control reactions included water and non-reverse-transcribed messenger RNA (mRNA). The specificity of the generated products was confirmed by melting curve analysis and agarose gel electrophoresis.

The threshold cycle (Ct) value for each gene was measured for each amplification using the MxPro QPCR software (Stratagene), with normalization of the value to GAPDH expression using the  $2^{-\Delta\Delta Ct}$  method (Frisch et al., 2016; Venkatesan et al., 2020a, 2020b).

#### **6.4. Statistical analysis**

Descriptive data are expressed as mean value  $\pm$  standard deviation (SD). Each condition *in vitro* was carried out in triplicate in three independent experiments with all samples and with all defects *in vivo*. Data were analyzed by two individuals blinded with respect to the different groups. The One-way ANOVA with Tukey's post-hoc test, t-test, Mann-Whitney Rank Sum test, and Wilcoxon signed-rank test were employed where appropriate. Calculations were performed using SPSS version 22.0 (SPSS Inc., Chicago, IL, USA), Stata (StataCorp LCC, College Station, TX, USA) and GraphPad Prism version 8.0.0 (GraphPad Software Inc., San Diego, CA, USA). Principal component analysis and heatmap visualization of macroscopic and histological scoring outcomes were performed with Biovinci version 1.1.5 (BioTutoring Inc., San Diego, CA, USA). Correlation between micro-CT parameters and histological score was analyzed with Pearson correlation coefficient. *P* values < 0.05 were considered statistically significant.

## 7. RESULTS

Results are presented in three sections corresponding to the three hypotheses.

### 7.1. SOX9 *in vivo* study

#### 7.1.1. Effects of SOX9 overexpression via rAAV-FLAG-hsox9/PEO-PPO-PEO hydrogel mediated gene transfer on the repair processes in minipig chondral defects

Upon macroscopic evaluation, no joint effusion, inflammation, periarticular osteophyte formation, nor adhesions were observed in any of the treatment groups (**Figure 11a**).

Semiquantitative scoring of macroscopic cartilage repair (Goebel et al., 2012) (**Figures 11e and 11f and Table 7**) revealed significantly improved total scores with the *sox9*/hydrogel ( $P = 0.026$  versus *lacZ*/hydrogel,  $P = 0.018$  versus *lacZ*) with less new blood vessels covering the repair tissue of defects treated with the *sox9*/hydrogel ( $P = 0.026$  versus *lacZ*/hydrogel,  $P = 0.028$  versus *lacZ*) (**Figures 11g and 11h and Table 7**).

Other individual parameters of the macroscopic scoring were not significantly different between groups ( $P \geq 0.093$ ) (**Figures 11g and 11h and Table 7**).

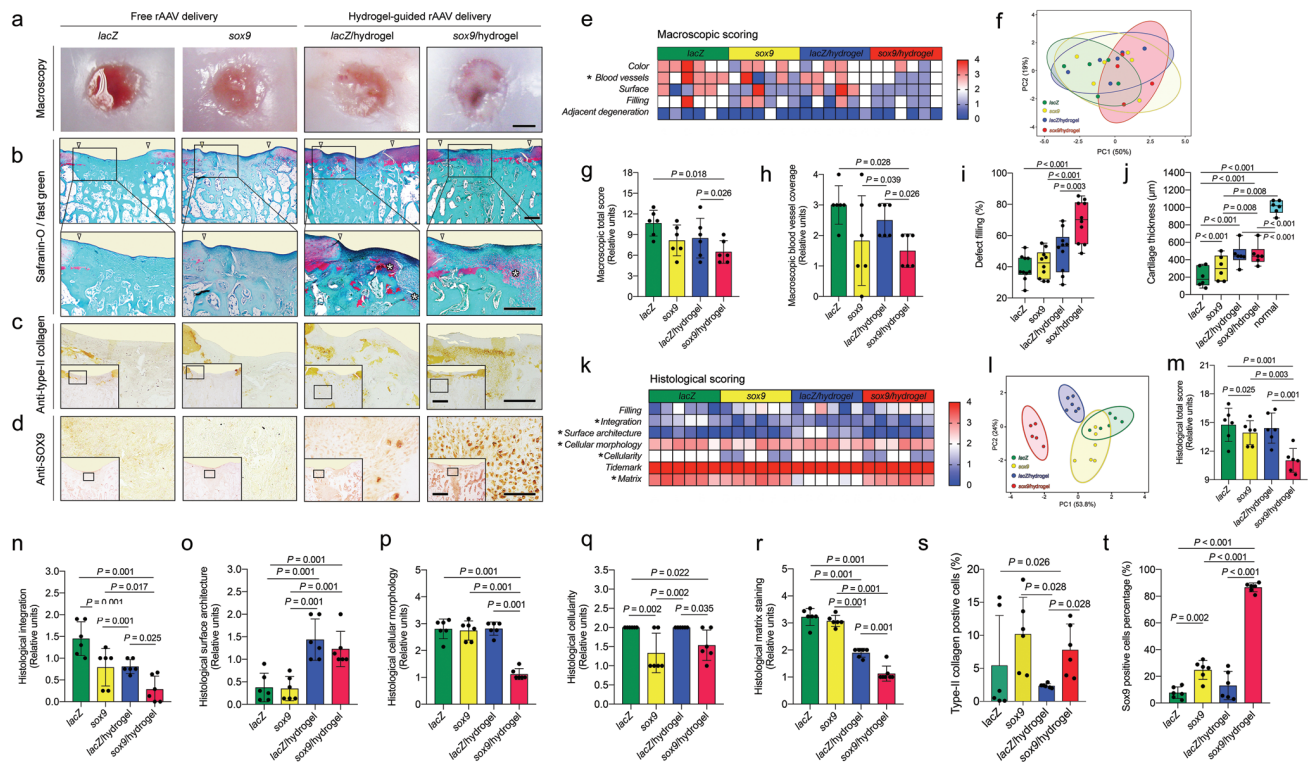


**Figure 11.** Cartilage repair in minipig chondral defects upon microfracture and application of *sox9*/hydrogel versus *lacZ*/hydrogel and free vector treatment. Macroscopic (**a**) and histological views (**b**: better repair and larger chondrogenic foci (\*) in the *sox9*/hydrogel defects) (all representative data). White triangles denote the defect borders. Immunodetection of type-II collagen deposition (**c**) and SOX9 expression (**d**) (all representative data). (**e**) Heat map of variables of the macroscopic scoring with (\*) indicating significant intergroup difference for blood vessels coverage. (**f**) Principal component analysis of total macroscopic score underlining the overlapped clusters without clear separations. Macroscopic total score (**g**) and blood vessel coverage (**h**). (**i**) Defect filling (%). (**j**) Cartilage thickness ( $\mu\text{m}$ ). (**k**) Heat map of variables of the histological scoring. Variables with significant intergroup differences are shown by (\*). (**l**) Principal component analysis of total histological score highlighting the evidently separated clusters of the *sox9*/hydrogel group from all other groups and the overlapping seen between free *sox9* and *lacZ* groups. Histological total score (**m**), integration score (**n**), surface architecture (**o**), cellular morphology (**p**), cellularity (**q**), and matrix staining (**r**). Cells expressing type-II collagen (**s**) and SOX9 (**t**). Scale bars: (**a**) 2.0 mm, (**b,c**) 0.5 mm, and (**d**) 0.1 mm (source: Madry\*, Gao\* et al., 2020a).

**Table 7.** Macroscopic scoring of cartilage repair in the defects (SOX9 study)

Parameter	Free rAAV application		Hydrogel-guided rAAV delivery		P value
	<i>lacZ</i>	<i>sox9</i>	<i>lacZ</i> /hydrogel	<i>sox9</i> /hydrogel	
Color of the repair tissue	2.83 ± 0.75	2.33 ± 0.82	2.17 ± 0.75	2.00 ± 0.63	n.s.
Blood vessels in the repair tissue	3.00 ± 0.63	1.83 ± 1.47	2.50 ± 0.55	1.50 ± 0.55	§,†,ε
Surface of the repair tissue	2.00 ± 1.26	1.50 ± 1.22	2.33 ± 1.21	1.17 ± 0.41	n.s.
Filling of the defect	2.33 ± 0.82	1.83 ± 0.98	1.33 ± 1.21	1.33 ± 0.52	n.s.
Degeneration of adjacent cartilage	0.50 ± 0.84	0.33 ± 0.82	0.17 ± 0.41	0.50 ± 0.84	n.s.
Average total score	10.67 ± 1.86	8.17 ± 2.23	8.50 ± 2.88	6.50 ± 1.64	§,ε

$P \leq 0.05$  for §*lacZ* versus *sox9*/hydrogel, †*sox9* versus *lacZ*/hydrogel, and ε*lacZ*/hydrogel versus *sox9*/hydrogel; n.s., not significant for all intergroup comparisons.

The histomorphometric analysis revealed that application of the *sox9*/hydrogel significantly improved the filling of the defects relative to all other groups ( $P \leq 0.003$ ) (**Figure 11i and Table 8**) while it enhanced the thickness of the cartilage versus free vector treatments ( $P \leq 0.008$ ) although it was significantly thinner than normal cartilage ( $P \leq 0.001$ ) (**Figure 11j and Table 8**). A histological analysis (**Figure 11b**) using a semiquantitative histological scoring of cartilage repair (Fortier et al., 2002) (**Figure 11k**) further showed that relative to all other groups, application of the *sox9*/hydrogel significantly improved the individual parameters of "integration" ( $P \leq 0.025$ ), "cellular morphology" ( $P = 0.001$ ), and "matrix staining" ( $P = 0.001$ ) (**Figures 11n, 11p, 11r and Table 9**) as well as the total histological score of cartilage repair ( $P \leq 0.003$ ) (**Figure 11m and Table 9**). The individual parameter of "surface architecture" was improved with the *sox9*/hydrogel versus *lacZ*/hydrogel ( $P = 0.001$ ) while "cellularity" was enhanced versus *lacZ* and *lacZ*/hydrogel ( $P \leq 0.022$ ) (**Figures 11o and 11q and Table 9**). Principal component analysis of the histological scoring (**Figure 11l**) detected a noteworthy separation among each dataset, indicating significant histological differences of cartilaginous repair tissue between groups.

**Table 8.** Filling and thickness of the defects

Parameter	Normal cartilage	Free rAAV application		Hydrogel-guided rAAV delivery		P value
		<i>lacZ</i>	<i>sox9</i>	<i>lacZ</i> /hydrogel	<i>sox9</i> /hydrogel	
Filling (%)	n.a.	39.16 ± 8.06	41.72 ± 9.04	50.26 ± 13.34	69.29 ± 13.29	§,λ,ε
Thickness (μm)	1,010.00 ± 76.85	348.00 ± 114.43	248.00 ± 144.78	434.00 ± 126.34	394.00 ± 119.38	#,§, λ,γ,η,κ,φ

$P \leq 0.05$  for <sup>#</sup>*lacZ* versus *lacZ*/hydrogel, <sup>§</sup>*lacZ* versus *sox9*/hydrogel, <sup>λ</sup>*sox9* versus *sox9*/hydrogel, <sup>ε</sup>*lacZ*/hydrogel versus *sox9*/hydrogel, <sup>γ</sup>normal cartilage versus *lacZ*, <sup>η</sup>normal cartilage versus *sox9*, <sup>κ</sup>normal cartilage versus *lacZ*/hydrogel, and <sup>φ</sup>normal cartilage versus *sox9*/hydrogel; n.a., not applicable (source: Madry\*, Gao\* et al., 2020a).

**Table 9.** Histological scoring of cartilage repair in the defects (SOX9 study)

Parameter	Free rAAV application		Hydrogel-guided rAAV delivery		P value
	<i>lacZ</i>	<i>sox9</i>	<i>lacZ</i> /hydrogel	<i>sox9</i> /hydrogel	
Filling	0.92 ± 0.68	1.65 ± 0.56	1.47 ± 0.98	1.71 ± 1.33	n.s.
Adjacent integration	1.45 ± 0.39	0.79 ± 0.43	0.81 ± 0.16	0.28 ± 0.30	#,§,λ,ε
Surface architecture	0.38 ± 0.32	0.35 ± 0.27	1.44 ± 0.46	1.23 ± 0.39	#,§,†,λ
Cellular morphology	2.81 ± 0.37	2.75 ± 0.36	2.81 ± 0.25	1.12 ± 0.21	§,λ,ε
Cellularity	2.00 ± 0.00	1.33 ± 0.52	2.00 ± 0.00	1.53 ± 0.40	*,§,†,ε
Tidemark	4.00 ± 0.00	4.00 ± 0.00	4.00 ± 0.00	4.00 ± 0.00	n.s.
Matrix staining	3.22 ± 0.31	3.07 ± 0.21	1.90 ± 0.17	1.15 ± 0.30	0.031
Average total score	14.77 ± 1.75	13.94 ± 1.26	14.42 ± 1.59	11.03 ± 1.25	*,§,λ,ε

$P \leq 0.05$  for <sup>\*</sup>*lacZ* versus *sox9*, <sup>#</sup>*lacZ* versus *lacZ*/hydrogel, <sup>§</sup>*lacZ* versus *sox9*/hydrogel, <sup>†</sup>*sox9* versus *lacZ*/hydrogel, <sup>λ</sup>*sox9* versus *sox9*/hydrogel, and <sup>ε</sup>*lacZ*/hydrogel versus *sox9*/hydrogel; n.s., not significant for all intergroup comparisons (source: Madry\*, Gao\* et al., 2020a).

Higher type-II collagen deposition was observed in the *sox9*/hydrogel defects compared with the *lacZ*/hydrogel group or with free *lacZ* application ( $P \leq 0.026$ ) (**Figures 11c and 11s and Table 10**), probably resulting from higher numbers of SOX9-positive cells in the *sox9*/hydrogel defects relative to all other groups ( $P \leq 0.001$ ) (**Figures 11d and 11t and Table 10**), indicating improved transgene expression via PEO-PPO-PEO-guided rAAV controlled release.

**Table 10.** Type-II collagen deposition and SOX9 expression in the defects

Parameter	Free rAAV application		Hydrogel-guided rAAV delivery		P value
	<i>lacZ</i>	<i>sox9</i>	<i>lacZ</i> /hydrogel	<i>sox9</i> /hydrogel	
Type-II collagen-positive cells (%)	5.44 ± 7.57	10.20 ± 5.57	2.35 ± 0.31	7.80 ± 3.92	§,†,λ
SOX9-positive cells (%)	7.69 ± 4.34	24.78 ± 7.05	13.08 ± 10.51	86.64 ± 3.32	*,§,λ,ε

$P \leq 0.05$  for \**lacZ* versus *sox9*, §*lacZ* versus *sox9*/hydrogel, †*sox9* versus *lacZ*/hydrogel, λ*sox9* versus *sox9*/hydrogel, and ε*lacZ*/hydrogel versus *sox9*/hydrogel (source: Madry\*, Gao\* et al., 2020a).

### 7.1.2. Effects of SOX9 overexpression via rAAV-FLAG-hsox9/PEO-PPO-PEO hydrogel mediated gene transfer on the immune response in minipig chondral defects

An immunohistochemical analysis on histological sections to detect potential CD3 (T-lymphocytes), CD11b (activated macrophages), and human leukocyte antigen isotype DR alpha (HLA-DRα) (class II major histocompatibility complex - MHC - antigens) expression (Rodeo et al., 2000) revealed the quasi absence of immune cells in all the defects without significant differences between groups ( $P \geq 0.220$ ) (**Figure 12 and Table 11**).

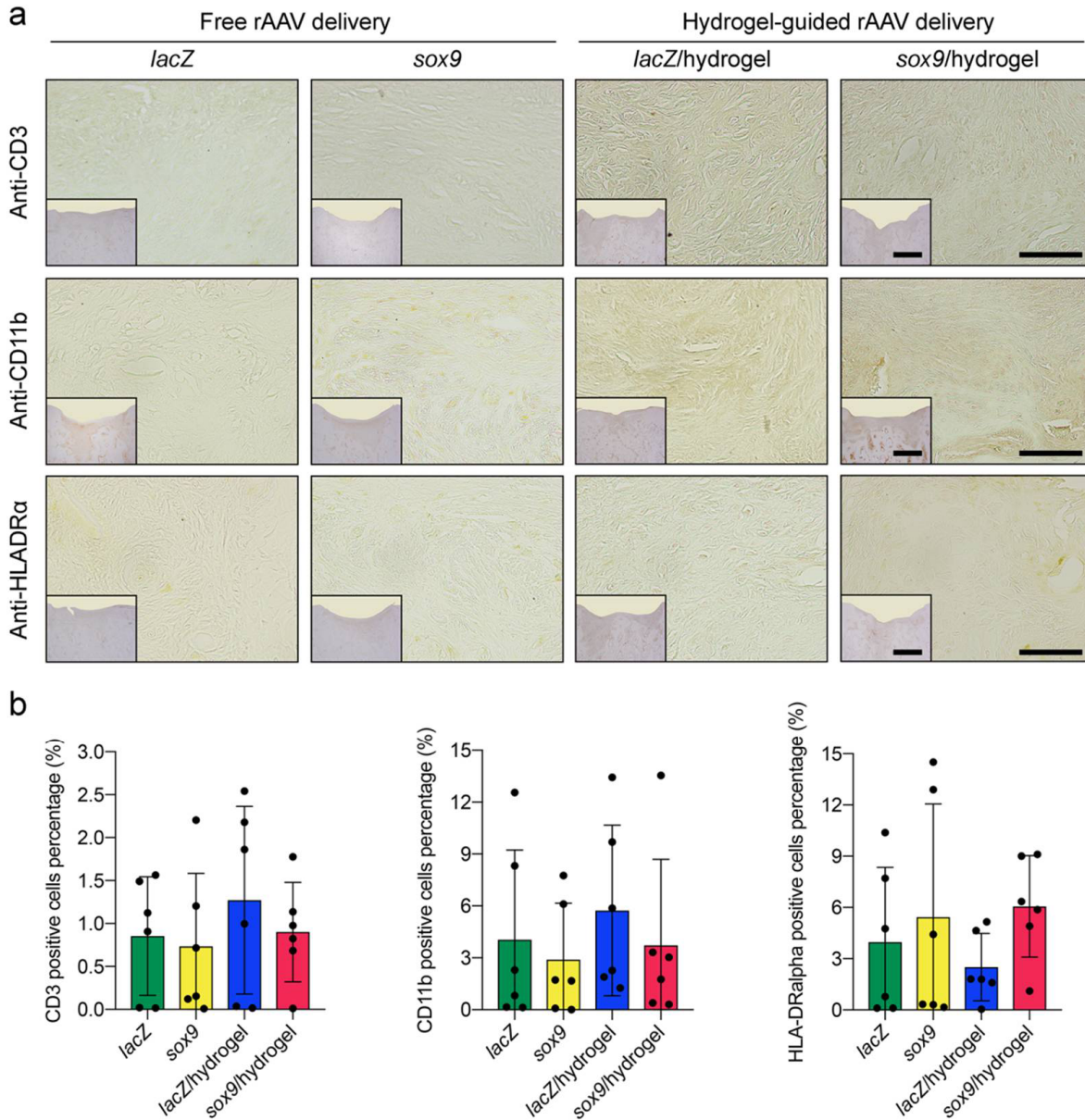


**Figure 12.** CD3, CD11b, and HLA-DR $\alpha$  expression in minipig chondral defects upon microfracture and application of *sox9*/hydrogel versus *lacZ*/hydrogel and free vector treatment. (a) Immunodetection of CD3, CD11b, and HLA-DR $\alpha$  expression (all representative data). (b) CD3-, CD11b-, and HLA-DR $\alpha$ -positive cells. Scale bars: 100  $\mu$ m and 40  $\mu$ m (insets) (source: Madry\*, Gao\* et al., 2020a).

**Table 11.** Analyses of CD3, CD11b, and HLA-DR $\alpha$  expression in the defects

Parameter	Free rAAV application		Hydrogel-guided rAAV delivery		P value
	<i>lacZ</i>	<i>sox9</i>	<i>lacZ</i> /hydrogel	<i>sox9</i> /hydrogel	
CD3-positive cells (%)	0.85 $\pm$ 0.69	0.73 $\pm$ 0.69	1.27 $\pm$ 1.09	0.90 $\pm$ 0.58	0.220 - 1.000
CD11b-positive cells (%)	4.05 $\pm$ 5.19	2.89 $\pm$ 3.26	5.74 $\pm$ 4.94	3.73 $\pm$ 4.97	0.592 - 0.992
HLA-DR $\alpha$ -positive cells (%)	3.94 $\pm$ 4.37	5.44 $\pm$ 4.37	2.50 $\pm$ 6.62	6.06 $\pm$ 2.97	0.504 - 0.994

<sup>a</sup>Range of *P* values from intergroup comparison (source: Madry\*, Gao\* et al., 2020a).

### 7.1.3. Effects of SOX9 overexpression via rAAV-FLAG-hsox9/PEO-PPO-PEO hydrogel mediated gene transfer on collagen orientation and distribution in minipig chondral defects

As such evaluations overall demonstrated superior cartilage repair via hydrogel-guided rAAV delivery over free rAAV vector treatment, we next focused on in-depth microstructural, comparative analyses in the *sox9*/hydrogel *versus lacZ*/hydrogel groups. An evaluation of collagen orientation and distribution detected visually better, and more collagens distributed in positive degree toward the subchondral bone plate in the basal zone of the *sox9*/hydrogel defects than in the *lacZ*/hydrogel defects (**Figure 13**). Further analyses revealed differences between groups in two sub-ROIs of the cartilaginous repair tissue (**Figures 14a-14c**). Compared with the surface zone of normal cartilage, significant less collagens oriented between -10° and 0° and between 80° and 90° were observed in either group compared with normal cartilage (**Figures 14d and 14f**). Within the basal zone of the cartilaginous repair tissue, collagen orientation in the *lacZ*/hydrogel defects showed significantly different patterns in multiple degree ranges (from -90° to -80°, -60° to -50°, 20° to 30°, 40° to 50°, and 80° to 90°; all *P*  $\leq$  0.05) compared with normal cartilage, while the *sox9*/hydrogel defects showed orientation and distribution of collagens more analogous to normal cartilage (**Figures 14e and 14g**).

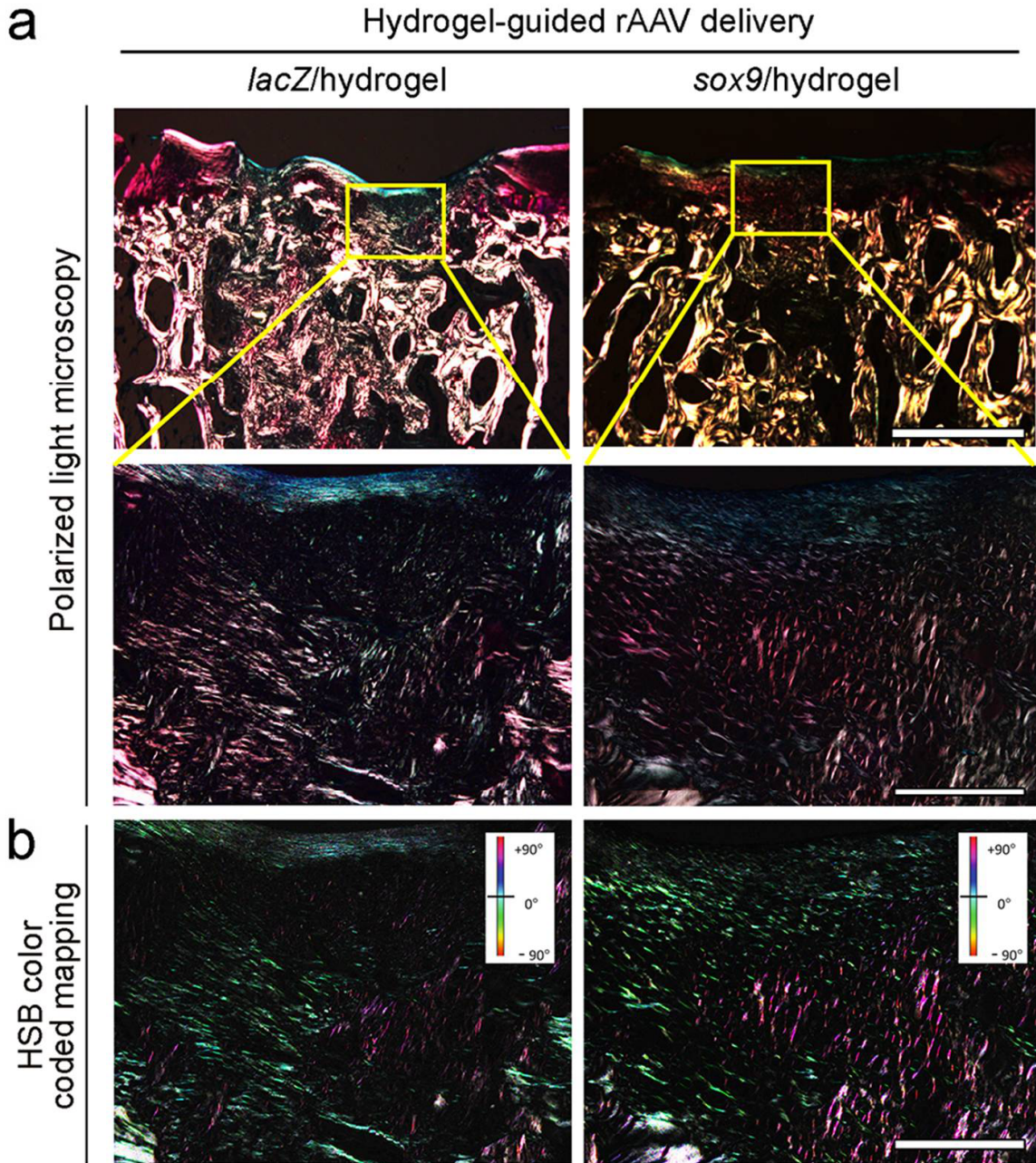


**Figure 13.** Collagen orientation in minipig chondral defects upon microfracture and application of *sox9*/hydrogel versus *lacZ*/hydrogel. (a) Polarized light microscopy (all representative data) and (b) HSB color-coded mapping of the same region of the lower row of (a), with more collagens distributed in positive degree towards the subchondral bone plate, approximating the normal zonal structure of normal cartilage, in the basal zone (purple coded regions) of the *sox9*/hydrogel defects than in the *lacZ*/hydrogel defects (scale bars: a, 0.5 mm and b, 0.1 mm) (source: Madry\*, Gao\* et al., 2020a).

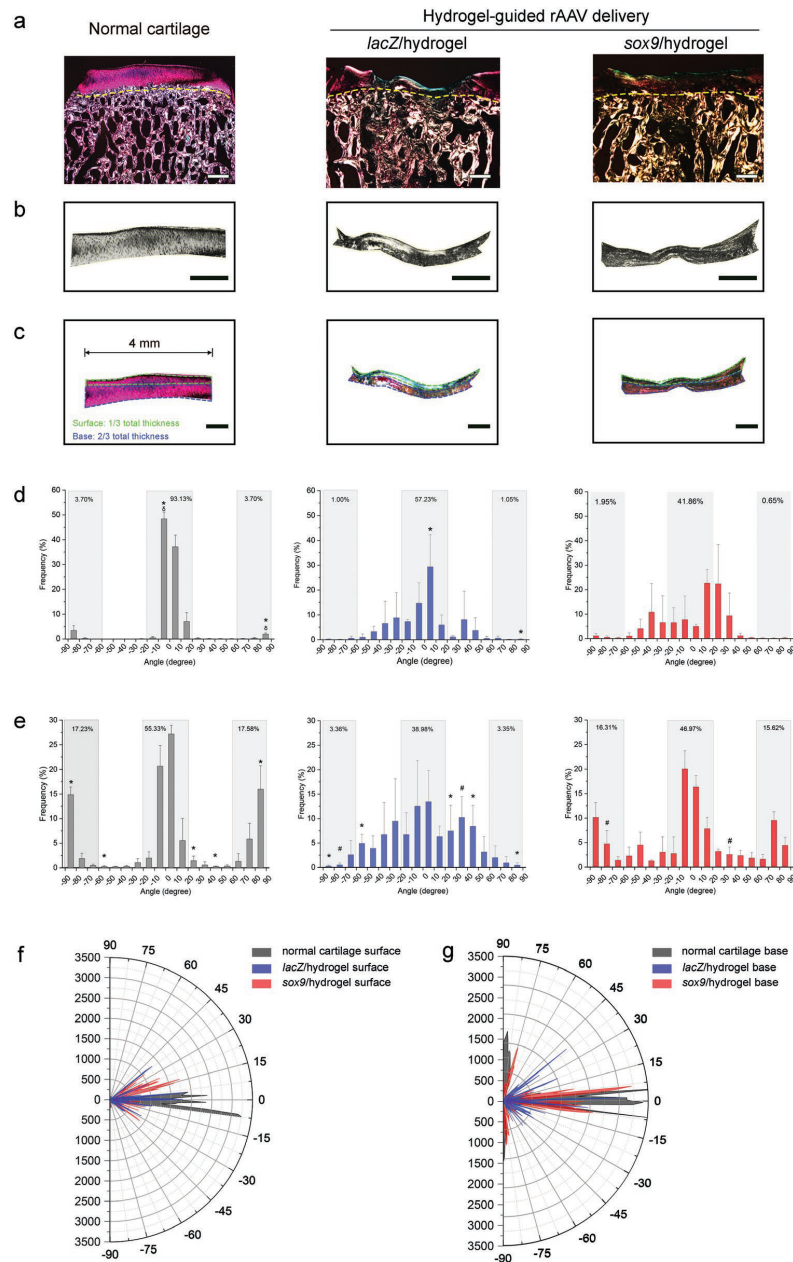


**Figure 14.** Quantitative analyses of collagen fiber orientation in minipig chondral defects upon microfracture and application of *sox9*/hydrogel versus *lacZ*/hydrogel. (a) Representative polarized microscopic views of normal cartilage and defects from both treatment groups. (b) Vector filled illustration. (c) Region of interests (ROIs) in the articular cartilage zone (surface ROI with 1/3 total thickness, base ROI with 2/3 total thickness). Collagen orientation in surface (d) and base ROIs (e). \* $P \leq 0.05$  between normal cartilage and *lacZ*/hydrogel defects;  $\delta P \leq 0.05$  between normal cartilage and *sox9*/hydrogel defects; # $P \leq 0.05$  between both groups. (f,g) Radar charts of collagen orientation within both surface (f) and base (g) ROIs (source: Madry\*, Gao\* et al., 2020a).

#### 7.1.4. Effects of SOX9 overexpression via rAAV-FLAG-hsox9/PEO-PPO-PEO hydrogel mediated gene transfer on the chondrogenesis and osteogenesis in minipig chondral defects

Histomorphometric analyses were performed to determine the effects of the rAAV/hydrogels on chondrogenesis and osteogenesis within the osteochondral unit *in vivo* (**Figures 15a and 15b**). Compared with the *lacZ*/hydrogel defects, the *sox9*/hydrogel defects exhibited a significantly larger area of mature chondrogenic foci ( $P = 0.046$ ) with a significantly improved area of chondrogenic foci/soft repair tissue ratio ( $P = 0.046$ ) (**Figure 15c and Table 12**). Moreover, significantly more chondrocytes, less MSCs, and higher cellularity ratio of chondrocytes *versus* MSCs were observed in the osteochondral repair tissue of the *sox9*/hydrogel defects compared with the control defects ( $P = 0.002$ ).

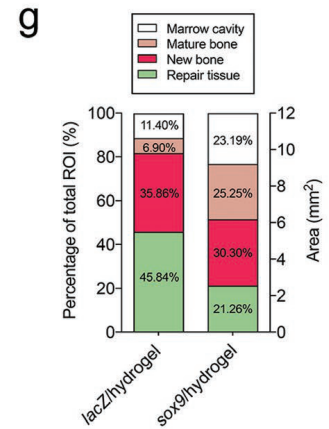
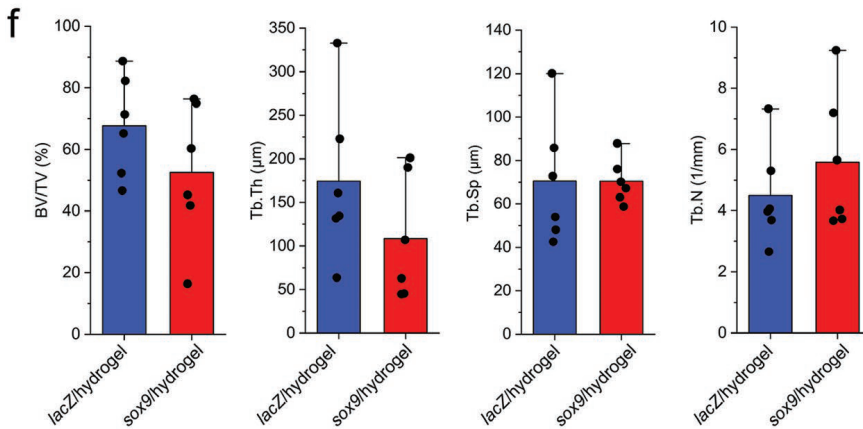
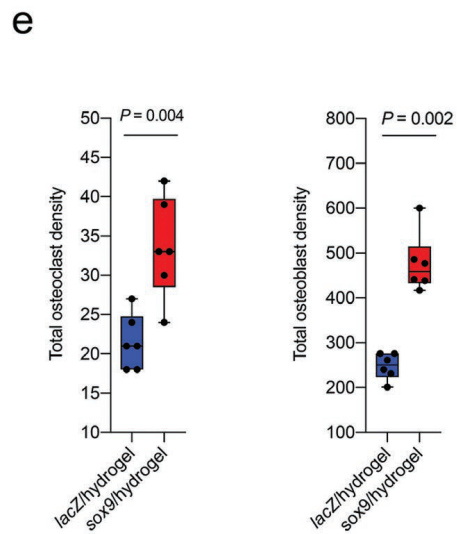
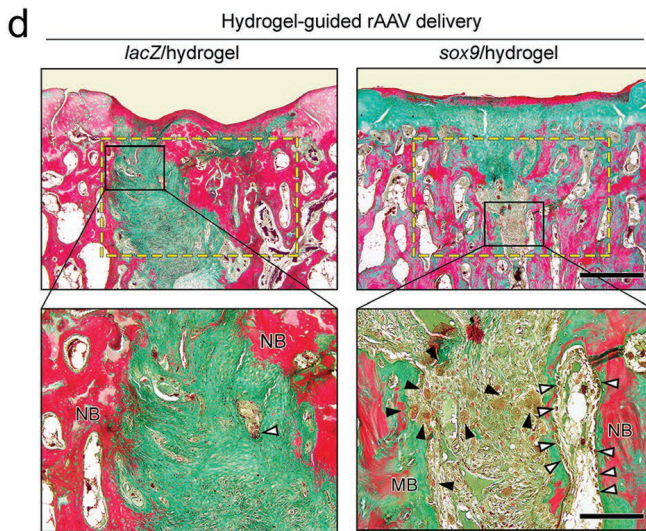
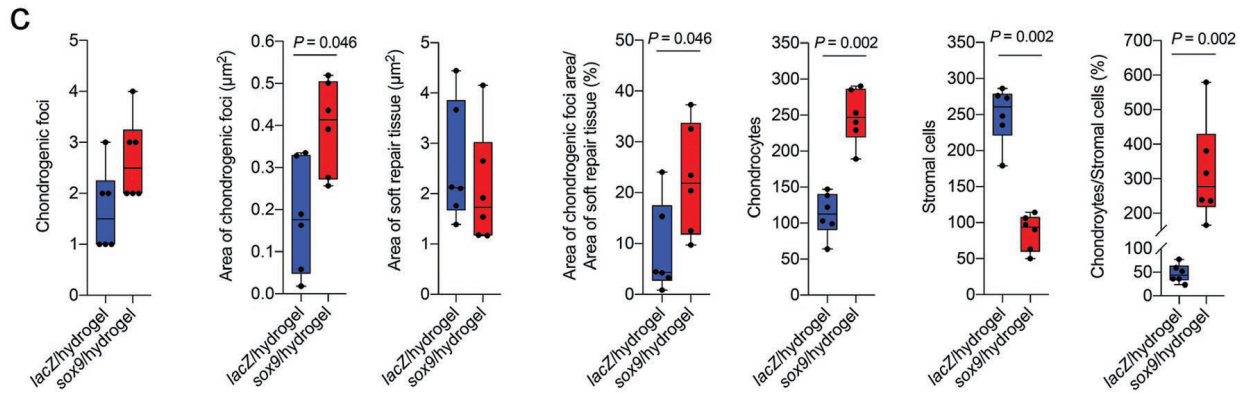
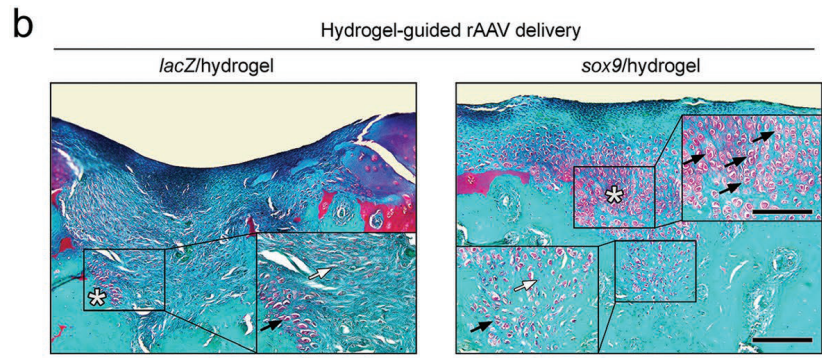
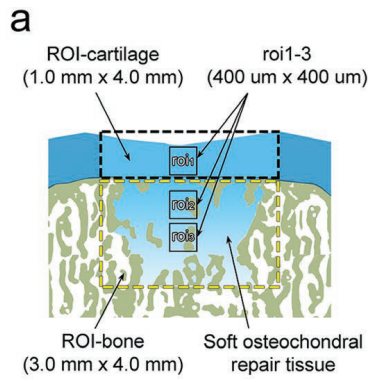


**Figure 15.** Histomorphometric analyses of chondrogenesis and osteogenesis in the osteochondral unit of minipig chondral defects upon microfracture and application of *sox9*/hydrogel versus *lacZ*/hydrogel. (a) Illustration of the regions of interest (ROIs). ROIs of the osteochondral unit include both articular cartilage (ROI-cartilage; black dashed rectangle) and subchondral bone (ROI-bone; yellow dashed rectangle). Quantification of chondrogenic foci was performed within both ROI-cartilage and ROI-bone, while quantification of chondrocytes and bone marrow-derived MSCs was achieved within the center of the osteochondral unit within up to three additional defined ROIs (roi1-3; black rectangles), depending on the depth of the soft osteochondral repair tissue. (b) Representative chondrogenic foci (white \*) with chondrocytes (black arrows) and MSCs (white arrows). Note the more mature and larger chondrogenic foci in the *sox9*/hydrogel defects than in the *lacZ*/hydrogel defects. (c) Significantly larger area of chondrogenic foci and area ratio of chondrogenic foci to soft repair tissue with considerably more chondrocytes, less MSCs, and higher cellularity ratio of chondrocytes to MSCs in the osteochondral repair tissue in the *sox9*/hydrogel defects than the *lacZ*/hydrogel defects. The numbers of chondrogenic foci and area of soft repair tissue are comparable between both groups (source: Madry\*, Gao\* et al., 2020a).

**Table 12.** Estimation of chondrogenic foci and stereological cells in the defects

Parameter	Hydrogel-guided rAAV delivery		P value
	<i>lacZ</i> /hydrogel	<i>sox9</i> /hydrogel	
Chondrogenic foci			
Foci number	1.67 ± 0.82	2.67 ± 0.82	0.093
Foci area (µm <sup>2</sup> )	0.18 ± 0.13	0.40 ± 0.11	0.046
Soft repair tissue area (µm <sup>2</sup> )	2.58 ± 1.20	2.10 ± 1.15	0.394
Foci area/soft repair tissue area (%)	8.71 ± 9.05	22.64 ± 10.85	0.046
Stereological cell counting			
Chondrocytes	112.17 ± 30.18	247.67 ± 37.59	0.002
MSCs	249.50 ± 39.42	86.67 ± 25.07	0.002
Chondrocytes/MSCs (%)	47.27 ± 19.39	319.70 ± 147.49	0.002

(source: Madry\*, Gao\* et al., 2020a).

### 7.1.5. Effects of SOX9 overexpression via rAAV-FLAG-hsox9/PEO-PPO-PEO hydrogel mediated gene transfer on the entire region below the cartilage defect in minipig chondral defects

As microfracture also exerts effects on the subchondral bone (Orth, Madry, 2015), we also searched for possible subchondral bone changes in the defects (**Figure 16**). Histomorphometric analyses evidence newly formed bone always located at the margin of the soft repair tissue. Application of the *sox9*/hydrogel led to a significantly higher total osteoclast ( $P = 0.004$ ) and osteoblast ( $P = 0.002$ ) density in the repair tissue and marrow cavity than the control group (**Figures 15d and 15e**). 2D bony structure parameters (bone volume fraction, BV/TV; trabecular thickness, Tb.Th; trabecular separation, and Tb.Sp; trabecular number, Tb.N) and measurements of structural components (marrow cavity, mature and new bone, and repair tissue) were not significantly different ( $P \geq 0.05$ ) (**Figures 15f and 15g and Table 13**).

Applying a micro-CT-based algorithm (Gao et al., 2016), residual microfracture holes, perihole bone resorption, and intralesional osteophytes (*lacZ*/hydrogel:  $n = 2$ ; *sox9*/hydrogel:  $n = 1$ ) were identified in both groups without significant differences ( $P \geq 0.05$ ) (**Figure 16**). An analysis of all 18 microfracture holes per group showed no significant differences in the perihole bone resorption and bone bridge height between groups ( $P \geq 0.05$ ) (**Tables 14 and 15**). Microstructural evaluation of the entire region below the cartilage defect revealed a considerable early affection of the subchondral bone plate in both groups, with decreased BV/TV, specific bone surface (BS/BV), bone surface density (BS/TV), and cortical thickness (Ct.Th) compared with the normal osteochondral unit (**Figure 17**). Of special importance, *sox9*/hydrogel treatment led to a significantly higher BV/TV of the subchondral bone plate than the control treatment ( $P = 0.002$ ), suggesting a preserving effect of the *sox9*/hydrogel on the subchondral bone plate. The subarticular spongiosa was less affected by such changes, as no differences of BV/TV, BS/BV, and Tb.Th were found between the normal osteochondral unit and defects treated by either the *lacZ*/hydrogel or the *sox9*/hydrogel ( $P \geq 0.05$ ). Treatment with the *lacZ*/hydrogel yielded significantly less BS/TV than the normal osteochondral unit ( $P = 0.002$ ) (**Table 16**).

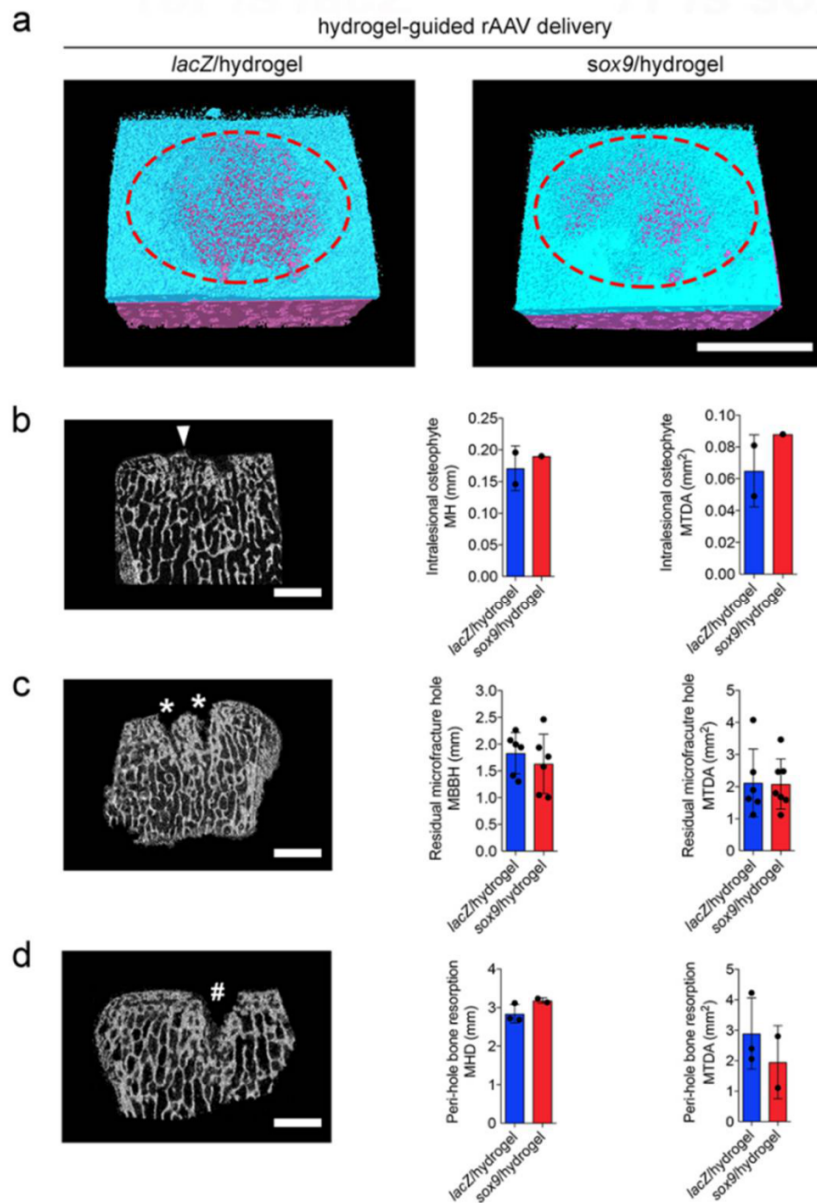


**Figure 16.** Qualitative analyses of subchondral bone changes in minipig chondral defects upon microfracture and application of *sox9*/hydrogel versus *lacZ*/hydrogel. (a) Representative 3D construction of defects with subchondral bone plate in blue and subarticular spongiosa in red (defect margin with a red dashed ellipse). Note the more intact subchondral bone plate within the defect region of the *sox9*/hydrogel defects than the *lacZ*/hydrogel defects. (b) Analysis of intralesional osteophytes (including maximal height (MH) and maximal two-dimensional area - MTDA). (c) Analysis of residual microfracture holes and maximal height of bone bridge (MBBH) and MTDA. (d) Analysis of peri-hole resorption. Scale bar: 2.0 mm (source: Madry\*, Gao\* et al., 2020a).

**Table 13.** Areas occupied by marrow cavity, mature bone, new bone, and repair tissue in ROIs of subchondral bone

Parameter	Hydrogel-guided rAAV delivery				P value
	<i>lacZ</i> /hydrogel		<i>sox9</i> /hydrogel		
	Area (mm <sup>2</sup> )	<sup>a</sup> Area percentage (%)	Area (mm <sup>2</sup> )	<sup>a</sup> Area percentage (%)	
Marrow cavity	1.37 ± 0.39	38.56	2.78 ± 1.06	23.19	0.109
Mature bone	0.83 ± 0.27	27.18	3.03 ± 1.01	25.25	0.109
New bone	4.30 ± 0.51	50.75	3.64 ± 0.21	30.30	0.109
Repair tissue	5.50 ± 1.12	112.01	2.55 ± 1.98	21.26	0.109

<sup>a</sup>Ratio of area of specific tissue type to area of region of interest of subchondral bone (12 mm<sup>2</sup>) (source: Madry\*, Gao\* et al., 2020a).

**Table 14.** Intralesional osteophytes in the defects

Systems	Defect number	Intralesional osteophytes			
		Number	MH (mm)	MW (mm)	MTDA (mm <sup>2</sup> )
<i>lacZ</i> /hydrogel	#1	1	0.146	0.471	0.049
	#2	1	0.196	0.376	0.081
	#3	0	n.a.	n.a.	n.a.
	#4	0	n.a.	n.a.	n.a.
	#5	0	n.a.	n.a.	n.a.
	#6	0	n.a.	n.a.	n.a.
<i>sox9</i> /hydrogel	#1	1	0.190	0.501	0.088
	#2	0	n.a.	n.a.	n.a.
	#3	0	n.a.	n.a.	n.a.
	#4	0	n.a.	n.a.	n.a.
	#5	0	n.a.	n.a.	n.a.
	#6	0	n.a.	n.a.	n.a.

MH, maximal height; MW, maximal width; MTDA, maximal two-dimensional area; n.a., not applicable (source: Madry\*, Gao\* et al., 2020a).

**Table 15.** Subchondral bone changes in the defects

Systems	Defect number	Residual microfracture holes				Peri-hole bone resorption						
		Number	MHD (mm)	MVD (mm)	MTDA (mm)	MBBH (mm)	Number	MHD (mm)	MVD (mm)	MTDA (mm)	MBBH (mm)	
<i>lacZ</i> /hydrogel	#1	2	1.146	1.856	1.124	2.072	0	n.a.	n.a.	n.a.	n.a.	
			1.303	2.609	2.450	1.996						
	#2	2	1.625	2.262	4.078	2.262	0	n.a.	n.a.	n.a.	n.a.	
			0.919	1.631	1.624	1.300						
	#3	0	n.a.	n.a.	n.a.	n.a.	1	3.114	2.137	2.055	-	
	#4	0	n.a.	n.a.	n.a.	n.a.	1	2.686	2.788	4.225	-	
	#5	0	n.a.	n.a.	n.a.	n.a.	1	2.718	2.069	2.393	-	
	#6	2	1.569	2.029	1.895	1.941	0	n.a.	n.a.	n.a.	n.a.	
			1.266	1.702	1.530	1.413						
	<i>sox9</i> /hydrogel	#1	0	n.a.	n.a.	n.a.	n.a.	1	3.232	2.890	2.800	1.340
		#2	0	n.a.	n.a.	n.a.	n.a.	1	3.134	0.836	1.105	0.655
		#3	2	1.245	1.332	1.679	1.048	0	n.a.	n.a.	n.a.	n.a.
1.726				2.400	3.464	1.767						
#4		2	1.232	1.552	1.114	1.003	0	n.a.	n.a.	n.a.	n.a.	
			1.068	2.009	1.585	1.582						
#5		1	1.815	2.187	2.479	n.a.	0	n.a.	n.a.	n.a.	n.a.	
#6		2	1.394	2.464	2.464	2.460	0	n.a.	n.a.	n.a.	n.a.	
			1.805	1.936	1.797	1.936						

MHD, maximal horizontal distance; MVD, maximal vertical distance; MTDA, maximal two-dimensional area; MBBH, maximal bone bridge height; n.a., not applicable (source: Madry\*, Gao\* et al., 2020a).

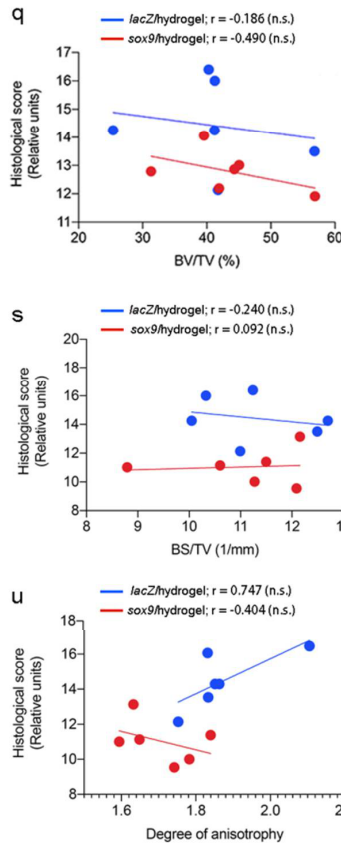
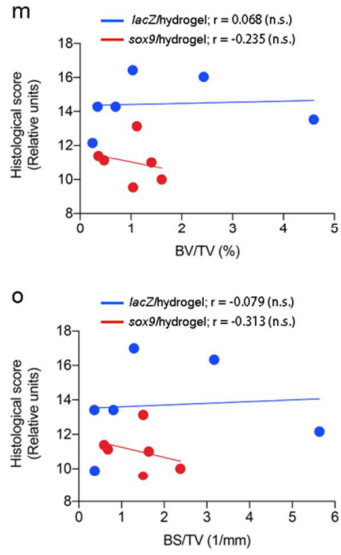
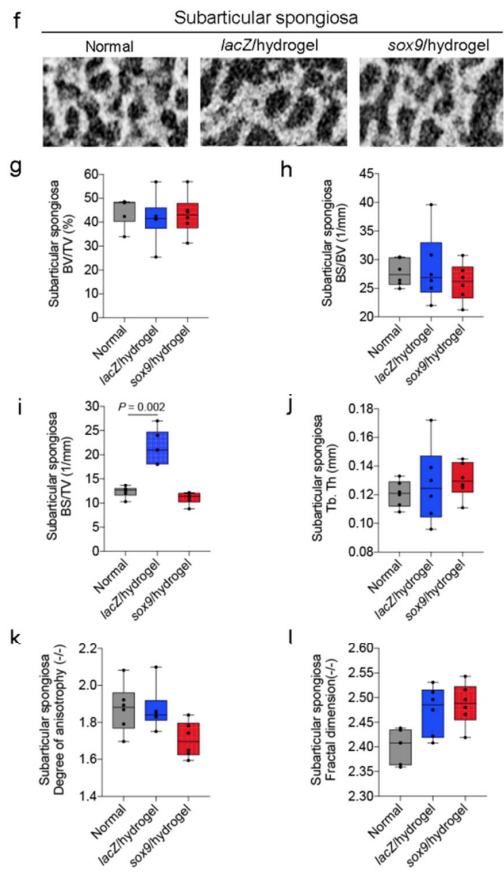
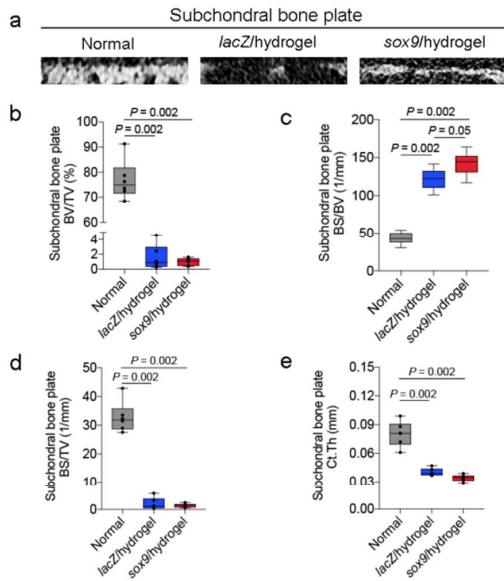


**Figure 17.** Quantitative analysis of subchondral bone changes in minipig chondral defects upon microfracture and application of *sox9*/hydrogel versus *lacZ*/hydrogel. **(a)** Representative micro-CT ROI of subchondral bone plate. **(b-e)** Compared with a normal osteochondral unit (adjacent to defects), both groups yielded significant decreases of BV/TV, BS/BV, BS/TV, and Ct.Th within the subchondral bone plate. No difference of micro-CT parameters (BV/TV, BS/TV, and Ct.Th) between both treatment groups were observed except the significantly less BS/BV of the subchondral bone plate in the *lacZ*/hydrogel defects than the *sox9*/hydrogel defects. **(f)** Representative micro-CT ROI of subarticular spongiosa. **(g-l)** No significant differences of BV/TV, BS/BV, BS/TV, Tb.Th, and DA, and FD between a normal osteochondral unit, *lacZ*/hydrogel defects, and *sox9*/hydrogel defects. Only significant difference was observed regarding BS/TV between a normal osteochondral unit and in the *lacZ*/hydrogel defects. **(m-p)** Correlation analysis between histological score and micro-CT parameters of the subchondral bone plate. Moderate negative correlation was identified between histological score and BV/TV and BS/TV in the *sox9*/hydrogel defects. **(q-v)** Correlation analysis between histological score and micro-CT parameters of the subarticular spongiosa (source: Madry\*, Gao\* et al., 2020a).

**Table 16.** Micro-CT parameters of the subchondral bone plate and subarticular spongiosa in the defects

Parameter	Hydrogel-guided rAAV delivery		Mean difference	<sup>a</sup> P value	Normal Osteochondral unit	<sup>b</sup> P value	<sup>c</sup> P value
	<i>lacZ</i> /hydrogel	<i>sox9</i> /hydrogel					
Subchondral bone plate							
BMD (mg/cm <sup>3</sup> )	674.62 ± 38.32	635.97 ± 17.82	38.65	0.070	752.33 ± 70.33	0.052	0.054
BV/TV (%)	1.68 ± 1.86	1.00 ± 0.50	0.68	1.000	78.92 ± 3.63	0.002	0.002
BS/BV (1/mm)	121.60 ± 15.40	142.23 ± 15.56	20.63	0.050	43.39 ± 10.19	0.002	0.002
BS/TV (1/mm)	2.08 ± 2.31	1.38 ± 0.66	0.70	0.930	34.02 ± 6.81	0.002	0.002
Ct.Th (mm)	0.09 ± 0.03	0.11 ± 0.03	0.02	0.130	0.70 ± 0.17	≤ 0.001	≤ 0.001
Subarticular spongiosa							
BMD (mg/cm <sup>3</sup> )	886.97 ± 112.43	864.55 ± 33.55	22.42	0.180	863.89 ± 63.23	0.662	1.000
BV/TV (%)	41.28 ± 11.12	43.16 ± 8.37	1.88	0.540	45.90 ± 5.64	0.329	0.589
BS/BV (1/mm)	28.76 ± 6.84	26.08 ± 3.31	2.68	0.660	28.08 ± 3.39	1.000	0.310
BS/TV (1/mm)	11.07 ± 1.26	11.31 ± 1.22	0.24	1.000	12.78 ± 1.29	0.026	0.126
Tb.Th (mm)	0.13 ± 0.03	0.13 ± 0.01	0	0.790	0.14 ± 0.04	0.792	0.818
Tb.Sp (mm)	0.22 ± 0.10	0.20 ± 0.04	0.02	1.000	0.41 ± 0.62	0.662	0.310
Tb.Pf (mm <sup>-1</sup> )	-1.76 ± 1.87	-3.69 ± 3.89	1.93	0.430	-1.77 ± 2.18	0.931	0.589
Tb.N (1/mm)	3.20 ± 0.45	3.32 ± 0.56	0.12	0.430	3.30 ± 1.53	0.126	0.240
SMI (-/-)	1.07 ± 0.63	0.55 ± 0.72	0.52	0.430	0.56 ± 0.35	0.126	1.000
DA (-/-)	1.82 ± 0.04	1.71 ± 0.10	0.11	0.050	0.45 ± 0.05	0.004	0.002
FD (-/-)	2.47 ± 0.05	2.49 ± 0.04	0.02	0.540	2.41 ± 0.06	0.126	0.041

BMD, bone mineral density; BV/TV, bone volume fraction; BS/BV, specific bone surface; BS/TV, bone surface density; Ct.Th, cortical thickness; Tb.Th, trabecular thickness; Tb.Sp, trabecular separation; Tb.Pf, trabecular pattern factor; Tb.N, trabecular number; SMI, structure model index; DA, degree of anisotropy; FD, fractal dimension. *P* value for <sup>a</sup>*lacZ*/hydrogel versus *sox9*/hydrogel, <sup>b</sup>*lacZ*/hydrogel versus normal osteochondral unit, and <sup>c</sup>*sox9*/hydrogel versus normal osteochondral unit (source: Madry\*, Gao\* et al., 2020a).

## 7.2. IGF-I *in vivo* study

### 7.2.1. Effective overexpression of IGF-I via rAAV/alginate-mediated gene transfer in chondral defects in minipigs *in vivo*

The IGF-I/AlgPH155 hydrogel system was applied to chondral defects in minipigs in a bilateral surgical approach to examine its ability to promote IGF-I gene delivery and overexpression over time (one year) relative to the *lacZ*/AlgPH155 hydrogel system without additional test conditions to comply with the 3R principle (Hampshire, Gilbert, 2019; Orth et al., 2013b). An estimation of IGF-I expression in the repair tissue of the defects after one year via immunohistochemical analysis showed significantly higher levels of IGF-I-positive cells in the defects treated with IGF-I/AlgPH155 relative to the *lacZ*/AlgPH155 defects ( $58.8\% \pm 13.9\%$  versus  $43.6\% \pm 14.4\%$  IGF-I-immunostained cells, i.e., a 1.3-fold difference,  $P = 0.034$ ) (**Figure 18**) (Cucchiaroni, Madry, 2014). Interestingly, IGF-I expression was also noted at this time point in the cartilage surrounding the IGF-I/AlgPH155 defects versus that of the *lacZ*/AlgPH155 defects ( $49.2\% \pm 3.3\%$  versus  $12.3\% \pm 2.5\%$  IGF-I-immunostained cells, i.e., a 4-fold difference,  $P \leq 0.001$ ) (**Figure 18**). No IGF-I expression was observed at broader sites (synovium, quadriceps muscle adjacent to the patella, infrapatellar pad, subchondral bone marrow).

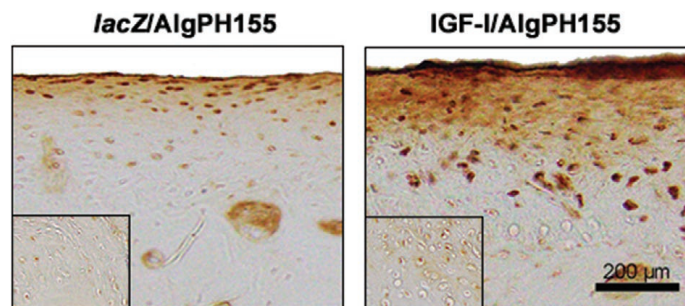


**Figure 18.** Transgene (IGF-I) expression in rAAV/AlgPH155-treated minipig chondral defects. The IGF-I/AlgPH155 and *lacZ*/AlgPH155 hydrogel systems ( $25 \mu\text{l}$  per defect;  $3.6 \times 10^5$  transgene copies) were implanted for one year in chondral defects (4 mm diameter, 5 mm depth) in the lateral, distal femur trochlea of minipigs following microfracture. The osteochondral units containing the defects were retrieved after one year and processed for immunodetection of IGF-I expression (insets: IGF-I in the cartilage surrounding the defects; all representative data) (source: Maihöfer\*, Madry\* et al., 2021).

7.2.2. Effects of IGF-I overexpression via rAAV/alginate-mediated gene transfer on the repair processes in minipig chondral defects over time

The rAAV/alginate-treated defects were processed to determine the effects of the IGF-I/AlgPH155 treatment on the macroscopic, histological, and biological repair processes over time *versus lacZ/AlgPH155*. After one year, there was no significant difference between IGF-I/AlgPH155 and *lacZ/AlgPH155* in the categories of a semiquantitative scoring system that grades the macroscopic repair of defects ( $P \geq 0.145$ ) (**Figure 19 and Table 17**) (Goebel et al., 2017) without osteophyte formation, macroscopic synovitis, nor of immune cell infiltration (absence of CD3, CD11b, and HLA-DR $\alpha$  expression).

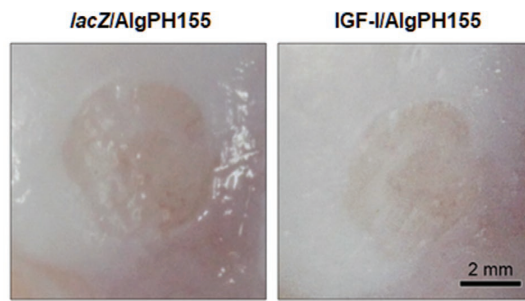


**Figure 19.** Macroscopic repair of rAAV/AlgPH155-treated minipig chondral defects. The IGF-I/AlgPH155 and *lacZ/AlgPH155* hydrogels were implanted in the defects and the osteochondral units containing the defects were retrieved after one year for macroscopic evaluation (all representative data) (source: Maihöfer\*, Madry\* et al., 2021).

**Table 17.** Macroscopic scoring of cartilage repair in the defects (IGF-I study)

Category	<i>lacZ/AlgPH155</i>	IGF-I/AlgPH155	P value
Color	1.38 ± 0.79	1.79 ± 0.81	0.145
Blood vessels	0.79 ± 0.60	1.13 ± 0.79	0.231
Surface	1.13 ± 0.66	1.08 ± 0.73	0.865
Filling	1.00 ± 0.94	1.38 ± 1.01	0.362
Adjacent cartilage	1.42 ± 0.89	1.79 ± 1.17	0.412
Total score	5.63 ± 2.62	7.08 ± 3.03	0.261

The macroscopic repair in the defects was evaluated using a semiquantitative score (Goebel et al., 2017). Values are given as mean ± SD.

Histological analysis performed on safranin O-stained sections using a validated inverse complex score that grades the microscopic structure of the repair tissue revealed significant improvements in the individual parameters "filling of the defect", "cellular morphology", and "architecture of the defect surface" (all  $P \leq 0.001$ ) at one year (Sellers et al., 1997). Most importantly, the total histological score was significantly ( $P = 0.015$ ) better in the IGF-I/AlgPH155 *versus* lacZ/AlgPH155 defects after one year, with a trend toward improved matrix staining and restrained architecture and subchondral bone plate ( $P \leq 0.019$ ) (**Figure 20 and Table 18**).

An evaluation of the cell densities on safranin O and HE-stained sections at this time point identified significantly higher values in the repair tissue of the defects treated with IGF-I/AlgPH155 compared with those that received lacZ/AlgPH155 (1.2-fold difference,  $P = 0.005$ ) (**Figure 20 and Table 19**) (Cucchiaroni, Madry, 2014; Frisch et al., 2014b).

An estimation of the type-II collagen intensities on immunostained sections using a semiquantitative score revealed a significantly stronger deposition of this major ECM component in the repair tissue of defects that received IGF-I/AlgPH155 *versus* lacZ/AlgPH155 after one year (1.3-fold difference,  $P = 0.037$ ) (**Figure 21a and Table 19**) (Orth et al., 2013a). Instead, there was no difference in the deposition of type-I collagen at this time point between the IGF-I/AlgPH155 and lacZ/AlgPH155 defects ( $P = 0.203$ ) (**Figure 21b and Table 19**) (Orth et al., 2013a).

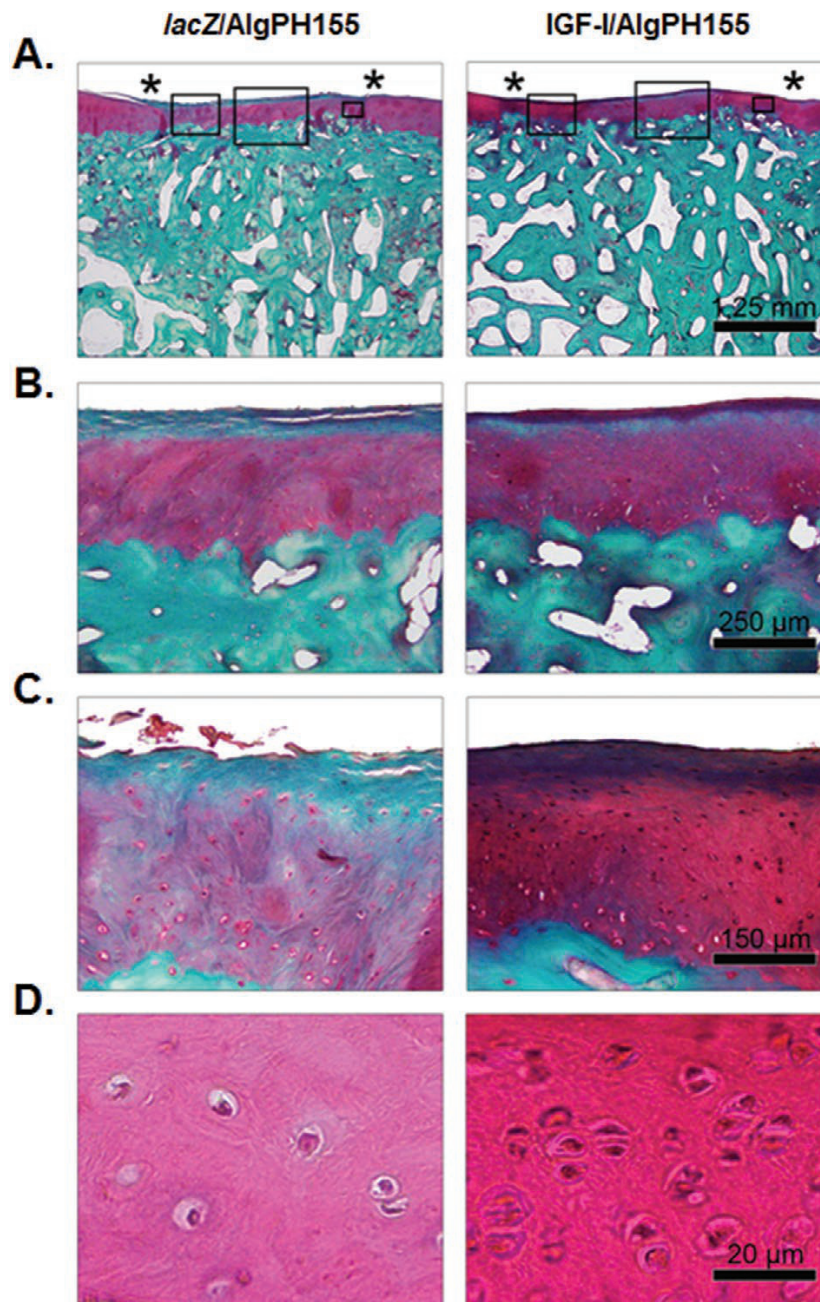


**Figure 20.** Histological repair of rAAV/AlgPH155-treated minipig chondral defects. The IGF-I/AlgPH155 and *lacZ*/AlgPH155 hydrogel systems were implanted in the minipig chondral defects and the osteochondral units containing the defects were retrieved after one year and processed for safranin O and HE staining. The (\*) indicate the integration sites and the boxes in (A) present the zones depicted in (B-D) (source: Maihöfer\*, Madry\* et al., 2021).

**Table 18.** Histological scoring of cartilage repair in the defects (IGF-I study)

Category	<i>lacZ/AlgPH155</i>	IGF-I/AlgPH155	P value
Filling of the defect	1.54 ± 0.89	0.92 ± 0.40	< 0.001*
Integration	1.13 ± 0.33	1.19 ± 0.40	0.183
Main staining	2.56 ± 0.75	2.49 ± 0.84	0.561
Cellular morphology	1.85 ± 0.47	1.59 ± 0.49	< 0.001*
Architecture of the defect	1.00 ± 0.65	1.31 ± 1.15	0.008*
Architecture of the surface	1.11 ± 0.36	0.86 ± 0.42	< 0.001*
Subchondral bone plate	1.14 ± 1.13	1.42 ± 0.96	0.019*
Tidemark	4.00 ± 0.00	3.96 ± 0.20	0.072
Total score	14.32 ± 2.67	13.74 ± 2.56	0.015*

The repair processes in the defects were evaluated on safranin O-stained histological sections using a semiquantitative inverse complex cartilage repair score (Sellers et al., 1997). Values are given as mean ± standard deviation (SD). \*Statistically significant *versus lacZ/AlgPH155* (source: Maihöfer\*, Madry\* et al., 2021).

**Table 19.** Cell densities and type-II/-I collagen deposition in the defects

Parameter	<i>lacZ/AlgPH155</i>	IGF-I/AlgPH155	P value
Cell densities (cells/mm <sup>2</sup> )	296 ± 67	366 ± 36	0.005*
Type-II collagen	2.3 ± 0.5	3.0 ± 0.6	0.037*
Type-I collagen	1.6 ± 0.5	1.9 ± 0.6	0.203

The cell densities were evaluated on safranin O and HE-stained histological sections. The deposition of type-II/-I collagen in the defects was evaluated on immunohistochemical sections using a semiquantitative score (0 = no immunoreactivity; 1 = significantly reduced immunoreactivity; 2 = moderately reduced immunoreactivity; 3 = similar immunoreactivity; 4 = stronger immunoreactivity compared with the controls) (Orth et al., 2013a). Values are given as mean ± standard deviation (SD). \*Statistically significant *versus lacZ/AlgPH155* (source: Maihöfer\*, Madry\* et al., 2021).

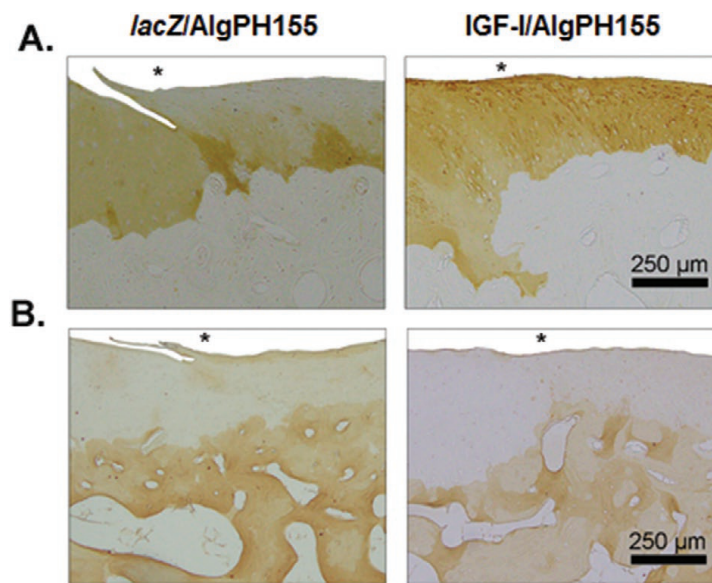


**Figure 21.** Expression of ECM components in rAAV/AlgPH155-treated minipig chondral defects. The IGF-I/AlgPH155 and *lacZ*/AlgPH155 hydrogel systems were implanted in the minipig chondral defects. (A,B) The osteochondral units containing the defects were retrieved after one year and processed to evaluate the deposition of type-II collagen (A) and type-I collagen (B) by immunohistochemistry (source: Maihöfer\*, Madry\* et al., 2021).

### 7.2.3. Effects of IGF-I overexpression via rAAV/alginate-mediated gene transfer on the inflammatory responses and perifocal OA in minipig chondral defects over time

The rAAV/alginate-treated defects were next examined to monitor a potential protection mediated by the IGF-I/AlgPH155 hydrogel system against inflammation and perifocal OA relative to *lacZ*/AlgPH155. An analysis of OA features in the cartilage adjacent to the defects using an established inverse OA score showed a significantly reduced overall perifocal OA around the defects treated with IGF-I/AlgPH155 relative to *lacZ*/AlgPH155 after one year (1.2-fold difference,  $P = 0.048$ ) (Little et al., 2010), with trends toward improved individual parameters of adjacent cartilage structure, cell cloning, interterritorial staining, and tidemark/subchondral bone at this time point (up to 1.6-fold difference,  $P \geq 0.081$ ) (Figure 22 and Table 20).

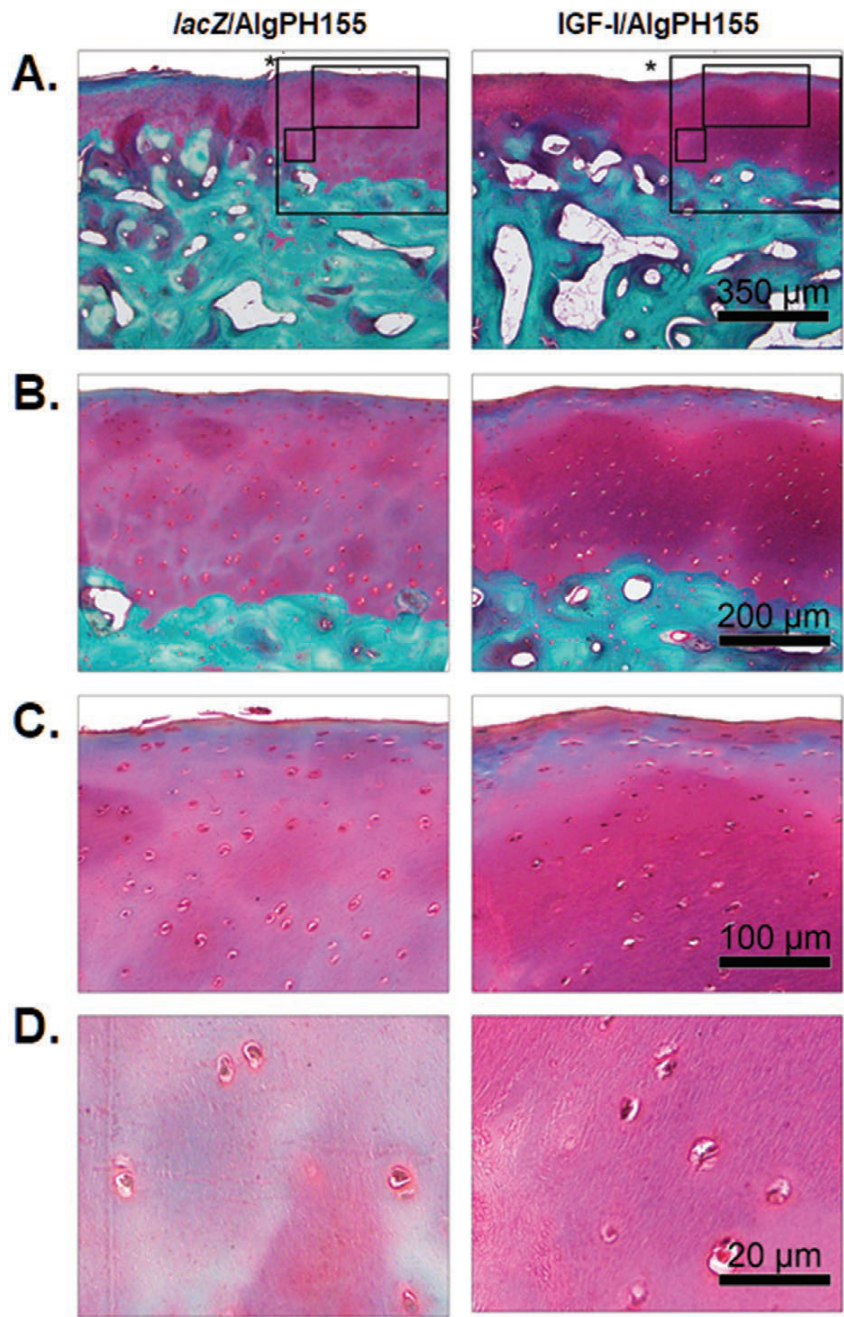


**Figure 22.** Histological analyses of the cartilage adjacent to rAAV/AlgPH155-treated minipig chondral defects. The IGF-I/AlgPH155 and *lacZ*/AlgPH155 hydrogel systems were implanted in the minipig chondral defects. The osteochondral units containing the defects were retrieved after one year and processed for safranin O staining. The (\*) indicate the integration sites and the boxes in (A) present the zones depicted in (B-D) (source: Maihöfer\*, Madry\* et al., 2021).

**Table 20.** OA signs in the cartilage adjacent to the defects

Category	<i>lacZ</i> /AlgPH155	IGF- <i>I</i> /AlgPH155	<i>P</i> value
Structure	1.18 ± 0.63	0.76 ± 0.68	0.081
Chondrocyte density	1.33 ± 0.47	1.39 ± 0.49	0.738
Cell cloning	3.54 ± 0.71	3.49 ± 0.81	0.946
Interterritorial staining	1.11 ± 0.32	1.07 ± 0.25	0.585
Tidemark, subchondral bone	1.83 ± 0.37	1.52 ± 0.69	0.159
Total score	9.00 ± 1.05	7.71 ± 2.46	0.048*

Signs of OA in the adjacent cartilage were evaluated on safranin O-stained sections using an established semiquantitative score (Little et al., 2010). Values are given as mean ± SD. \*Statistically significant *versus lacZ*/AlgPH155 (source: Maihöfer\*, Madry\* et al., 2021).

An evaluation of the inflammatory responses by immunohistochemistry revealed significantly decreased levels of IL-1 $\beta$  and TNF- $\alpha$  expression in the repair tissue of defects receiving IGF-*I*/AlgPH155 *versus lacZ*/AlgPH155 after one year (16% ± 3% *versus* 88% ± 4% IL-1 $\beta$ -immunostained cells, i.e., 5.6-fold decrease, and 4% ± 1% *versus* 86% ± 3% TNF- $\alpha$ -immunostained cells, i.e., a 22.8-fold decrease, always  $P \leq 0.001$ ) (**Figure 23**). Similar results were noted when evaluating the levels of IL-1 $\beta$  and TNF- $\alpha$  expression in the cartilage surrounding the defects (7% ± 3% *versus* 67% ± 3% IL-1 $\beta$ -immunostained cells, i.e., 10.3-fold decrease, and 4% ± 2% *versus* 72% ± 3% TNF- $\alpha$ -immunostained cells, i.e., an 18-fold decrease, always  $P \leq 0.001$ ) (**Figure 23**).

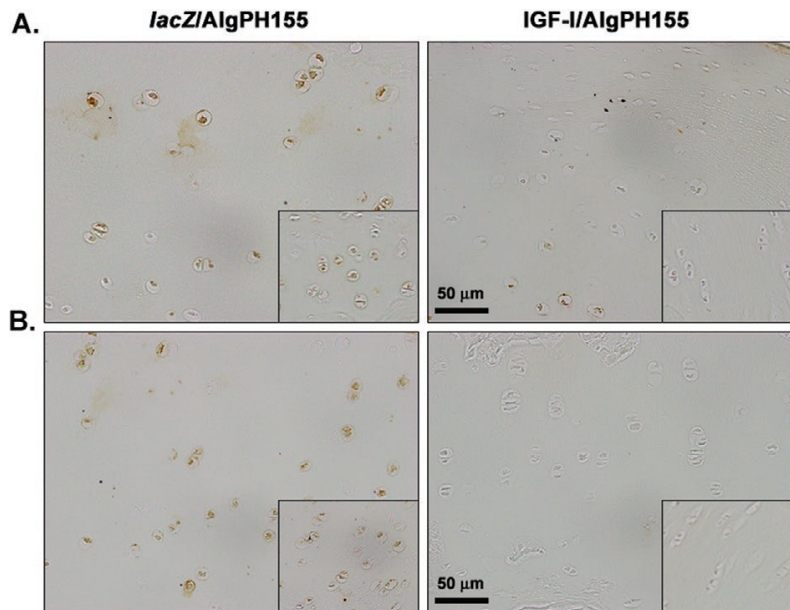


**Figure 23.** Inflammatory responses in the repair tissue and surrounding cartilage of rAAV/AlgPH155-treated minipig chondral defects. The IGF-I/AlgPH155 and *lacZ*/AlgPH155 hydrogel systems were implanted in the minipig chondral defects. **(A,B)** The osteochondral units containing the defects were retrieved after one year and processed to evaluate the expression of IL-1 $\beta$  **(A)** and TNF- $\alpha$  **(B)** by immunohistochemistry in the repair tissue of the defects and in the surrounding cartilage (insets) (source: Maihöfer\*, Madry\* et al., 2021).

### 7.3. TGF- $\beta$ *ex vivo* study

#### 7.3.1. Effective TGF- $\beta$ overexpression via rAAV/pNaSS-grafted PCL films in human bone marrow aspirates

The candidate rAAV-hTGF- $\beta$  vector was coated on pNaSS-grafted PCL films (TGF- $\beta$ /pNaSS-grafted PCL) *versus* ungrafted films (TGF- $\beta$ /ungrafted PCL) to evaluate the capacity of the system to promote TGF- $\beta$  expression over time in human bone marrow aspirates compared with other treatments (pNaSS-grafted and ungrafted PCL films lacking rAAV i.e. no vector/pNaSS-grafted PCL and no vector/ungrafted PCL, respectively) (Venkatesan et al., 2020a, 2020b).

Efficient overexpression of TGF- $\beta$  via rAAV gene delivery was noted in human bone marrow aspirates treated with the TGF- $\beta$ /pNaSS-grafted and TGF- $\beta$ /ungrafted PCL films for 21 days in chondrogenic medium as evidenced by significantly higher levels of TGF- $\beta$  immunodetection *versus* samples receiving films without vector coating (up to 4-fold difference of % TGF- $\beta^+$  cells,  $P \leq 0.001$ ) (**Figure 24 and Table 21**). Notably, the % of TGF- $\beta^+$  cells were higher when providing TGF- $\beta$ /pNaSS-grafted films relative to TGF- $\beta$ /ungrafted films (1.3-fold difference,  $P \leq 0.001$ ) (**Figure 24 and Table 21**).

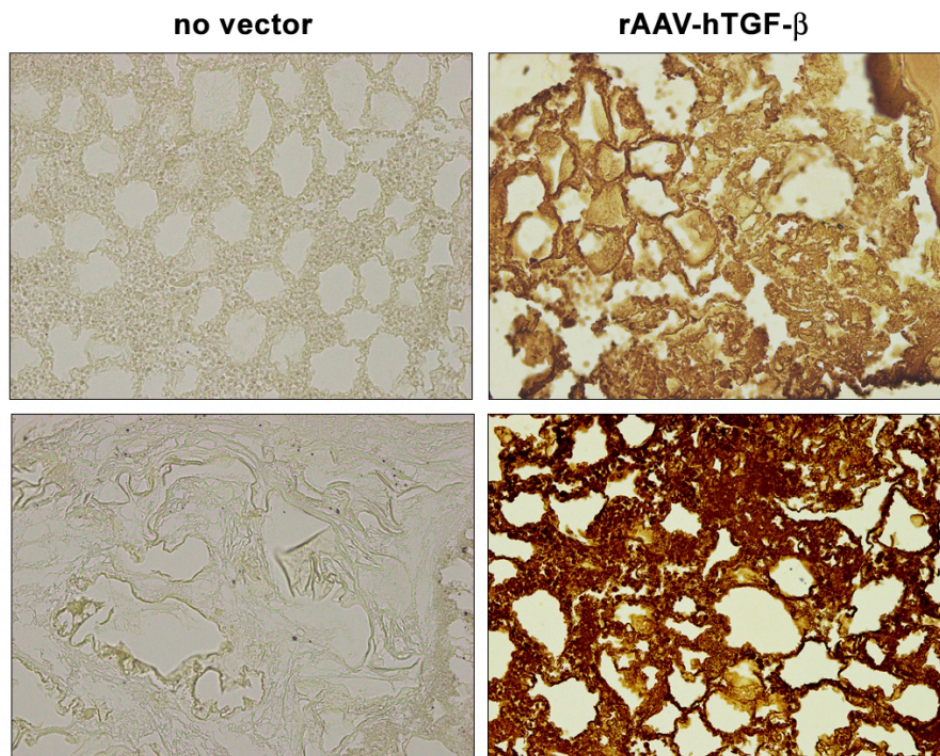


**Figure 24.** Detection of transgene (TGF- $\beta$ ) overexpression in human bone marrow aspirates treated with rAAV TGF- $\beta$ -coated PCL films. pNaSS-grafted and ungrafted PCL films (macroscopic photographs) were coated with rAAV-hTGF- $\beta$  (40  $\mu$ l,  $8 \times 10^5$  transgene copies) or left without vector coating before incubation with the aspirates in chondrogenic medium (150  $\mu$ l,  $6.1 \times 10^7$  hMSCs, i.e., MOI = 75). TGF- $\beta$  expression was monitored by immunohistochemistry after 21 days of culture (magnification x20; all representative data) (source: Venkatesan\*, Cai\* et al., 2021).

**Table 21.** Histomorphometric and biological analyses in human bone marrow aspirates treated with rAAV-coated PCL films

Parameters	No vector/ ungrafted PCL	No vector/ pNaSS-grafted PCL	TGF- $\beta$ / ungrafted PCL	TGF- $\beta$ / pNaSS-grafted PCL
	TGF- $\beta$	1.8 $\pm$ 0.8	2.4 $\pm$ 1.1	72.8 $\pm$ 4.5 <sup>a,b</sup>
Toluidine blue	1.2 $\pm$ 0.4	1.4 $\pm$ 0.5	3.2 $\pm$ 0.4 <sup>a,b</sup>	3.8 $\pm$ 0.4 <sup>a,b,c</sup>
Proteoglycans	35.0 $\pm$ 2.6	35.0 $\pm$ 4.4	45.7 $\pm$ 0.6 <sup>b</sup>	52.7 $\pm$ 1.2 <sup>a,b,c</sup>
Type-II collagen	1.0 $\pm$ 0.7	0.8 $\pm$ 0.8	2.8 $\pm$ 0.4 <sup>a,b</sup>	3.6 $\pm$ 0.5 <sup>a,b,c</sup>
Cell densities	3,850 $\pm$ 120	4,125 $\pm$ 175	5,201 $\pm$ 76 <sup>a,b</sup>	6,475 $\pm$ 89 <sup>a,b,c</sup>
WST-1	0.49 $\pm$ 0.04	0.50 $\pm$ 0.04	0.60 $\pm$ 0.04 <sup>a,b</sup>	1.14 $\pm$ 0.17 <sup>a,b,c</sup>
Alizarin red	2.8 $\pm$ 0.4	2.6 $\pm$ 0.5	1.4 $\pm$ 0.5 <sup>a,b</sup>	0.6 $\pm$ 0.5 <sup>a,b,c</sup>
Type-I collagen	3.2 $\pm$ 0.4	3.4 $\pm$ 0.5	3.0 $\pm$ 0.7	3.2 $\pm$ 0.4
Type-X collagen	3.8 $\pm$ 0.4	3.6 $\pm$ 0.5	3.4 $\pm$ 0.5	1.6 $\pm$ 0.5 <sup>a,b,c</sup>

TGF- $\beta$  is in % TGF- $\beta$ <sup>+</sup> cells/total cell numbers on immunohistochemically stained sections. Sections for toluidine blue staining, type-II/-I/-X collagen immunostaining, and alizarin red staining were scored using a modified Bern grading score with 0 = no staining, 1 = heterogeneous and/or weak staining, 2 = homogeneous and/or moderate staining, 3 = homogeneous and/or intense staining, and 4 = very intense staining (Venkatesan et al., 2020a, 2020b). The proteoglycan contents are in ng/ $\mu$ g total proteins, the cell densities on HE-stained sections in cells/mm<sup>2</sup>, and the results of the WST-1 assay as OD<sup>450</sup> nm. Values are provided as mean  $\pm$  standard deviation (SD). Statistically significant relative to <sup>a</sup>no vector/ungrafted PCL, <sup>b</sup>no vector/pNaSS-grafted PCL, and <sup>c</sup>TGF- $\beta$ /ungrafted PCL (source: Venkatesan\*, Cai\* et al., 2021).

These results were corroborated by the findings of a TGF- $\beta$  ELISA revealing prolonged, significantly higher and levels of growth factor production when applying films coated with rAAV-hTGF- $\beta$  relative to the other treatments (up to 12.4-fold difference,  $P \leq 0.001$ ) and a superior effect when using pNaSS-grafted PCL films (up to 2.3-fold difference relative to ungrafted films,  $P \leq 0.001$ ) (**Table 22**). Of further note, increases in

TGF- $\beta$  expression were significantly measured over time when using films coated with rAAV-hTGF- $\beta$  (up to 2.3-fold difference between days 14 and 21,  $P \leq 0.001$ ) (**Table 22**).

**Table 22.** Transgene (TGF- $\beta$ ) expression in human bone marrow aspirates treated with rAAV-coated PCL films

Days post-treatment	No vector/ ungrafted PCL	No vector/ pNaSS-grafted PCL	TGF- $\beta$ / ungrafted PCL	TGF- $\beta$ / pNaSS-grafted PCL
	14	114.3 $\pm$ 4.1	165.6 $\pm$ 5.2	672.2 $\pm$ 10.3 <sup>a,b</sup>
21	128.1 $\pm$ 3.7	177.6 $\pm$ 4.3	696.5 $\pm$ 8.8 <sup>a,b</sup>	1,585.6 $\pm$ 19.3 <sup>a,b,c,d</sup>

Values are expressed as mean  $\pm$  SD in  $\mu\text{g/ml}/24$  h. Statistically significant relative to <sup>a</sup>no vector/ungrafted PCL, <sup>b</sup>no vector/pNaSS-grafted PCL, <sup>c</sup>TGF- $\beta$ /ungrafted PCL, and <sup>d</sup>earlier time point (source: Venkatesan\*, Cai\* et al., 2021).

### 7.3.2. Effects of TGF- $\beta$ overexpression via rAAV/pNaSS-grafted PCL films on the deposition of proteoglycans and type-II collagen and on cell viability in human bone marrow aspirates

The rAAV-hTGF- $\beta$  candidate vector was next provided to human bone marrow aspirates via coating on pNaSS-grafted *versus* ungrafted PCL films to evaluate the potential of the systems to stimulate over time the biological activities and the chondrogenic events in these samples over time compared with other conditions.

Application of rAAV-hTGF- $\beta$  using the pNaSS-grafted and ungrafted PCL films promoted significantly stronger proteoglycan deposition in the aspirates maintained for 21 days in chondrogenic medium as seen by a more important toluidine blue staining relative to the other treatments (up to 3.2-fold difference,  $P \leq 0.001$ ) and with a superior effect when using pNaSS-grafted PCL films (1.2-fold difference relative to ungrafted films,  $P = 0.033$ ) (**Figure 25 and Table 21**). These findings were substantiated by an estimation of the proteoglycan contents in the samples, with higher levels achieved with TGF- $\beta$ /pNaSS-grafted and TGF- $\beta$ /ungrafted PCL films relative to the other treatments (up to 1.5-fold difference,  $P \leq 0.007$ ) and with a superior effect of following pNaSS grafting (1.2-fold difference relative to ungrafted films,  $P \leq 0.001$ ) (**Table 21**). Similar findings were noted

when monitoring type-II collagen deposition, with stronger type-II collagen immunostaining using TGF- $\beta$ /pNaSS-grafted or TGF- $\beta$ /ungrafted PCL films relative to the other treatments (up to 4.5-fold difference,  $P \leq 0.001$ ) and with a superior effect when applying pNaSS-grafted PCL films (1.3-fold difference relative to ungrafted films,  $P = 0.018$ ) (**Figure 25 and Table 21**). Furthermore, gene transfer of rAAV-hTGF- $\beta$  using the pNaSS-grafted and ungrafted PCL films significantly increased the cell proliferation indices in the aspirates relative to the other treatments (cell densities: up to 1.7-fold difference,  $P \leq 0.001$ ; WST-1 assay: up to 2.3-fold difference,  $P \leq 0.001$ ) and with a superior effect when using pNaSS-grafted PCL films (cell densities: 1.2-fold difference relative to ungrafted films,  $P \leq 0.001$ ; WST-1 assay: 1.9-fold difference relative to ungrafted films,  $P \leq 0.001$ ) (**Figure 25 and Table 21**).

### *7.3.3. Effects of TGF- $\beta$ overexpression via rAAV/pNaSS-grafted PCL films on mineralization and type-X collagen deposition in human bone marrow aspirates*

The rAAV-hTGF- $\beta$  candidate vector was then administered to human bone marrow aspirates via coating on pNaSS-grafted *versus* ungrafted PCL films to determine the potential of the systems to limit premature osteogenic events and hypertrophy in these samples over time compared with other conditions.

Application of rAAV-hTGF- $\beta$  using the pNaSS-grafted and ungrafted PCL films significantly decreased matrix mineralization in the aspirates maintained for 21 days in osteogenic medium as seen by a reduced alizarin red staining relative to the other treatments (up to 4.7-fold difference,  $P \leq 0.001$ ) and with a superior effect when using pNaSS-grafted PCL films (2.3-fold difference relative to ungrafted films,  $P = 0.025$ ) (**Figure 26 and Table 21**). In addition, while there was no significant effect of rAAV-hTGF- $\beta$  on osteogenic type-I collagen deposition in the aspirates relative to the other treatments, regardless of the type of film applied ( $P \geq 0.173$ ) (**Figure 26 and Table 21**), administration of the therapeutic candidate via the pNaSS-grafted films significantly decreased hypertrophic type-X collagen deposition relative to the use of ungrafted PCL films and to the other treatments (up to 2.4-fold difference,  $P \leq 0.001$ ) (**Figure 26 and Table 21**).

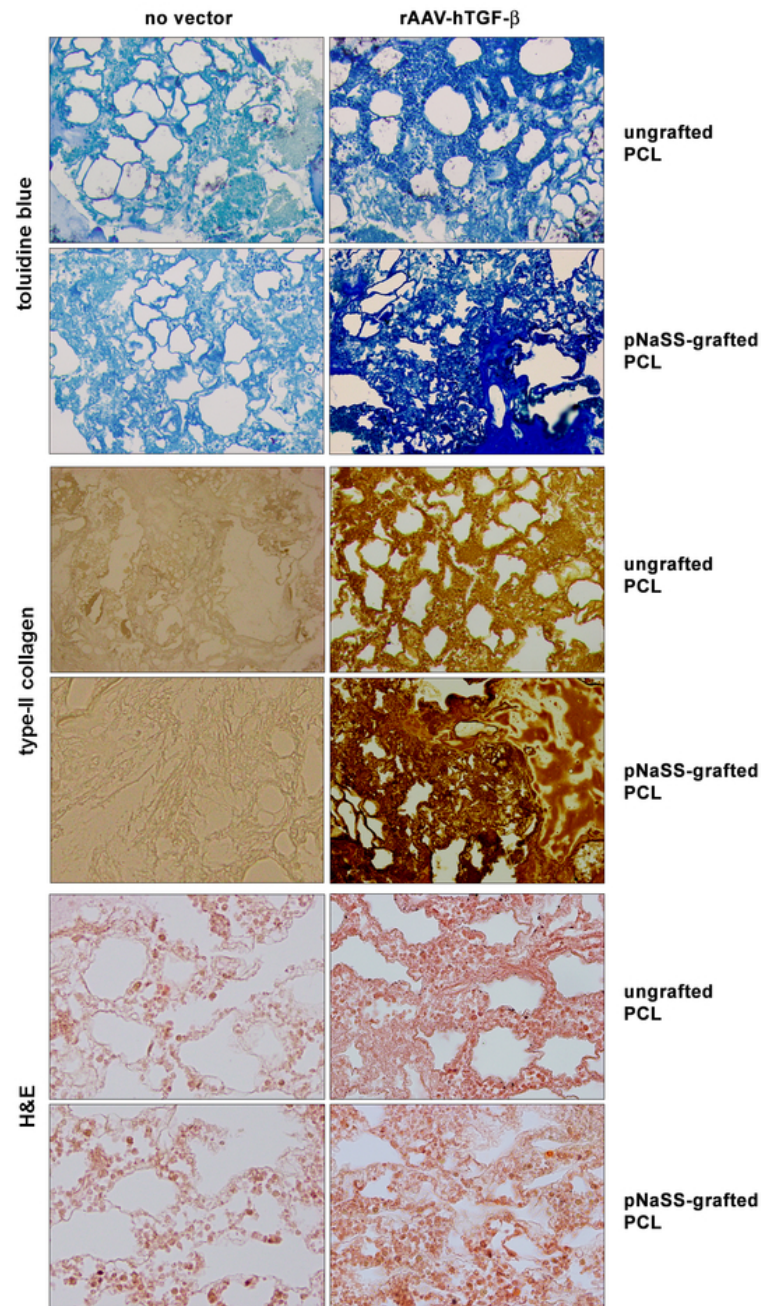


**Figure 25.** Chondroreparative activities in human bone marrow aspirates treated with rAAV-TGF- $\beta$ -coated PCL films. pNaSS-grafted and ungrafted PCL films were coated with rAAV-hTGF- $\beta$  or left without vector coating before incubation with the aspirates in chondrogenic medium. Matrix proteoglycans (toluidine blue staining), type-II collagen (immunohistochemistry), and cellularity (HE staining) were assessed after 21 days of culture (magnification x20 except for HE at magnification x40; all representative data) (source: Venkatesan\*, Cai\* et al., 2021).

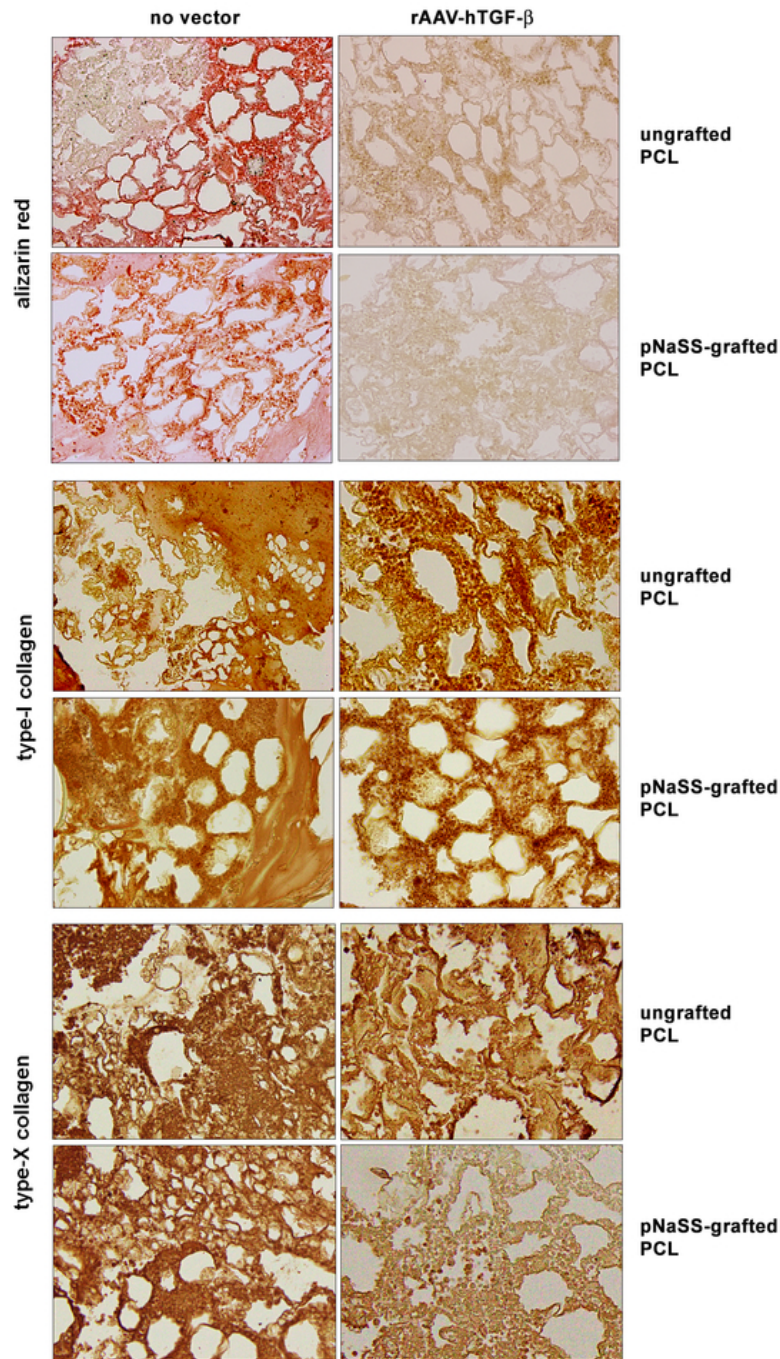


**Figure 26.** Mineralization and type-I and -X collagen deposition in human bone marrow aspirates treated with rAAV-hTGF- $\beta$ -coated PCL films. pNaSS-grafted and ungrafted PCL films were coated with rAAV-hTGF- $\beta$  or left without vector coating before incubation with the aspirates in osteogenic medium. Mineralization (alizarin red staining) and type-I and -X collagen (immunohistochemistry) were assessed after 21 days of culture (magnification x20; all representative data) (source: Venkatesan\*, Cai\* et al., 2021).

#### 7.3.4. Effects of TGF- $\beta$ overexpression via rAAV/pNaSS-grafted PCL films on the chondrogenic expression profiles in human bone marrow aspirates

Overall, such findings were confirmed by real-time RT-PCR analyses of gene expression profiles in the aspirates after 21 days of culture with the candidate rAAV-hTGF- $\beta$  vector provided with pNaSS-grafted and ungrafted PCL films *versus* the other treatments.

In a chondrogenic environment, application of rAAV-hTGF- $\beta$  using the pNaSS-grafted and ungrafted PCL films significantly increased the levels of chondrogenic SOX9, COL2A1, and ACAN expression in the aspirates relative to each respective control treatment (2-, 2.4-, and 1.5-fold difference in the TGF- $\beta$ /ungrafted compared with the ungrafted PCL films, respectively; 12.8-, 5.1-, and 2.4-fold difference, in the TGF- $\beta$ /pNaSS-grafted compared with the pNaSS-grafted PCL films, respectively;  $P \leq 0.001$ ) (**Figures 27a and 27b**) and with a superior effect when using pNaSS-grafted PCL films (14.5-, 4.6-, and 2.2-fold difference in the TGF- $\beta$ /pNaSS-grafted compared with the TGF- $\beta$ /ungrafted PCL films, respectively;  $P \leq 0.001$ ) (**Figure 27c**).

In an osteogenic environment, while there was no significant effect of rAAV-hTGF- $\beta$  on osteogenic COL1A1 expression in the aspirates relative to the other treatments, regardless of the type of film applied ( $P \geq 0.165$ ) (**Figures 26a-26c**), application of rAAV-hTGF- $\beta$  using the pNaSS-grafted PCL films significantly decreased the levels of hypertrophic COL10A1 expression in the aspirates relative to the use of ungrafted PCL films and to the other treatments (up to 3.5-fold difference;  $P \leq 0.001$ ) (**Figures 27a-27c**).

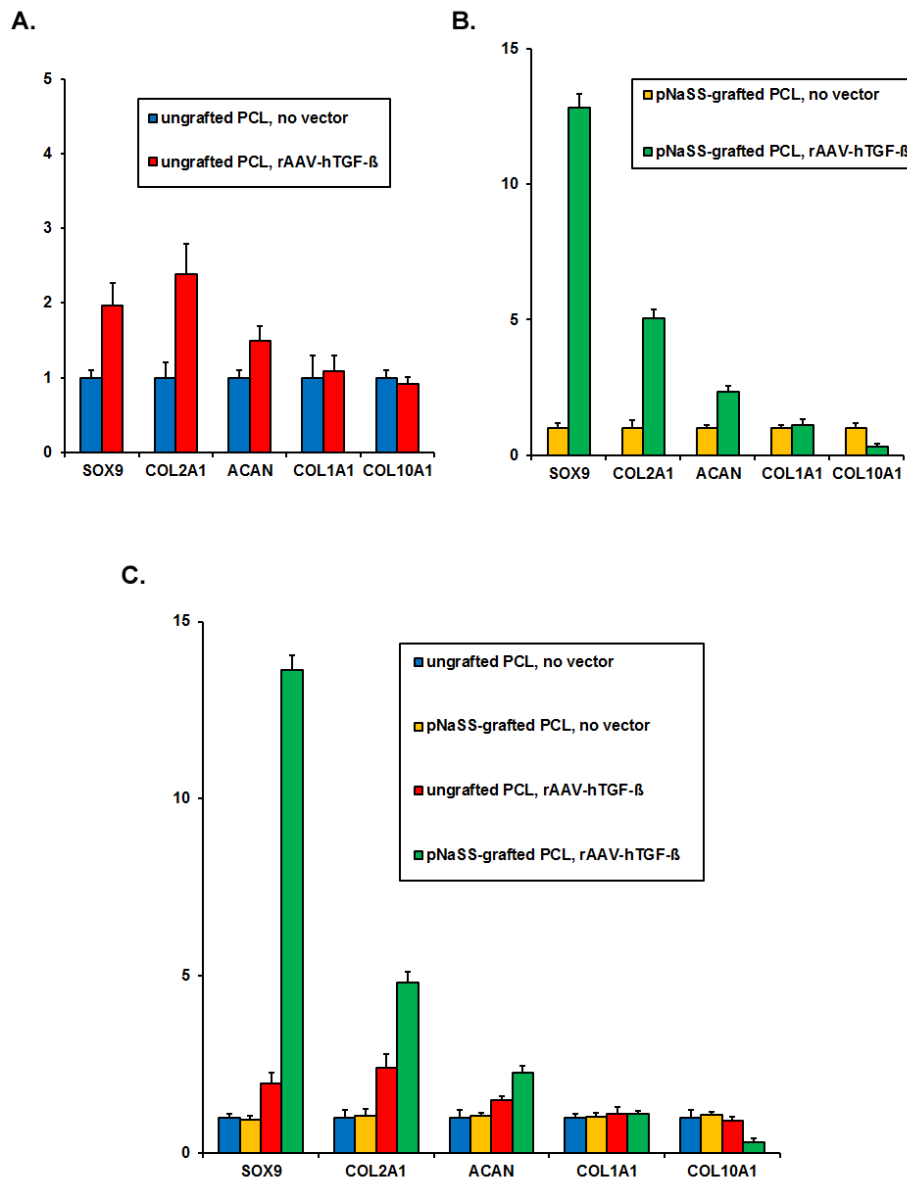


**Figure 27.** Gene expression profiles in human bone marrow aspirates treated with rAAV-hTGF- $\beta$ -coated PCL films. pNaSS-grafted and ungrafted PCL films were coated with rAAV-hTGF- $\beta$  or left without vector coating before incubation with the aspirates. The SOX9, COL2A1, ACAN, COL1A1, and COL10A1 expression profiles were evaluated by real-time RT-PCR *versus* GAPDH after 21 days of culture (SOX9, COL2A1, ACAN: chondrogenic medium; COL1A1, COL10A1: osteogenic medium) (**A,B**: fold inductions relative to samples receiving each respective PCL films without rAAV; **C**: fold inductions relative to samples receiving ungrafted PCL films without rAAV; data from all patients) (source: Venkatesan\*, Cai\* et al., 2021).

## 8. DISCUSSION

In the present study, we tested the hypothesis that thermosensitive PEO-PPO-PEO hydrogel efficiently transfers and overexpress the rAAV SOX9 vector as a means to heal chondral defects *in vivo*. Thermosensitive hydrogel based on PEO-PPO-PEO poloxamers controlling the release of a therapeutic (SOX9) rAAV vector significantly improves the repair of full-thickness chondral defects in a clinically relevant large animal model *in vivo*. We also tested the hypotheses that hydrogel-guided, rAAV-mediated IGF-I overexpression affords long-term cartilage repair and protects against inflammation and the potential development of perifocal OA in a minipig model of a full-thickness chondral defect treated with microfracture surgery after one year *in vivo*. The present study demonstrates the potential benefits of hydrogel (alginate)-guided therapeutic rAAV gene delivery to improve cartilage repair *in vivo* while advantageously reducing perifocal OA and inflammation over an extended period of time. Finally, tested the third hypothesis that PCL films transfer and overexpress the rAAV TGF- $\beta$  vector efficiently to enhance the chondrogenic potential of human bone marrow aspirates *ex vivo* as possible material for future transplantation in cartilage defects. The work reveals the ability of PCL films to deliver a therapeutic rAAV TGF- $\beta$  vector in human bone marrow aspirates as an effective off-the-shelf compound for chondroreparative purposes, especially upon functionalization by pNaSS grafting.

### 8.1. SOX9 *in vivo* study

The current results extend our previous *in vitro* findings on the effectiveness of such hydrogel systems as valid delivery platforms for therapeutic rAAV vectors in MSCs, the major cell type responsible for cartilage repair in this *in vivo* model, as already shown using hMSCs and human articular chondrocytes (Díaz-Rodríguez et al., 2015; Rey-Rico et al., 2016a, 2017, 2018). These findings are also in good agreement with the enhanced *in vitro* chondrogenesis of MSCs and with the improved repair of osteochondral defects in rabbit knee joints by direct, hydrogel-free *sox9* gene transfer (Cucchiaroni et al., 2013; Tao et al., 2016a). The absence of immune response in the current design, even after a long time body exposure to the vectors, is in good

agreement with our previous findings *in vivo* using rAAV vectors in a free form and with the observation that PEO-PPO-PEO poloxamers can protect rAAV-mediated gene transfer from neutralization by antibodies directed against the AAV capsid *in vitro* and in experimental cartilage defects (Cucchiari et al., 2013; Rey-Rico et al., 2015a, 2016a). Overall, these observations further confirm the benefits of applying this class of gene vehicles for clinical purposes compared with the effective but highly immunogenic and transient adenoviral vectors (Bellavia et al., 2018; Evans et al., 2001).

These findings suggest that *sox9*/hydrogel delivery yielded a better approximation of the normal zonal collagen network than the control condition, especially in the basal zone. Mimicking the primary vertical orientation in the base zone of the normal cartilage, these restored collagen fibrils by SOX9 treatment may significantly increase the stiffness of the tissue and protect the solid matrix against large distortions and strains at the subchondral junction (Meng et al., 2017), possibly yielding a persistent and enhanced cartilaginous repair tissue. Taken together, these data indicate that SOX9 treatment via PEO-PPO-PEO hydrogel-guided delivery significantly improved major parameters of a stratified zonal *in situ* chondrogenesis (Chevrier et al., 2011).

Such early loss of the subchondral bone induced by microfracture suggests that stimulation of new bone formation underlying the treated defects possibly occurs at later time points and, from a clinical perspective, highlights the importance of a protected weight-bearing within the first 6 weeks postoperatively when performing marrow stimulation in the tibiofemoral compartment (Gao et al., 2017; Madry et al., 2017; Steadman et al., 2001). Of special importance, *sox9*/hydrogel treatment led to a significantly higher BV/TV of the subchondral bone plate than the control treatment ( $P = 0.002$ ), suggesting a preserving effect of the *sox9*/hydrogel on the subchondral bone plate.

This study holds some limitations. First, the 4-week time point selected for assessment of early osteochondral repair does not allow for a final assessment of the long-term effectiveness. Second, the full postoperative weight-bearing as requested by animal welfare is not comparable to a clinical rehabilitation. The strengths of the study include the use of a translational animal model at an early time point, allowing for an in-depth analysis of the very early outcomes of marrow stimulation, and the comprehensive

analyses of the entire osteochondral unit based on a variety of robust evaluation methods using categorical and continuous data.

## **8.2. IGF-I *in vivo* study**

The current results critically demonstrate that the IGF-I/AlgPH155 hydrogel system was capable of significantly inducing higher levels of IGF-I expression in minipig chondral defects *in vivo* compared with control *lacZ*/AlgPH155 treatment over an extended period of time (one year). The findings corroborate and expand our previous study showing the ability of rAAV-hIGF-I to support IGF-I overexpression in rabbit osteochondral defects for three weeks *in vivo* using a hydrogel-free gene vector delivery approach and are probably resulting from the prolonged controlled release of rAAV from the AlgPH155 hydrogel as reported by us *in vitro* (Cucchiari, Madry, 2014; Díaz-Rodríguez et al., 2015). Such data also support the concept of employing rAAV for *in vivo* protocols over other classes of vectors that may be more immunogenic and functional only over short periods of time (adenoviral vectors) and of using noninvasive (Goodrich et al., 2006), cell-free (rAAV) gene transfer approaches *versus* complex strategies based on the reimplantation of genetically modified cells (Goodrich et al., 2007; Griffin et al., 2016; Madry et al., 2005, 2013; Orved et al., 2015). Interestingly, expression of IGF-I *in vivo* here was also noted in the cartilage surrounding the IGF-I/AlgPH155 defects but not in the synovium, quadriceps muscle adjacent to the patella, infrapatellar pad, or subchondral bone marrow, possibly due to the effective release of rAAV from the hydrogel in the defects and at close distance, but not to an undesirable vector spreading and dissemination at broader sites.

The data next demonstrate that after one year, there was no evidence of deleterious effects of either the IGF-I/AlgPH155 or *lacZ*/AlgPH155 treatment in minipig chondral defects *in vivo*, without signs of osteophytes, synovitis, or immune cell infiltration. This observation confirms the safety of the rAAV/hydrogel system and of rAAV-mediated IGF-I gene transfer as previously noted when testing the current rAAV/hydrogel system *in vitro* and when applying the rAAV-hIGF-I vector to rabbit osteochondral defects in a hydrogel-free form (Cucchiari, Madry, 2014; Díaz-Rodríguez et al., 2015).

The results further reveal that local application of IGF-I/AlgPH155 significantly and persistently enhanced the processes of cartilage repair in minipig chondral defects for at least one year *in vivo* relative to control *lacZ*/AlgPH155 treatment, with significantly improved microstructural repair, significantly enhanced cellularity, and significantly higher ECM deposition (stronger type-II collagen deposition, trend toward more proteoglycans, absence of undesirable type-I collagen), in good agreement with the properties of the growth factor (Nixon et al., 1999; Osborn et al., 1989). These findings expand our previous observations in rabbit osteochondral defects using the rAAV-hIGF-I vector in a hydrogel-free form for three weeks (Cucchiari, Madry, 2014), even though type-I collagen expression was reduced with IGF-I in the rabbits probably due to the difference in time points evaluated (three weeks *versus* one year here) (Cucchiari, Madry, 2014), as the amounts of vector added were in the same range in both studies ( $2 \times 10^5$  *versus*  $3.6 \times 10^5$  transgene copies here). For comparison, significant benefits of IGF-I overexpression were reported in complex cell-based approaches for only 28 weeks in rabbit osteochondral defects using IGF-I-transfected chondrocytes using a poly(glycolic acid) (PGA) scaffold and for eight months in horse chondral defects treated with rAAV-treated chondrocytes (Griffin et al., 2016; Madry et al., 2013; Orved et al., 2015). Our current off-the-shelf, cell-free strategy is also more adapted and durable than the use of recombinant IGF-I as tested by other groups who applied the factor at a very high dose ( $25 \mu\text{g}$  *versus* up to  $\approx 13.5 \text{ ng}$  here, i.e.,  $\approx 1,850$ -fold difference) to achieve therapeutic effects in rabbit osteochondral defects for only 12 weeks using an oligo(poly(ethylene glycol) fumarate)/gelatin composite hydrogel and in horse chondral defects for 6-8 months using fibrin alone or chondrocyte-fibrin composites (Kim et al., 2013; Nixon et al., 1999, 2005). The reduced parameters of "defect architecture" and "subchondral bone plate" were caused by a large osteochondral cleft in one of the treated defects that was not excluded from scoring.

Finally, the present findings reveal that the IGF-I/AlgPH155 hydrogel system was capable of significantly reducing the long-term development of perifocal OA in the cartilage adjacent to the minipig chondral defects, with trends toward improved microscopic structure after one year and decreased expression of detrimental proinflammatory mediators (IL-1 $\beta$ , TNF- $\alpha$ ) in the defects and surrounding cartilage relative to the *lacZ*/AlgPH155 condition, possibly due to the overexpression of IGF-I from

the candidate hydrogel system at a close distance, in good agreement with the protective effects of the growth factor against OA pathomechanisms (cartilage degradation, inflammation) and with our previous work showing a reduction of OA changes in the cartilage surrounding rabbit osteochondral defects treated with IGF-I-transfected chondrocytes/PGA constructs for 28 weeks (Loffredo et al., 2014; Madry et al., 2013; Nixon et al., 2005; Rogachefsky et al., 1993; Weimer et al., 2012).

A limitation of the study is the absence of quantitative biochemical analysis and of the assessment of the mechanical function of the repaired cartilage and adjacent tissues. As complete regeneration was not achieved in the conditions tested here, coadministration of other candidates might be desirable, like the chondroreparative and anti-hypertrophic cartilage specific SOX9 transcription factor (Bi et al., 1999; Cucchiaroni et al., 2013; Madry et al., 2020a; Venkatesan et al., 2012). This might be performed by simultaneous or independent gene transfer of various rAAV via alginate since co-treatment of such vectors can be successfully established without viral interference (Cucchiaroni et al., 2009; Rendahl et al., 1998).

### **8.3. TGF- $\beta$ *ex vivo* study**

In the current study, we examined the feasibility of delivering a highly chondrogenic TGF- $\beta$  sequence via rAAV in human bone marrow aspirates using solid PCL films functionalized with a bioactive pNaSS molecule (Frisch et al., 2016; Leroux et al., 2019; Rohman et al., 2015; Venkatesan et al., 2020a), as a non-invasive strategy to further stimulate the chondroregenerative processes in these samples relative to the outcomes achieved when applying a candidate rAAV SOX9 construct (Venkatesan et al., 2020b). The present data first show that TGF- $\beta$  can be successfully overexpressed via rAAV in human bone marrow aspirates following vector delivery via PCL films for up to 21 days (the longest time point evaluated), especially using films grafted with pNaSS (92.6% gene transfer efficiencies) relative to the other conditions, probably due to the effective controlled release of rAAV from such films evidenced in our earlier work using reporter vectors (Venkatesan et al., 2020a). These findings also extend our previous observations in similar samples treated with film-free rAAV-hTGF- $\beta$  gene delivery and confirm similar observations using an rAAV SOX9 vector (Frisch et al., 2016;

Venkatesan et al., 2020b). Remarkably, the levels of TGF- $\beta$  production achieved using PCL films, especially those grafted with pNaSS, increased over the period of evaluation, in contrast to findings where rAAV-hTGF- $\beta$  was applied to bone marrow aspirates in a free form, showing significant but decreasing TGF- $\beta$  synthesis over time (from 113 to 16 pg/mg total proteins/24 hours between days 14 and 21) (Frisch et al., 2016), again possibly due to the effective controlled release of rAAV from such films (Venkatesan et al., 2020a).

The findings next demonstrate that effective TGF- $\beta$  overexpression via application of rAAV vectors coated on PCL films led to higher levels of matrix proteoglycans and type-II collagen and of cell proliferation after 21 days in the bone marrow aspirates, particularly when using films grafted with pNaSS, compared with the other conditions, concordant with the activities of the TGF- $\beta$  and with our previous work using similar samples treated with film-free rAAV-hTGF- $\beta$  (Frisch et al., 2016). The increases in matrix compound deposition were probably due to the enhanced expression of SOX9 in the corresponding samples as noted by real-time RT-PCR analysis, in good agreement with the properties of this transcription factor (Guo et al., 2006b). Interestingly, while the levels of matrix components achieved via PCL-guided TGF- $\beta$  overexpression here were in the range of those reported when using film-free rAAV TGF- $\beta$  administration (53-60 ng/mg total proteins) (Frisch et al., 2016), the indices of cell proliferation were higher than those reached when using film-free rAAV TGF- $\beta$  gene transfer ( $5,201 \pm 76$  and  $6,475 \pm 89$  cells/mm<sup>2</sup> with ungrafted and pNaSS-grafted films, respectively, *versus*  $119 \pm 27$  cells/mm<sup>2</sup> at similar vector doses, i.e. an up to 54.4-fold difference) (Frisch et al., 2016). Such stimulating effects of PCL-guided rAAV TGF- $\beta$  delivery on cell proliferation demonstrate the potential additional benefits of using this candidate gene for reparative purposes relative to the transfer of an rAAV SOX9 construct using similar films that promoted higher matrix deposition (70-83 *versus* 48-53 ng/mg total proteins here) but had not proliferative effects in bone marrow aspirates (Venkatesan et al., 2020b).

Equally important, PCL-guided administration of rAAV-hTGF- $\beta$  was capable of reducing premature matrix mineralization and hypertrophy (type-X collagen expression) in the aspirates for 21 days, especially when applying the films grafted with pNaSS,

compared with the other conditions, as noted when employing film-free rAAV-hTGF- $\beta$  gene delivery or when transferring an rAAV SOX9 construct with the films (Frisch et al., 2016; Venkatesan et al., 2020b), possibly due to the increased expression of anti-hypertrophic SOX9 in the TGF- $\beta$ -treated samples (Pagnotto et al., 2007). Interestingly, there was no effect of rAAV-hTGF- $\beta$  on type-I collagen expression regardless of the type of film employed, in contrast to findings using film-free rAAV-hTGF- $\beta$  gene transfer where expression of this marker was significantly decreased (Frisch et al., 2016). Nevertheless, in this previous study, free rAAV-hTGF- $\beta$  was applied at a lower MOI (10 *versus* 75 here), suggesting that high rAAV-hTGF- $\beta$  doses may have a limited impact on type-I collagen in such a system, in contrast to the administration of an rAAV SOX9 construct via similar films at the same MOI (75) that was capable of significantly reducing the levels of this osteogenic marker (Venkatesan et al., 2020b), in agreement with the activities of the transcription factor (Ivkovic et al., 2010).

The possible chondroreparative benefits and immune protection of the PCL-guided rAAV TGF- $\beta$  gene transfer are currently being evaluated over free gene vector delivery in orthotopic models of cartilage defects *in vivo* (Cucchiarini et al., 2018; Goomer et al., 2001; Guo et al., 2006a, 2006b; Ivkovic et al., 2010; Li et al., 2013; Pagnotto et al., 2007), where anti-AAV immune responses may occur (Cottard et al., 2004). The therapeutic benefits of this system may further be improved by combined delivery of additional rAAV constructs, like for instance, an rAAV SOX9 vector that may further stimulate matrix deposition and reduce osteogenic and terminal differentiation in the aspirates (Venkatesan et al., 2020b). This might be performed by simultaneous or independent coating of various rAAV on the films since co-treatment of such vectors can be successfully established without viral interference (Cucchiarini et al., 2009; Rendahl et al., 1998).

#### **8.4. Conclusions**

*In vivo*, we provided scaffold-guided rAAV vectors within focal cartilage defects to monitor cartilage repair over time. For the SOX9 *in vivo* study, a thermosensitive hydrogel based on PEO-PPO-PEO poloxamers controlling the release of a therapeutic (SOX9) rAAV vector significantly improves the repair of full-thickness chondral defects in

a clinically relevant large animal model. This hydrogel is a highly promising system for *in vivo* rAAV delivery, supporting cartilage repair in conditions where protection against potentially damaging host immune responses may need to be afforded. The data support the concept of biomaterial-guided gene delivery as an attractive therapeutic option for cartilage repair, enabling for a controlled and minimally invasive delivery of genes without loss of the therapeutic gene product *in vivo* (Ashammakhi et al., 2019). From a clinical translational point of view, such biomaterial-guided gene vector delivery is particularly attractive for cartilage defects that are arthroscopically treated with microfracture and may represent a major step toward improved cartilage repair in the near future. The IGF-I *in vivo* study demonstrates the potential benefits of hydrogel (alginate)-guided therapeutic rAAV gene delivery to improve cartilage repair *in vivo* while advantageously reducing perifocal OA and inflammation over an extended period of time. The current findings highlight the value of the rAAV/AlgPG155 hydrogel system as a future direction, a minimally invasive off-the-shelf solution for enhanced surgical therapies to repair cartilage defects clinical scenarios. From a future clinical perspective, such a hydrogel-guided, rAAV-mediated overexpression of therapeutic gene sequences will ideally be performed during arthroscopic marrow stimulation given the symmetric pattern of enhanced long-term cartilage repair and protection against perifocal OA.

*Ex vivo*, we modified chondroreparative human bone marrow aspirates via the controlled release of therapeutic rAAV vectors as novel implantable platforms for the treatment of cartilage injuries including OA. This work reveals the ability of PCL films to deliver a therapeutic rAAV TGF- $\beta$  vector in human bone marrow aspirates as an effective off-the-shelf compound for chondroreparative purposes, especially upon functionalization by pNaSS grafting. Such a scaffold-guided gene therapy approach to enhance the chondrogenic potential of noninvasively prepared human bone marrow aspirates has a broad potential in translational applications that aim at reinforcing the processes of healing by implantation of the modified aspirates in cartilage defects. Alternatively, therapeutic rAAV-coated scaffolds may also directly be applied to sites of cartilage damage as a means to stimulate the chondrogenic activities of local bone marrow cells that repopulate the defects. Taken together, this study provides evidence supporting the concept of applying therapeutic rAAV vectors using hydrogels and solid scaffolds in clinical protocols aiming at improved cartilage repair in patients.

## 9. REFERENCES

- Alvarez-Lorenzo C, Sosnik A, Concheiro A (2011) PEO-PPO block copolymers for passive micellar targeting and overcoming multidrug resistance in cancer therapy. *Curr Drug Targets* 12:1112-1130
- Ashammakhi N, Ahadian S, Darabi MA, El Tahchi M, Lee J, Suthiwanich K, Sheikhi A, Dokmeci MR, Oklu R, Khademhosseini A (2019) Minimally invasive and regenerative therapeutics. *Adv Mater* 31:e1804041
- Bellavia D, Veronesi F, Carina V, Costa V, Raimondi L, De Luca A, Alessandro R, Fini M, Giavaresi G (2018) Gene therapy for chondral and osteochondral regeneration: is the future now? *Cell Mol Life Sci* 75:649-667
- Bi W, Deng JM, Zhang Z, Behringer RR, de Crombrughe B (1999) Sox9 is required for cartilage formation. *Nat Genet* 22:85-89
- Brunger JM, Huynh NPT, Guenther CM, Perez-Pinera P, Moutos FT, Sanchez-Adams J, Gersbach CA, Guilak F (2014) Scaffold-mediated lentiviral transduction for functional tissue engineering of cartilage. *Proc Natl Acad Sci U S A* 111:E798
- Chevrier A, Hoemann CD, Sun J, Buschmann MD (2007) Chitosan-glycerol phosphate/blood implants increase cell recruitment, transient vascularization and subchondral bone remodeling in drilled cartilage defects. *Osteoarthritis Cartilage* 15:316-327
- Chevrier A, Hoemann CD, Sun J, Buschmann MD (2011) Temporal and spatial modulation of chondrogenic foci in subchondral microdrill holes by chitosan-glycerol phosphate/blood implants. *Osteoarthritis Cartilage* 19:136-144
- Christensen BB, Foldager CB, Olesen ML, Vingtoft L, Rölfing JHD, Ringgaard S, Lind M (2015) Experimental articular cartilage repair in the Göttingen minipig: the influence of multiple defects per knee. *J Exp Orthop* 2:13-13
- Cottard V, Valvason C, Falgarone G, Lutomski D, Boissier MC, Bessis N (2004) Immune response against gene therapy vectors: influence of synovial fluid on adeno-associated virus mediated gene transfer to chondrocytes. *J Clin Immunol* 24:162-169
- Cucchiari M, Asen AK, Goebel L, Venkatesan JK, Schmitt G, Zurakowski D, Menger MD, Laschke MW, Madry H (2018) Effects of TGF- $\beta$  overexpression via rAAV

- gene transfer on the early repair processes in an osteochondral defect model in minipigs. *Am J Sports Med* 46:1987-1996
- Cucchiari M, Henrionnet C, Mainard D, Pinzano A, Madry H (2015) New trends in articular cartilage repair. *J Exp Orthop* 2:8-8
- Cucchiari M, Madry H (2019) Biomaterial-guided delivery of gene vectors for targeted articular cartilage repair. *Nat Rev Rheumatol* 15:18-29
- Cucchiari M, Madry H (2014) Overexpression of human IGF-I via direct rAAV-mediated gene transfer improves the early repair of articular cartilage defects in vivo. *Gene Ther* 21:811-819
- Cucchiari M, Orth P, Madry H (2013) Direct rAAV SOX9 administration for durable articular cartilage repair with delayed terminal differentiation and hypertrophy in vivo. *J Cell Mol Med* 91:625-636
- Cucchiari M, Terwilliger EF, Kohn D, Madry H (2009) Remodelling of human osteoarthritic cartilage by FGF-2, alone or combined with Sox9 via rAAV gene transfer. *J Cell Mol Med* 13:2476-2488
- Cucchiari M, Thurn T, Weimer A, Kohn D, Terwilliger EF, Madry H (2007) Restoration of the extracellular matrix in human osteoarthritic articular cartilage by overexpression of the transcription factor SOX9. *Arthritis Rheum* 56:158-167
- Díaz-Rodríguez P, Rey-Rico A, Madry H, Landin M, Cucchiari M (2015) Effective genetic modification and differentiation of hMSCs upon controlled release of rAAV vectors using alginate/poloxamer composite systems. *Int J Pharm* 496:614-626
- Evans CH, Ghivizzani SC, Oligino TA, Robbins PD (2001) Future of adenoviruses in the gene therapy of arthritis. *Arthritis Res* 3:142-146
- Fahy N, Farrell E, Ritter T, Ryan AE, Murphy JM (2015) Immune modulation to improve tissue engineering outcomes for cartilage repair in the osteoarthritic joint. *Tissue Eng Part B Rev* 21:55-66
- Fortier L, Mohammed H, Lust G, Nixon A (2002) Insulin-like growth factor-I enhances cell-based repair of articular cartilage. *J Bone Joint Surg Br* 84:276-288
- Frisch J, Rey-Rico A, Venkatesan JK, Schmitt G, Madry H, Cucchiari M (2016) TGF- $\beta$  gene transfer and overexpression via rAAV vectors stimulates chondrogenic events in human bone marrow aspirates. *J Cell Mol Med* 20:430-440

- Frisch J, Venkatesan JK, Rey-Rico A, Schmitt G, Madry H, Cucchiarini M (2014a) Determination of the chondrogenic differentiation processes in human bone marrow-derived mesenchymal stem cells genetically modified to overexpress transforming growth factor- $\beta$  via recombinant adeno-associated viral vectors. *Hum Gene Ther* 25:1050-1060
- Frisch J, Venkatesan JK, Rey-Rico A, Schmitt G, Madry H, Cucchiarini M (2014b) Influence of insulin-like growth factor I overexpression via recombinant adeno-associated vector gene transfer upon the biological activities and differentiation potential of human bone marrow-derived mesenchymal stem cells. *Stem Cell Res Ther* 5:103
- Gao L, Orth P, Müller-Brandt K, Goebel LKH, Cucchiarini M, Madry H (2017) Early loss of subchondral bone following microfracture is counteracted by bone marrow aspirate in a translational model of osteochondral repair. *Sci Rep* 7:45189
- Goebel L, Orth P, Cucchiarini M, Pape D, Madry H (2017) Macroscopic cartilage repair scoring of defect fill, integration and total points correlate with corresponding items in histological scoring systems - a study in adult sheep. *Osteoarthritis Cartilage* 25:581-588
- Goebel L, Orth P, Müller A, Zurakowski D, Bückler A, Cucchiarini M, Pape D, Madry H (2012) Experimental scoring systems for macroscopic articular cartilage repair correlate with the MOCART score assessed by a high-field MRI at 9.4 T-- comparative evaluation of five macroscopic scoring systems in a large animal cartilage defect model. *Osteoarthritis Cartilage* 20:1046-1055
- Gomoll AH, Madry H, Knutsen G, van Dijk N, Seil R, Brittberg M, Kon E (2010) The subchondral bone in articular cartilage repair: current problems in the surgical management. *Knee Surg Sports Traumatol Arthrosc* 18:434-447
- Goodrich L, Hidaka C, Robbins P, Evans CH, Nixon A (2007) Genetic modification of chondrocytes with insulin-like growth factor-1 enhances cartilage healing in an equine model. *J Bone Joint Surg Br* 89:672-685
- Goodrich LR, Brower-Toland BD, Warnick L, Robbins PD, Evans CH, Nixon AJ (2006) Direct adenovirus-mediated IGF-I gene transduction of synovium induces persisting synovial fluid IGF-I ligand elevations. *Gene Ther* 13:1253-1262

- Goomer RS, Deftos LJ, Terkeltaub R, Maris T, Lee MC, Harwood FL, Amiel D (2001) High-efficiency non-viral transfection of primary chondrocytes and perichondrial cells for ex-vivo gene therapy to repair articular cartilage defects. *Osteoarthritis Cartilage* 9:248-256
- Grande DA, Schwartz JA, Brandel E, Chahine NO, Sgaglione N (2013) Articular cartilage repair: where we have been, where we are now, and where we are headed. *Cartilage* 4:281-285
- Griffin DJ, Orved KF, Nixon AJ, Bonassar LJ (2016) Mechanical properties and structure-function relationships in articular cartilage repaired using IGF-I gene-enhanced chondrocytes. *J Orthop Res* 34:149-153
- Guermazi A, Hayashi D, Roemer FW, Niu J, Quinn EK, Crema MD, Nevitt MC, Torner J, Lewis CE, Felson DT (2017) Brief report: partial-and full-thickness focal cartilage defects contribute equally to development of new cartilage damage in knee osteoarthritis: the multicenter osteoarthritis study. *Arthritis Rheumatol* 69:560-564
- Guo T, Zeng X, Hong H, Diao H, Wangrui R, Zhao J, Zhang J, Li J (2006a) Gene-activated matrices for cartilage defect repair. *Int J Artif Organs* 29:612-621
- Guo X, Zheng Q, Yang S, Shao Z, Yuan Q, Pan Z, Tang S, Liu K, Quan D (2006b) Repair of full-thickness articular cartilage defects by cultured mesenchymal stem cells transfected with the transforming growth factor beta1 gene. *Biomed Mater* 1:206-215
- Haffner-Luntzer M, Heilmann A, Heidler V, Liedert A, Schinke T, Amling M, Yorgan TA, Vom Scheidt A, Ignatius A (2016) Hypochlorhydria-induced calcium malabsorption does not affect fracture healing but increases post-traumatic bone loss in the intact skeleton. *J Orthop Res* 34:1914-1921
- Hampshire VA, Gilbert SH (2019) Refinement, reduction, and replacement (3R) strategies in preclinical testing of medical devices. *Toxicol Pathol* 47:329-338
- Hoemann C, Kandel R, Roberts S, Saris DBF, Creemers L, Mainil-Varlet P, Méthot S, Hollander AP, Buschmann MD (2011) International Cartilage Repair Society (ICRS) recommended guidelines for histological endpoints for cartilage repair studies in animal models and clinical trials. *Cartilage* 2:153-172
- Hotaling NA, Bharti K, Kriel H, Simon CG, Jr. (2015) DiameterJ: A validated open source nanofiber diameter measurement tool. *Biomaterials* 61:327-338

- Ivkovic A, Pascher A, Hudetz D, Maticic D, Jelic M, Dickinson S, Loparic M, Haspl M, Windhager R, Pecina M (2010) Articular cartilage repair by genetically modified bone marrow aspirate in sheep. *Gene Ther* 17:779-789
- Kelly DC, Raftery RM, Curtin CM, O'Driscoll CM, O'Brien FJ (2019) Scaffold-based delivery of nucleic acid therapeutics for enhanced bone and cartilage repair. *J Orthop Res* 37:1671-1680
- Kim K, Lam J, Lu S, Spicer PP, Lueckgen A, Tabata Y, Wong ME, Jansen JA, Mikos AG, Kasper FK (2013) Osteochondral tissue regeneration using a bilayered composite hydrogel with modulating dual growth factor release kinetics in a rabbit model. *J Control Release* 168:166-178
- Kwon H, Brown WE, Lee CA, Wang D, Paschos N, Hu JC, Athanasiou KA (2019) Surgical and tissue engineering strategies for articular cartilage and meniscus repair. *Nat Rev Rheumatol* 15:550-570
- Lee HH, Haleem AM, Yao V, Li J, Xiao X, Chu CR (2011) Release of bioactive adeno-associated virus from fibrin scaffolds: effects of fibrin glue concentrations. *Tissue Eng Part A* 17:1969-1978
- Leroux A, Venkatesan JK, Castner DG, Cucchiari M, Migonney V (2019) Analysis of early cellular responses of anterior cruciate ligament fibroblasts seeded on different molecular weight polycaprolactone films functionalized by a bioactive poly(sodium styrene sulfonate) polymer. *Biointerphases* 14:041004
- Li B, Yang J, Ma L, Li F, Tu Z, Gao C (2013) Fabrication of poly(lactide-co-glycolide) scaffold filled with fibrin gel, mesenchymal stem cells, and poly(ethylene oxide)-b-poly(L-lysine)/TGF- $\beta$ 1 plasmid DNA complexes for cartilage restoration in vivo. *J Biomed Mater Res A* 101:3097-3108
- Little CB, Smith MM, Cake MA, Read RA, Murphy MJ, Barry FP (2010) The OARSI histopathology initiative - recommendations for histological assessments of osteoarthritis in sheep and goats. *Osteoarthritis Cartilage* 18 Suppl 3:S80-S92
- Loffredo FS, Pancoast JR, Cai L, Vannelli T, Dong JZ, Lee RT, Patwari P (2014) Targeted delivery to cartilage is critical for in vivo efficacy of insulin-like growth factor 1 in a rat model of osteoarthritis. *Arthritis Rheumatol* 66:1247-1255

- Madry H, Gao L, Eichler H, Orth P, Cucchiarini M (2017) Bone marrow aspirate concentrate-enhanced marrow stimulation of chondral defects. *Stem Cells Int* 2017:1609685
- Madry H\*, Gao L\*, Rey-Rico A, Venkatesan JK, Müller-Brandt K, Cai X, Goebel L, Schmitt G, Speicher-Mentges S, Zurakowski D, Menger MD, Laschke MW, Cucchiarini M (2020a) Thermosensitive hydrogel based on PEO-PPO-PEO poloxamers for a controlled in situ release of recombinant adeno-associated viral vectors for effective gene therapy of cartilage defects. *Adv Mater* 32:e1906508 (\*shared authorship)
- Madry H, Kaul G, Cucchiarini M, Stein U, Zurakowski D, Remberger K, Menger MD, Kohn D, Trippel SB (2005) Enhanced repair of articular cartilage defects in vivo by transplanted chondrocytes overexpressing insulin-like growth factor I (IGF-I). *Gene Ther* 12:1171-1179
- Madry H, Kaul G, Zurakowski D, Vunjak-Novakovic G, Cucchiarini M (2013) Cartilage constructs engineered from chondrocytes overexpressing IGF-I improve the repair of osteochondral defects in a rabbit model. *Eur Cell Mater* 25:229-247
- Madry H, Orth P, Cucchiarini M (2011) Gene therapy for cartilage repair. *Cartilage* 2:201-225
- Madry H, van Dijk CN, Mueller-Gerbl M (2010) The basic science of the subchondral bone. *Knee Surg Sports Traumatol Arthrosc* 18:419-433
- Madry H, Venkatesan JK, Carballo-Pedrares N, Rey-Rico A, Cucchiarini M (2020b) Scaffold-mediated gene delivery for osteochondral repair. *Pharmaceutics* 12: 930
- Maihöfer J\*, Madry H\*, Rey-Rico A, Venkatesan JK, Goebel L, Schmitt G, Speicher-Mentges S, Cai X, Meng W, Zurakowski D, Menger MD, Laschke MW, Cucchiarini M (2021) Hydrogel-guided, rAAV-mediated IGF-I overexpression enables long-term cartilage repair and protection against perifocal osteoarthritis in a large-animal full-thickness chondral defect model at one year in vivo. *Adv Mater* 33:e2008451 (\*shared authorship)
- Mandal K, Wang I, Vitiello E, Orellana LAC, Balland M (2014) Cell dipole behaviour revealed by ECM sub-cellular geometry. *Nat Comm* 5:5749

- McCarty WJ, Luan A, Sundaramurthy P, Urbanczyk C, Patel A, Hahr J, Sotoudeh M, Ratcliffe A, Sah RL (2011) An arthroscopic device to assess articular cartilage defects and treatment with a hydrogel. *Ann Biomed Eng* 39:1306-1312
- Medvedeva EV, Grebenik EA, Gornostaeva SN, Telpuhov VI, Lychagin AV, Timashev PS, Chagin AS (2018) Repair of damaged articular cartilage: current approaches and future directions. *Int J Mol Sci* 19:2366
- Meng Q, An S, Damion RA, Jin Z, Wilcox R, Fisher J, Jones A (2017) The effect of collagen fibril orientation on the biphasic mechanics of articular cartilage. *J Mech Behav Biomed Mater* 65:439-453
- Moreira Teixeira LS, Bijl S, Pully VV, Otto C, Jin R, Feijen J, van Blitterswijk CA, Dijkstra PJ, Karperien M (2012) Self-attaching and cell-attracting in-situ forming dextran-tyramine conjugates hydrogels for arthroscopic cartilage repair. *Biomaterials* 33:3164-3174
- Moutos FT, Guilak F (2010) Functional properties of cell-seeded three-dimensionally woven poly(epsilon-caprolactone) scaffolds for cartilage tissue engineering. *Tissue Eng Part A* 16:1291-1301
- Nixon AJ, Fortier LA, Williams J, Mohammed H (1999) Enhanced repair of extensive articular defects by insulin-like growth factor-I-laden fibrin composites. *J Orthop Res* 17:475-487
- Nixon AJ, Haupt JL, Frisbie DD, Morisset SS, McIlwraith CW, Robbins PD, Evans CH, Ghivizzani S (2005) Gene-mediated restoration of cartilage matrix by combination insulin-like growth factor-I/interleukin-1 receptor antagonist therapy. *Gene Ther* 12:177-186
- O'Driscoll SW (1998) Current concepts review-the healing and regeneration of articular cartilage. *J Bone Joint Surg Am* 80:1795-1812
- Oh KT, Bronich TK, Kabanov AV (2004) Micellar formulations for drug delivery based on mixtures of hydrophobic and hydrophilic pluronic block copolymers. *J Control Release* 94:411-422
- Orth P, Cucchiaroni M, Zurakowski D, Menger MD, Kohn DM, Madry H (2013a) Parathyroid hormone [1-34] improves articular cartilage surface architecture and integration and subchondral bone reconstitution in osteochondral defects in vivo. *Osteoarthritis Cartilage* 21:614-624

- Orth P, Goebel L, Wolfram U, Ong MF, Gräber S, Kohn D, Cucchiari M, Ignatius A, Pape D, Madry H (2012) Effect of subchondral drilling on the microarchitecture of subchondral bone: analysis in a large animal model at 6 months. *Am J Sports Med* 40:828-836
- Orth P, Madry H (2015) Advancement of the subchondral bone plate in translational models of osteochondral repair: implications for tissue engineering approaches. *Tissue Eng Part B Rev* 21:504-520
- Orth P, Rey-Rico A, Venkatesan JK, Madry H, Cucchiari M (2014) Current perspectives in stem cell research for knee cartilage repair. *Stem Cells Cloning* 7:1-17
- Orth P, Zurakowski D, Alini M, Cucchiari M, Madry H (2013b) Reduction of sample size requirements by bilateral versus unilateral research designs in animal models for cartilage tissue engineering. *Tissue Eng Part C Methods* 19:885-891
- Ortved KF, Begum L, Mohammed HO, Nixon AJ (2015) Implantation of rAAV5-IGF-I transduced autologous chondrocytes improves cartilage repair in full-thickness defects in the equine model. *Mol Ther* 23:363-373
- Osborn KD, Trippel SB, Mankin HJ (1989) Growth factor stimulation of adult articular cartilage. *J Orthop Res* 7:35-42
- Pagnotto MR, Wang Z, Karpie JC, Ferretti M, Xiao X, Chu CR (2007) Adeno-associated viral gene transfer of transforming growth factor-beta1 to human mesenchymal stem cells improves cartilage repair. *Gene Ther* 14:804-813
- Parfitt AM, Mathews CH, Villanueva AR, Kleerekoper M, Frame B, Rao DS (1983) Relationships between surface, volume, and thickness of iliac trabecular bone in aging and in osteoporosis. Implications for the microanatomic and cellular mechanisms of bone loss. *J Clin Invest* 72:1396-1409
- Rendahl KG, Leff SE, Otten GR, Spratt SK, Bohl D, Van Roey M, Donahue BA, Cohen LK, Mandel RJ, Danos O, Snyder RO (1998) Regulation of gene expression in vivo following transduction by two separate rAAV vectors. *Nat Biotechnol* 16:757-761
- Rey-Rico A, Cucchiari M (2016) Controlled release strategies for rAAV-mediated gene delivery. *Acta Biomater* 29:1-10

- Rey-Rico A, Cucchiarini M (2018) PEO-PPO-PEO tri-block copolymers for gene delivery applications in human regenerative medicine-an overview. *Int J Mol Sci* 19:775
- Rey-Rico A, Frisch J, Venkatesan JK, Schmitt G, Rial-Hermida I, Taboada P, Concheiro A, Madry H, Alvarez-Lorenzo C, Cucchiarini M (2016a) PEO-PPO-PEO carriers for rAAV-mediated transduction of human articular chondrocytes in vitro and in a human osteochondral defect model. *ACS Appl Mater Interfaces* 8:20600-20613
- Rey-Rico A, Madry H, Cucchiarini M (2016b) Hydrogel-based controlled delivery systems for articular cartilage repair. *Biomed Res Int* 2016:1215263
- Rey-Rico A, Venkatesan JK, Frisch J, Rial-Hermida I, Schmitt G, Concheiro A, Madry H, Alvarez-Lorenzo C, Cucchiarini M (2015a) PEO-PPO-PEO micelles as effective rAAV-mediated gene delivery systems to target human mesenchymal stem cells without altering their differentiation potency. *Acta Biomater* 27:42-52
- Rey-Rico A, Venkatesan JK, Frisch J, Schmitt G, Monge-Marcet A, Lopez-Chicon P, Mata A, Semino C, Madry H, Cucchiarini M (2015b) Effective and durable genetic modification of human mesenchymal stem cells via controlled release of rAAV vectors from self-assembling peptide hydrogels with a maintained differentiation potency. *Acta Biomater* 18:118-127
- Rey-Rico A, Venkatesan JK, Schmitt G, Concheiro A, Madry H, Alvarez-Lorenzo C, Cucchiarini M (2017) rAAV-mediated overexpression of TGF- $\beta$  via vector delivery in polymeric micelles stimulates the biological and reparative activities of human articular chondrocytes in vitro and in a human osteochondral defect model. *Int J Nanomedicine* 12:6985-6996
- Rey-Rico A, Venkatesan JK, Schmitt G, Speicher-Mentges S, Madry H, Cucchiarini M (2018) Effective remodelling of human osteoarthritic cartilage by sox9 gene transfer and overexpression upon delivery of rAAV vectors in polymeric micelles. *Mol Pharm* 15:2816-2826
- Rezakhaniha R, Agianniotis A, Schrauwen JT, Griffa A, Sage D, Bouten CV, van de Vosse FN, Unser M, Stergiopoulos N (2012) Experimental investigation of collagen waviness and orientation in the arterial adventitia using confocal laser scanning microscopy. *Biomech Model Mechanobiol* 11:461-473

- Rodeo SA, Seneviratne A, Suzuki K, Felker K, Wickiewicz TL, Warren RF (2000) Histological analysis of human meniscal allografts: a preliminary report. *J Bone Joint Surg* 82:1071
- Rogachefsky RA, Dean DD, Howell DS, Altman RD (1993) Treatment of canine osteoarthritis with insulin-like growth factor-1 (IGF-1) and sodium pentosan polysulfate. *Osteoarthritis Cartilage* 1:105-114
- Rohman G, Huot S, Vilas-Boas M, Radu-Bostan G, Castner DG, Migonney V (2015) The grafting of a thin layer of poly(sodium styrene sulfonate) onto poly( $\epsilon$ -caprolactone) surface can enhance fibroblast behavior. *J Mater Sci Mater Med* 26:206
- Samulski RJ, Chang LS, Shenk T (1989) Helper-free stocks of recombinant adeno-associated viruses: normal integration does not require viral gene expression. *J Virol* 63:3822-3828
- Samulski RJ, Chang LS, Shenk T (1987) A recombinant plasmid from which an infectious adeno-associated virus genome can be excised in vitro and its use to study viral replication. *J Virol* 61:3096-3101
- Schneider CA, Rasband WS, Eliceiri KW (2012) NIH Image to ImageJ: 25 years of image analysis. *Nat Methods* 9:671-675
- Sellers RS, Peluso D, Morris EA (1997) The effect of recombinant human bone morphogenetic protein-2 (rhBMP-2) on the healing of full-thickness defects of articular cartilage. *J Bone Joint Surg Am* 79:1452-1463
- Sophia Fox AJ, Bedi A, Rodeo SA (2009) The basic science of articular cartilage: structure, composition, and function. *Sports Health* 1:461-468
- Steadman JR, Rodkey WG, Rodrigo JJ (2001) Microfracture: surgical technique and rehabilitation to treat chondral defects. *Clin Orthop Relat Res* 391 Suppl:S362-S369
- Tao K, Frisch J, Rey-Rico A, Venkatesan JK, Schmitt G, Madry H, Lin J, Cucchiari M (2016a) Co-overexpression of TGF- $\beta$  and SOX9 via rAAV gene transfer modulates the metabolic and chondrogenic activities of human bone marrow-derived mesenchymal stem cells. *Stem Cell Res Ther* 7:20-20
- Tao K, Rey-Rico A, Frisch J, Venkatesan JK, Schmitt G, Madry H, Lin J, Cucchiari M (2017) Effects of combined rAAV-mediated TGF- $\beta$  and sox9 gene transfer and

- overexpression on the metabolic and chondrogenic activities in human bone marrow aspirates. *J Exp Orthop* 4:4
- Tao K, Rey-Rico A, Frisch J, Venkatesan JK, Schmitt G, Madry H, Lin J, Cucchiari M (2016b) rAAV-mediated combined gene transfer and overexpression of TGF- $\beta$  and SOX9 remodels human osteoarthritic articular cartilage. *J Orthop Res* 34:2181-2190
- Vega SL, Kwon MY, Burdick JA (2017) Recent advances in hydrogels for cartilage tissue engineering. *Eur Cell Mater* 33:59-75
- Venkatesan JK\*, Cai X\*, Meng W, Rey-Rico A, Schmitt G, Speicher-Mentges S, Falentin-Daudré C, Leroux A, Madry H, Migonney V, Cucchiari M (2021) pNaSS-grafted PCL film-guided rAAV TGF- $\beta$  gene therapy activates the chondrogenic activities in human bone marrow aspirates. *Hum Gene Ther* doi:10.1089/hum.2020.329 (\*shared authorship)
- Venkatesan JK, Ekici M, Madry H, Schmitt G, Kohn D, Cucchiari M (2012) SOX9 gene transfer via safe, stable, replication-defective recombinant adeno-associated virus vectors as a novel, powerful tool to enhance the chondrogenic potential of human mesenchymal stem cells. *Stem Cell Res Ther* 3:22
- Venkatesan JK, Falentin-Daudré C, Leroux A, Migonney V, Cucchiari M (2020a) Biomaterial-guided recombinant adeno-associated virus delivery from poly(sodium styrene sulfonate)-grafted poly( $\epsilon$ -caprolactone) films to target human bone marrow aspirates. *Tissue Eng Part A* 26:450-459
- Venkatesan JK, Falentin-Daudré C, Leroux A, Migonney V, Cucchiari M (2018) Controlled release of gene therapy constructs from solid scaffolds for therapeutic applications in orthopedics. *Discov Med* 25:195-203
- Venkatesan JK, Meng W, Rey-Rico A, Schmitt G, Speicher-Mentges S, Falentin-Daudré C, Leroux A, Madry H, Migonney V, Cucchiari M (2020b) Enhanced chondrogenic differentiation activities in human bone marrow aspirates via sox9 overexpression mediated by pNaSS-grafted PCL film-guided rAAV gene transfer. *Pharmaceutics* 12:280
- Visser J, Peters B, Burger TJ, Boomstra J, Dhert WJ, Melchels FP, Malda J (2013) Biofabrication of multi-material anatomically shaped tissue constructs. *Biofabrication* 5:035007

Xiao X, Li J, Samulski RJ (1996) Efficient long-term gene transfer into muscle tissue of immunocompetent mice by adeno-associated virus vector. *J Virol* 70:8098-8108

Zhao R-l, Zhang X-m, Jia L-n, Song W, Sun Y-l, Meng X-y, Peng X-x (2019) P<sup>+</sup>NNS-conjugated chitosan mediated IGF-1 and miR-140 overexpression in articular chondrocytes improves cartilage repair. *BioMed Res Int* 2019:2761241

## 10. PUBLICATIONS AND PRESENTATIONS

### 10.1. Publications

1. **Cai X**, Gao L, Cucchiari M, Madry H. Association of nicotine with osteochondrogenesis and osteoarthritis development: the state of the art of preclinical research. *J Clin Med*. 2019;8(10):1699. Impact factor: 3.303 (2019)
2. **Cai X**, Xu T, Xun C, Abulizi Y, Liu Q, Sheng W, Han Z, Gao L, Maierdan M. Establishment and initial testing of a medium-sized, surgically feasible animal model for Brucellar Spondylodiscitis: a preliminary study. *Biomed Res Int*. 2019;2019:7368627. Impact factor: 2.276 (2019)
3. Madry H\*, Gao L\*, Rey-Rico A, Venkatesan JK, Müller-Brandt K, **Cai X**, Goebel L, Schmitt G, Speicher-Mentges S, Zurakowski D, Menger MD, Laschke MW, Cucchiari M. Thermosensitive hydrogel based on PEO-PPO-PEO poloxamers for a controlled in situ release of recombinant adeno-associated viral vectors for effective gene therapy of cartilage defects. *Adv Mater*. 2020;32:e1906508 (\*shared authorship). Impact factor: 27.398 (2019)
4. **Cai X**, Daniels O, Cucchiari M, Madry H. Ectopic models recapitulating morphological and functional features of articular cartilage. *Ann Anat*. 2021;19; 237:151721. Impact factor: 2.388 (2019)
5. Venkatesan JK\*, **Cai X\***, Meng W, Rey-Rico A, Schmitt G, Speicher-Mentges S, Falentin-Daudré C, Leroux A, Madry H, Migonney V, Cucchiari M. pNaSS-grafted PCL film-guided rAAV TGF- $\beta$  gene therapy activates the chondrogenic activities in human bone marrow aspirates. *Hum Gene Ther*. 2021;doi:10.1089/hum.2020.329 (\*shared authorship). Impact factor: 4.510 (2019)
6. Oláh T, **Cai X**, Michaelis JC, Madry H. Comparative anatomy and morphology of the knee in translational models for articular cartilage disorders. Part I: large animals. *Ann Anat*. 2021;235:151680. Impact factor: 2.388 (2019)
7. Oláh T, Michaelis JC, **Cai X**, Cucchiari M, Madry H. Comparative anatomy and morphology of the knee in translational models for articular cartilage disorders. Part II: small animals. *Ann Anat*. 2021;234:151630. Impact factor: 2.388 (2019)
8. Venkatesan JK, Rey-Rico, A, Meng W, **Cai X**, Pons F, Lebeau L, Migonney V, Madry H, Cucchiari M. Biomaterial-assisted gene therapy for translational approaches to treat musculoskeletal disorders. *Mater Today Adv*. 2021;9:100126.

9. Abulizi Y\*, **Cai X\***, Xu T, Xun C, Sheng W, Gao L, Maimaiti M. Diagnosis and surgical treatment of human Brucellar Spondylodiscitis. *J Vis Exp*. 2021:e61840 (\*shared authorship). Impact factor: 1.200 (2019)
10. Maihöfer J\*, Madry H\*, Rey-Rico A, Venkatesan JK, Goebel L, Schmitt G, Speicher-Mentges S, **Cai X**, Meng W, Zurakowski D, Menger MD, Laschke MW, Cucchiarini M. Hydrogel-guided, rAAV-mediated IGF-I overexpression enables long-term cartilage repair and protection against perifocal osteoarthritis in a large animal full-thickness chondral defect model at one year in vivo. *Adv Mater*. 2021;18:e2008451 (\*shared authorship). Impact factor: 27.398 (2019)
11. Li Z, Zhang S, He M, Zhao D, Yang X, Habulihan H, **Cai X<sup>+</sup>**, Cheng H<sup>+</sup>. Single-stage transverse process resection, debridement, interbody fusion, and internal fixation for the treatment of lumbar spinal tuberculosis via posterior-only approach. *Orthop Surg*. *in press*. \*corresponding author. Impact factor: 1.718 (2019)

## 10.2. Oral presentations

1. **Cai X**, Xu T, Xun C, Abulizi Y, Liu Q, Sheng W, Han Z, Gao L, Maierdan M. A novel middle-size and surgically feasible animal model for Brucellar spondylodiscitis. The 14<sup>th</sup> Annual Congress of Chinese Orthopaedic Association, 11/2021, Shanghai, P. R. China.

## 10.3. Poster presentations

1. **Cai X**, Li Z, Zhang S, He M, Zhao D, Yang X, Habulihan H, Cheng H. Single-stage transverse process resection, debridement, interbody fusion, and internal fixation for the treatment of lumbar spinal tuberculosis via posterior-only approach. Global Spine Congress, 11/2021, Paris, France.
2. **Cai X**, Xu T, Xun C, Abulizi Y, Liu Q, Sheng W, Han Z, Gao L, Maierdan M. Establishment and validation of the middle-size, surgically feasible rabbit for Brucellar spondylodiscitis. Global Spine Congress, 11/2021, Paris, France.

## 11. ACKNOWLEDGEMENTS

First and foremost, I would like to extend my deepest gratitude to my director, Prof. Dr. med. Henning Madry and my supervisor, Prof. Dr. rer. nat. Magali Cucchiarini Madry, for their precious guidance and continuous support on my research works. I'm indebted to them, not just for their supervisory aid but also for their encouragement, wisdom, and friendship over the last three years. Without their meticulous patience and insightful guidance, I was unable to finish this dissertation successfully.

Secondly, my heart-felt thanks also go to Dr. rer. nat. Jagadeesh K. Venkatesan and Dr. rer. nat. Tamás Oláh for their valuable advice and technical assistance on my research project. Dr. rer. nat. Jagadeesh K. Venkatesan helped me with the data analysis and manuscript writing during the experiments and accompanied me during the whole project. Dr. rer. nat. Tamás Oláh introduced me to the method of the micro-CT analysis and gave me many practical suggestions for my research. I would like to extend my sincere gratitude to Mrs. Gertrud Schmitt for the lab facilities and kind help during my research. She spent a lot of time helping me with the cell culture, sample cutting, and histological staining. My grateful thanks to Mrs. Susanne Speicher-Mentges, who helped me during the histological staining tasks and gave me a lot of practical advice. Special thanks must be sent to Ms. Sonja Ramin, who helped me reduce the burden of documentation and formalities. Many thanks to Dr. med. Liang Gao for the unreserved support of my work, scientific guidance, and invaluable suggestions for the improvement of the scientific manuscripts. I would also like to credit my old friend, Dr. Weikun Meng, who always takes care of me and help me with everything. To all the current and former members of the Center of Experimental Orthopaedics, especially to Dr. rer. nat. Mahnaz Amini and Dr. Wei Liu: many thanks to you for the excellent working atmosphere and support in my work.

Thirdly, I would also like to express my sincere thanks to Prof. Dr. med. Matthias Laschke and the outstanding team from Institute for Clinical and Experimental Surgery for providing the experimental surgical facilities and for their professional support during the animal surgeries.

Finally, to my parents, my fiancée Ms. Jarkenay Abduray, all my family (especially the Nagys), and my friends: I thank you very much for your selfless support, concern, and love. Your loving considerations and help are the sources of my strength.

## **12. CURRICULUM VITAE**

The curriculum vitae was removed from the electronic version of the doctoral thesis for reasons of data protection.